REACTION KINETICS AND MECHANISMS OF LOW TEMPERATURE SO_2 REMOVAL BY DRY CALCIUM-BASED SORBENTS

A Dissertation Presented to

The Faculty of the College of Engineering and Technology

Ohio University

In Partial Fulfillment

of the Requirement for the Degree

Doctor of Philosophy

by

Lotfi Ben-Said

November, 1993

ABSTRACT

Ben-Said, Lotfi, Ph.D. November, 1993
Chemical Engineering

Reaction Kinetics and Mechanisms of Low Temperature SO_2 Removal by Dry Calcium-Based Sorbents (181pp.)

Director of Dissertation: Michael E. Prudich

Bench-scale integral reactor experimental studies which investigated the effects of inlet SO_2 concentration, flue gas relative humidity, and limestone particle size were performed to test the performance of a 2 inch diameter by 6 inch deep fixed-bed reactor.

Bench-scale experiments using differential reactor techniques were conducted to obtain kinetic data under dry/humidified conditions and to investigate key experimental conditions that included limestone type, flue gas relative humidity and limestone particle size.

An extension to an existing resistance-in-series kinetic model describing the reaction between SO_2 and limestone was developed. The upgraded model included the effects of $CaSO_3/CaSO_4$ product layer blinding as well as the effects of dry sorbent capture. The model for the precipitate layer blinding idealizes the limestone surface by dividing it into blinded and non-blinded regions. As the reaction between SO_2 and limestone progresses, the blinded area gradually increases until the limestone becomes entirely unreactive. The precipitate layer blinding model takes the form of an empirical equation which

ACKNOWLEDGEMENTS

It has been my pleasure and an honor for me to work with my dissertation advisor, Professor Michael E. Prudich. His gentle guidance, sound advice, and steadfast encouragement throughout this research are very much appreciated. His great ideas and motivations were very essential in completing this work. Special thanks are due to Professor Kendree J. Sampson for his valuable suggestions and constructive criticisms along the way.

I would like to take this opportunity to express my appreciation to the other members of my dissertation committee, Professor Nicholas Dinos in the Chemical Engineering Department and Professor Jared Butcher in the Department of Chemistry.

I would like to thank the Coal Development Office of the Ohio Department of Development for providing partial financial support for this work.

i am very grateful to my wife Naima for her confidence and patient understanding throughout the years we spent in the United States. I owe a special debt to my Caring and loving mother Gmar and I ask forgiveness for being far from her for so many years.

This dissertation is dedicated to my wife Naima and my children Oussama, Mohamed and Mona.

TABLE OF CONTENTS

LIST OF FIGURES

LIST OF TABLES

1.0 INTRODUCTION

The need for better and more advanced flue gas desulfurization (FGD) processes continues to grow very rapidly in the United States and in many other developed countries. This is mainly caused by the acid rain problem, which accounts for a broad range of adverse environmental and health effects potentially associated with air pollutants such as sulfur dioxide and nitrogen oxides. The major source of acid rain has been sulfur dioxide, although other pollutants such as nitrogen oxides contribute quite a bit to acid rain deposition.

Flue gas desulfurization processes have emerged as a result of the limitations on emissions imposed by governmental regulations. Many control proposals have focused on controlling sulfur dioxide emissions from utilities, which account for about two thirds of the annual sulfur dioxide emissions in the United States. The 1990 amendments to the Clean Air Act will result in limiting SO_2 emissions to less than 10 million tons per year by the year 2000.

Better control methods which have the capability of removing sulfur dioxide cheaply and effectively from flue gases will enable the use of high-sulfur coals. Dry scrubbing injection methods which involve the reaction of sulfur dioxide with a dry sorbent seem to be very promising and effective because of their lower capital cost requirements compared to conventional wet scrubbing techniques [Ireland et al., 1988]. For high-sulfur coals, these methods may not be economical owing to higher operating costs resulting from poor sorbent utilization [Offen, 1987].

It is clear that dry scrubbing technologies suffer from poor sorbent utilization and low sulfur dioxide removal, and any work that could be done to overcome these limitations would make these processes more economically feasible. A closer look at factors limiting process performance will generate a better and clearer understanding of what is taking place in the FGD processes.

Prudich et al. [1988] have developed a novel wet/dry post-furnace desulfurization process [Limestone Emission Control (LEC) process] which uses a fixed bed of limestone. In this process, water is introduced to the fixed bed either by condensation from a humidified flue gas or by an over-bed water spray. Pilot plant studies have shown that the LEC process is capable of achieving 99 % sulfur dioxide removal over extended operating periods with an average percent removal of greater than 90 %.

A three resistance-in-series model for the reaction of sulfur dioxide with limestone was developed by Visneski et al. [1990]. This mathematical kinetic model included the gas-phase diffusional resistance of sulfur dioxide, liquid-phase diffusional resistances of both dissolved sulfur and calcium species, and the solid-phase dissolution resistance of limestone. The kinetic model was incorporated into a process model for the fixed-bed LEC reactor, and computer simulation results were compared to experimental data obtained from the small LEC pilot plant installed at Ohio University. The three resistance-in-series model neglected the effects of the sulfite/sulfate precipitate layer which gradually covers the limestone active surface as the reaction progresses. In addition,

bench-scale experimental data as well as results from the small LEC pilot plant demonstration indicated that a significant amount of SO_2 removal (i.e. about 5 to 20 %) takes place in that part of the limestone bed that is nominally dry, but humidified. This effect was not included in the development of the three resistance-in-series model.

Presented herein is an extension to the kinetic model that includes the effects of $CaSO_3/CaSO_4$ product layer blinding as well as the effects of dry sorbent capture. The model for the precipitate layer blinding divides the total limestone surface area into blinded (i.e. nonactive area) and non-blinded (i.e. active area) regions. As the reaction progresses, the blinded area gradually increases until the limestone becomes entirely unreactive. The model takes the form of an empirical equation which relates the surface area available for mass transfer to the extent of reaction. The model for dry sorbent capture has been developed based on experimentally observed behavior. Bench-scale experimental studies at 140°F and at dry conditions using various raw limestones [Ben-Said et al., 1993] revealed an exponential increase in the reaction rate as the gas relative humidity is increased. The model for dry capture effects also takes the form of an empirical equation which relates the fractional liquid coverage (i.e. ratio of liquid surface area to area available for mass transfer) to the gas relative humidity.

Along with the mathematical modeling, bench-scale experiments have been designed to generate kinetic data for the SO_2/limestone reaction at low

temperature. Differential reactor techniques were used to obtain reaction rates for five different raw limestones ranging from highly calcitic (i.e. high $CaCO_3$ content) to dolomitic (i.e. roughly equal $CaCO_3/MgCO_3$ content). The most important parameters investigated included limestone type (i.e. having different chemical and physical properties), flue gas relative humidity (40-95%), and limestone particle size (53-180 microns). The results of this experimental study have been used for determining the parameters of the dry capture and the blinding models. Bench-scale integral experiments that included the effects of inlet SO_2 concentration (500-1750 ppm), flue gas relative humidity (25-75%), and limestone particle size (0.55-2.18 mm) have also been carried out to study the SO_2 removal performance of a 2 inch diameter by 6 inch deep fixed-bed reactor filled with raw Maxville limestone.

2.0 LITERATURE REVIEW

2.1 Background on Current Flue Gas Desulfurization Processes

Flue gas desulfurization (FGD) processes are classified as either recovery or throwaway [Maurin, 1985]. This designation refers to the residues rather than the equipment being used. The throw-away processes produce a waste stream that must be disposed of. The recovery, or marketable systems, on the other hand, are designed to convert sulfur oxides into valuable by-products such as elemental sulfur, sulfuric acid, or ammonium sulfate. These systems are usually more expensive than the throw-away systems, and few of them have been installed, primarily on large utility-sized boilers. The most widely used FGD techniques are the throw-away systems. These technologies include wet scrubbing techniques which use sodium or calcium-based sorbents such as hydrated lime or limestone, sodium alkali or seawater, and dry scrubbing techniques, in which a lime or alkaline slurry is brought in contact with flue gas in a spray dryer. The dry FGD systems generate a dry product, usually a powder, for disposal.

2.1.1 Wet Flue Gas Desulfurization Processes

In wet FGD systems, the flue gas is contacted with an aqueous stream or a slurry of a caustic reagent to remove sulfur oxides. The slurry absorbs the SO_2, and the reaction product which is usually calcium sulfate and/or sulfite is discharged as a wet sludge. Wet scrubbers available for sulfur oxides removal include packed, tray and spray absorbers. These scrubbers have different

removal efficiencies in terms of sulfur oxides and particulates because of their different mechanical operations. High removal efficiencies of both sulfur oxides and particulates are achieved through a multi-stage wet-scrubber process. In this case, an electrostatic precipitator or fabric filter and a venturi scrubber are used ahead of the SO_2 absorber for particulate removal.

A spray scrubber, as shown in Figure 2-1, uses spray nozzles to atomize the scrubbing liquid. Nozzles are operated at very high pressures to ensure fine droplet size and consequently large surface area. The spray absorbers have higher sulfur oxides removal efficiencies than other systems because of the high liquid-gas contact achieved by atomizing the scrubbing liquid. On the other hand, they have low particulate removal efficiencies.

In a tray scrubber, the flue gas passes through small orifices and then encounters an impingement plate. These types of scrubbers have relatively high particulate and sulfur oxides removal efficiencies (about 90 %). However, these systems are subject to scale formation, plugging and corrosion.

Packed-bed absorbers are usually operated in a vertical countercurrent flow or a horizontal cross-flow configuration. These types of scrubbers have reasonable sulfur oxides removal efficiencies; however, they are not suitable for particulate removal.

Among the types of wet FGD processes are three common set-ups which use lime or limestone, sodium alkali, or dual alkali (i.e. uses two alkali feed streams such as lime and soda ash) (McInnes and Royen, 1990).

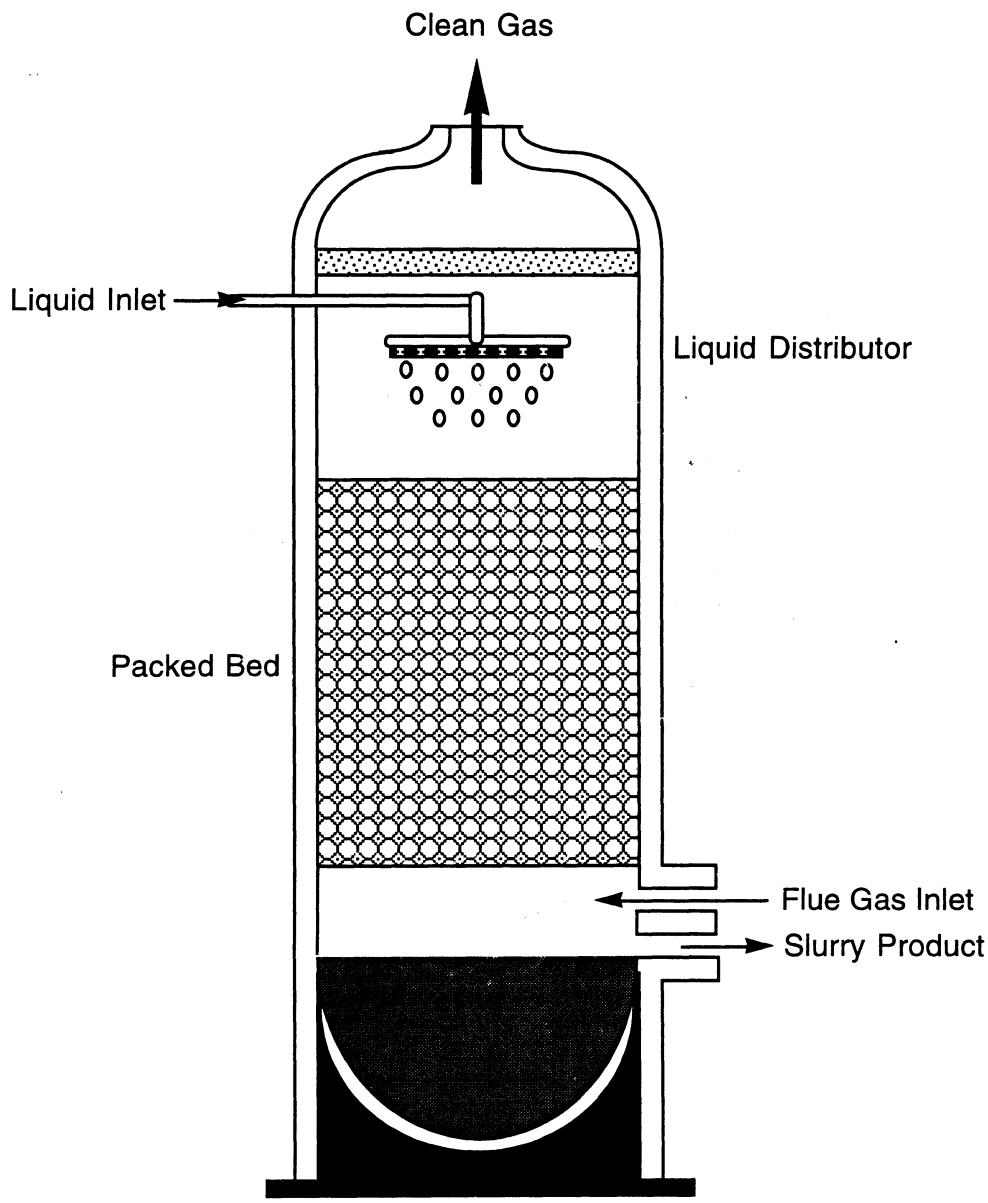

Figure 2-1: Spray Scrubber in Wet FGD System.

In the lime/limestone process (Figure 2-2), a slurry of calcium hydroxide or calcium carbonate is contacted with flue gas to remove sulfur dioxide. Calcium sulfite and calcium sulfate are formed as a result of the chemical reaction between sulfur dioxide and lime or limestone. These products are slightly soluble in water, and they ultimately precipitate. The slurry product drains from the scrubber into a holding tank in which dissolution of lime/limestone and precipitation of calcium sulfite/sulfate take place. Fresh lime or limestone and make-up water are continuously added to the tank. A large portion of the slurry is recirculated to the scrubber, and the remainder is withdrawn and treated to reduce water pollution before it is disposed.

In the sodium-alkali processes, sulfur dioxide from flue gas is absorbed by a solution of sodium hydroxide, sodium carbonate or sodium bicarbonate. In this case, sulfur dioxide chemically reacts with the salts to form sodium sulfite and sodium bisulfite, which are soluble in water and remain dissolved in the solution. Some of the sodium sulfite reacts with oxygen in the flue gas to produce sodium sulfate. The salt products are then removed as liquid waste. The sodium-alkali processes are different from the other two types of processes in that a lot of liquid waste containing salts are generated instead of solid wastes.

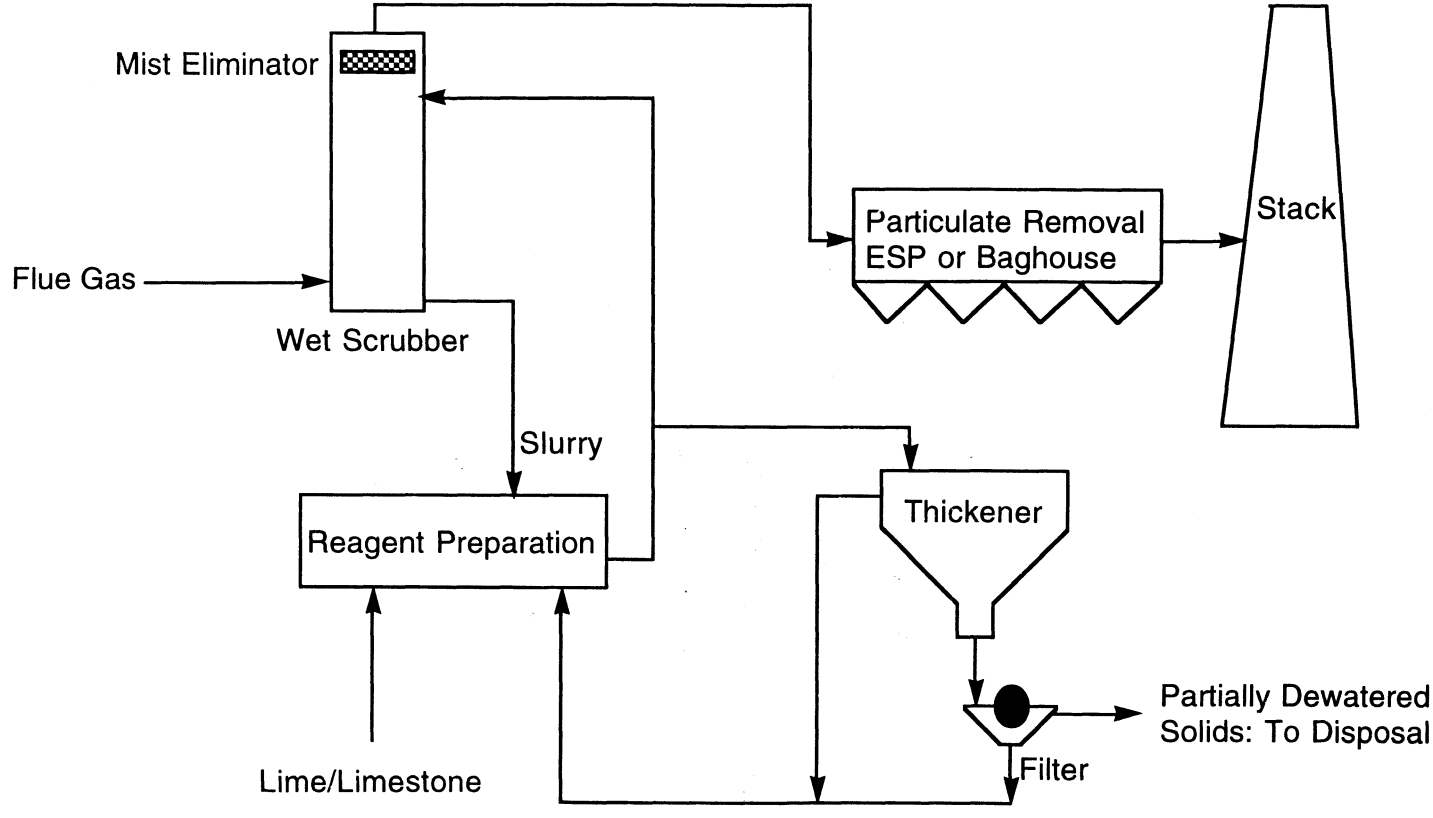

Figure 2-2: Wet Lime/Limestone Flue Gas Desulfurization Process.

In the dual-alkali processes, sulfur dioxide is absorbed by a solution of sodium-based alkali that contains sodium carbonate, sodium bicarbonate, sodium sulfite, and sodium hydroxide to form sodium sulfite, sodium bisulfite, and sodium sulfate. The solution is reacted with lime to regenerate the sodium-based alkali for recycling to the scrubber. Calcium sulfite and calcium sulfate which are generated during this step precipitate from the solution, and they are treated for disposal. The dual-alkali processes produce solid waste which is easily disposed of, as opposed to liquid waste which require complicated waste water treatment. Other wet FGD processes use saltwater alone or in combination with some chemical additives. These types of scrubbing techniques produce a waste stream resembling natural seawater, and this waste product can be released into the ocean. In this process, seawater is introduced into a packed tower, where it is countercurrently contacted with flue gas. Upon leaving the tower, the gas flows through a mist eliminator to remove the entrained water and the acid gases. The acidic seawater containing the absorbed SO_2 flows through a water treatment facility. The acidic seawater is neutralized by the addition of fresh seawater. Air is introduced to the neutralized seawater to oxidize SO_2 to SO_4^{2-}. Before being discharged to the ocean, the resulting solution is analyzed for pH and oxygen to make sure it is of sufficient quality.

Although wet FGD systems achieve high sulfur oxides removal ($> 90\%$), they have not been considered very attractive recently because of their intrinsic

disadvantages. They require expensive alloys that protect against corrosion. In general, they have high capital and operating costs compared to dry FGD systems. Because of the slurry waste, wet scrubbers require additional complicated steps and equipment for product disposal and waste water treatment.

2.1.2 Dry Flue Gas Desulfurization Processes

Very recently, industrial coal-fired boiler users have turned to the consideration of dry scrubbing techniques because of the many potential advantages these systems offer over conventional wet scrubbing methods. Since dry FGD systems produce dry waste products, they do not require any complicated steps for waste disposal and they do not involve any waste water treatment as opposed to wet systems. Because of their simplicity and flexibility of operation, maintenance and personnel requirements are reduced. Process design and control of dry FGD systems is much simpler than that of wet scrubbing systems. Dry processes use more additives than wet processes for similar SO_2 removal rates because they have shorter gas to liquid contact times.

Dry FGD methods are classified by the temperature of the flue gas at the point of contact with the dry sorbent. They include in-furnace injection where the flue gas temperature is between 1800 and 2200 °F, economizer zone injection where the flue gas temperature ranges between 800 and 1100 °F, and post air preheater injection where the flue gas temperature is below 350 °F with enough water added to get significant SO_2 removal.

The in-furnace scrubbing process which operates at about 2000 °F includes the calcination or thermal decomposition of $CaCO_3$ or $Ca(OH)_2$ to active CaO and the reaction of SO_2 with CaO according to the following scheme:

a. Thermal Decomposition of Raw Sorbent

$$CaCO_3\ (s) \rightarrow CaO\ (s) + CO_2\ (g) \qquad (2\text{-}1)$$

$$Ca(OH)_2\ (s) \rightarrow CaO\ (s) + H_2O\ (g) \qquad (2\text{-}2)$$

b. Sulfation Reaction

$$CaO\ (s) + SO_2\ (g) + 1/2\ O_2\ (g) \rightarrow CaSO_4\ (s) \qquad (2\text{-}3)$$

Typical sorbent utilizations for these systems range from 25 to 35 %. The U.S. Environmental Protection Agency (EPA) and later the U.S. Department of Energy have sponsored the development and operation of a full-scale demonstration in-furnace injection facility, the LIMB (Limestone Injection Multistage Burner) process, since 1981. This process has achieved an average SO_2 removal efficiency of 65% using commercial hydrated lime at a Ca:S addition ratio of 2.

The economizer zone injection process which operates at about 1000 °F involves the direct reaction between SO_2 and the sorbent according to the following:

$$Ca(OH)_2\ (s) + SO_2\ (g) \rightarrow CaSO_3\ (s) + H_2O\ (g) \qquad (2\text{-}4)$$

This process shows higher SO_2 removal rates compared to the in-furnace injection process. At a temperature below 900 °F and in the absence of water, the SO_2 removal rate sharply decreased and became negligible at temperatures

below 500 °F.

In the post air preheater injection process which operates at temperatures below 350 °F, lime or limestone and water in the form of vapor or liquid are injected into the flue gas. The dry scrubbing methods can be classified into two types depending on the amount of water introduced in the system : dry/dry and wet/dry systems. In dry/dry processes, a few monolayers of water are physically adsorbed onto the sorbent surface. In wet/dry systems, however, a bulk phase of liquid water is present in the reaction *medium*. Examples of the later process include slurry spray drying and the Limestone Emission Control (LEC) described by Prudich et al. [1988].

In spray dryers, Figure 2-3, the flue gas is contacted with a finely atomized spray of alkaline slurry or solution. The sulfur oxides in the flue gas are absorbed by the alkali slurry or solution. The hot gas dries the reaction products and unreacted additives. These solid products, along with the fly ash, are carried out from the dryer to a particulate removal device such as a fabric filter or an electrostatic precipitator. Slaked lime or soda ash are used as additives because limestone is not sufficiently reactive for many dry FGD processes. No equipment for dewatering is needed, and the reaction products and ash are removed as a dry material. Some of the dry solids-fly ash material collected by the fabric filter or precipitator can be recycled to the spray dryer, thus reducing additive consumption. For spray drying, significant sulfur oxides removal efficiencies (more than 90 %) can be achieved by using lime or

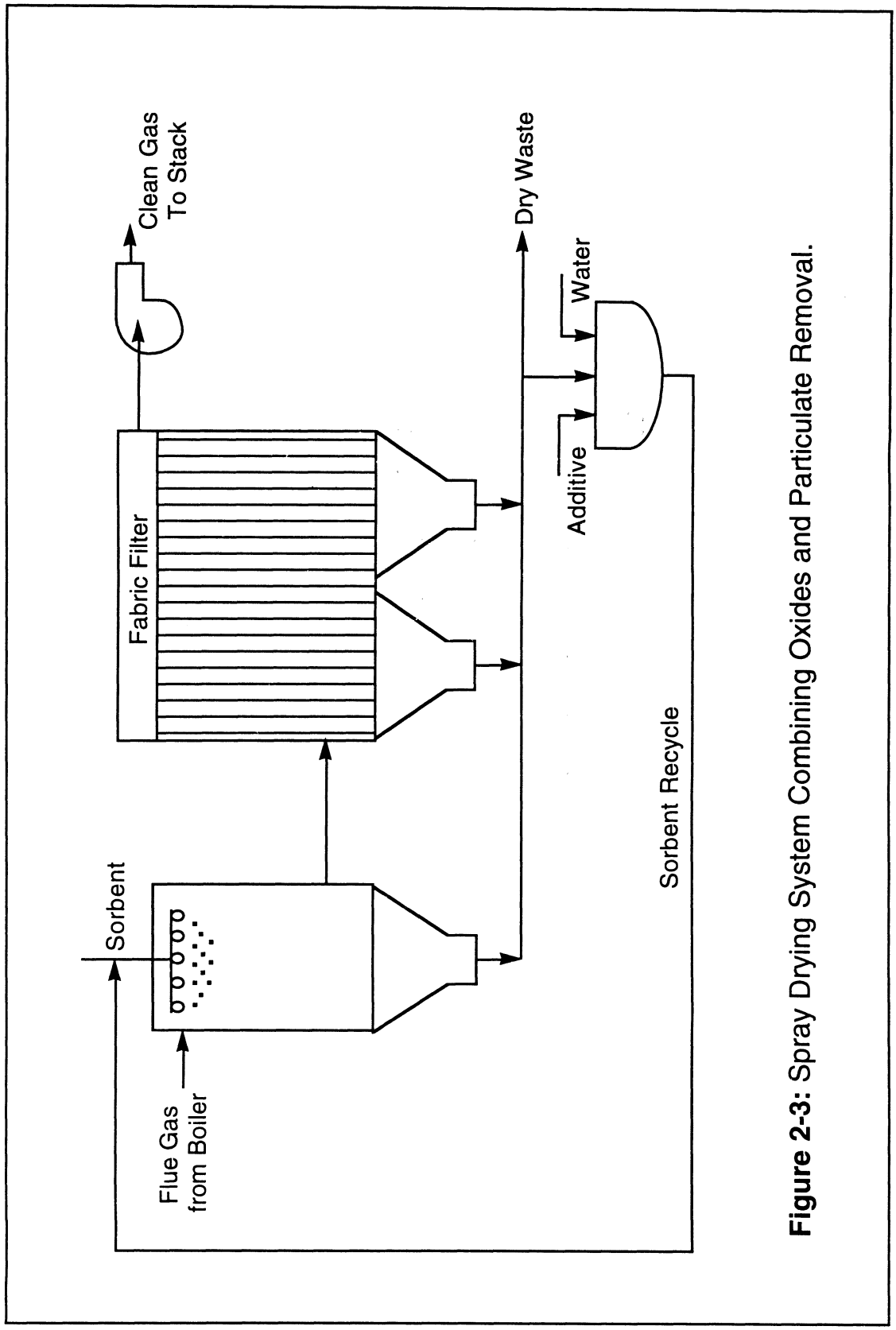

Figure 2-3: Spray Drying System Combining Oxides and Particulate Removal.

sodium-based sorbents and high reagent feed rates. Sodium-based reagents such as sodium hydroxide and sodium carbonate are more reactive than calcium-based sorbents such as lime or limestone.

The Limestone Emission Control (LEC) process is a novel scrubbing technique developed by Prudich et al. [1988]. A schematic diagram of the LEC system is shown in Figure 2-4. In this process, the flue gas passes through a spray chamber where it is humidified. The humidified gas enters the LEC reactor, which was basically a fixed bed of granular limestone. Water could be introduced into the system by humidifying the flue gas, pre-wetting the limestone bed or spraying over the sorbent bed. Upon exiting the reactor, the gas was analyzed for SO_2 concentration. A removable limestone bed is used in the LEC process to allow for sorbent regeneration while another bed is in operation. Regeneration of used limestone is done through an attritor mill that removes the sulfite/sulfate product layers. The reactor bed is designed in a way that accommodates various limestone depths. Experimental tests performed on the LEC unit were done at a temperature range of 170 to 300 °F. At the temperature range used in the LEC process and in the presence of a bulk water phase, the following reaction scheme is believed to take place:

a. Ionic Dissociation of SO_2 in Water

$$SO_2\,(g) + H_2O\,(l) \rightleftarrows H^+ + HSO_3^- \qquad (2\text{-}5)$$

$$HSO_3^- \rightleftarrows H^+ + SO_3^{2-} \qquad (2\text{-}6)$$

b. Dissolution of Limestone

$$CaCO_3 \rightleftarrows Ca^{2+} + CO_3^{2-} \qquad (2\text{-}7)$$

c. Reaction of Dissolved Sorbent with Dissolved SO_2

$$Ca^{2+} + SO_3^{2-} \rightleftarrows CaSO_3 \qquad (2\text{-}8)$$

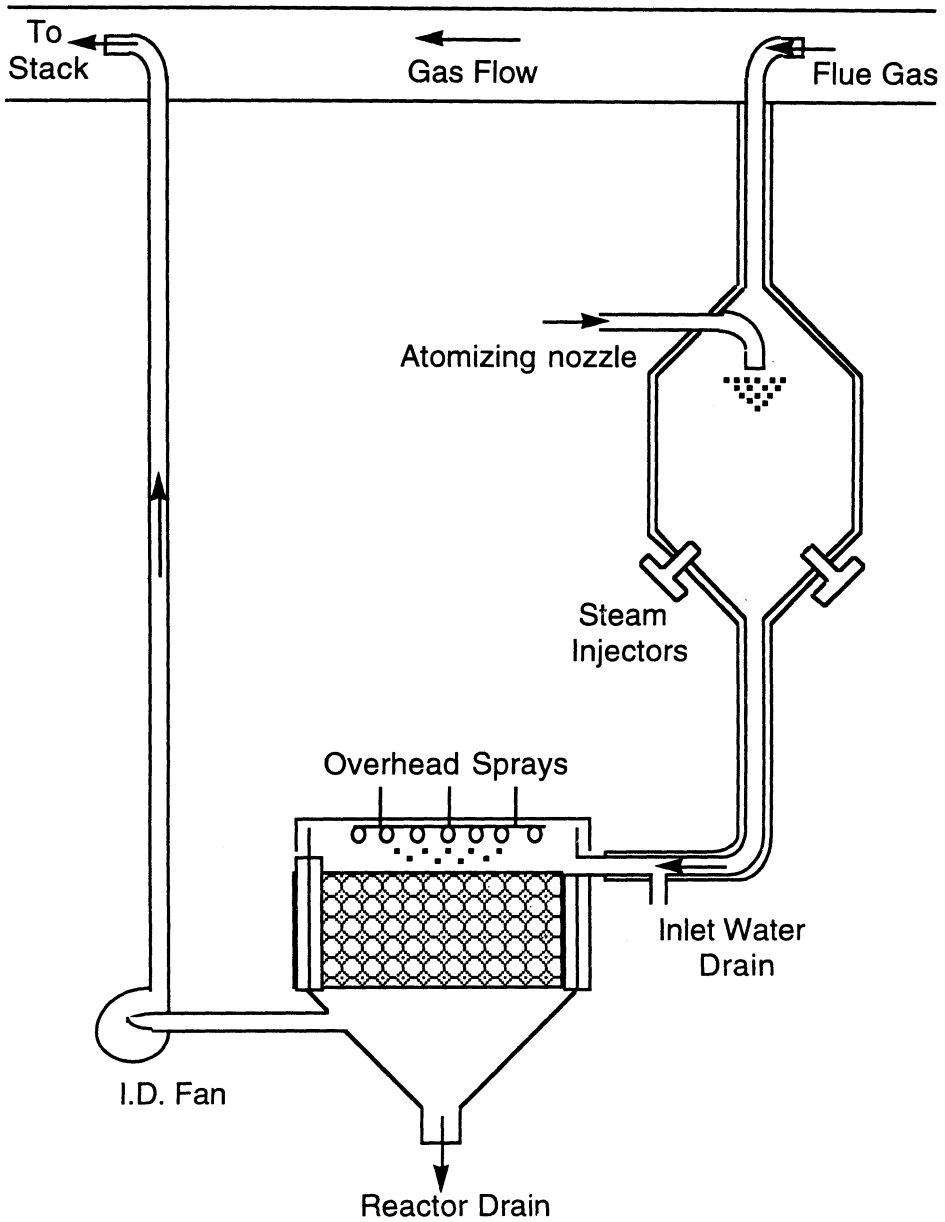

Figure 2-4: Schematic Diagram of the LEC Process.

The pilot plant results showed that the LEC process was capable of achieving 99% SO_2 removal, with an average percent removal of greater than 90% over extended operating periods. The LEC system was shown to have a significant economic advantage over many conventional wet and dry scrubbing systems.

In addition to the LEC fixed-bed configuration, a moving-bed reactor has been adopted for the LEC process. In this case, as shown in Figure 2-5, the flue gas is drawn horizontally across a limestone bed which moves vertically downward. Experimental tests on this unit showed SO_2 removal efficiencies (i.e. more than 90%) comparable to those achieved using the LEC fixed bed unit.

2.2 Sorbents and Additives

2.2.1 Sorbent Forms

Sorbents used in FGD systems include calcium-based and sodium-based compounds. Commercial, as well as lab-produced, hydrated limes have been used in the low temperature regime. Low temperature desulfurization studies done by Yoon et al. [1986] using high BET surface area (i.e. 10-50 m^2/g) calcitic hydrates prepared in their laboratory showed a very strong correlation between sorbent conversion and hydrate BET surface area. Their results indicated that higher calcium utilization was achieved with the higher surface area hydrate sample.

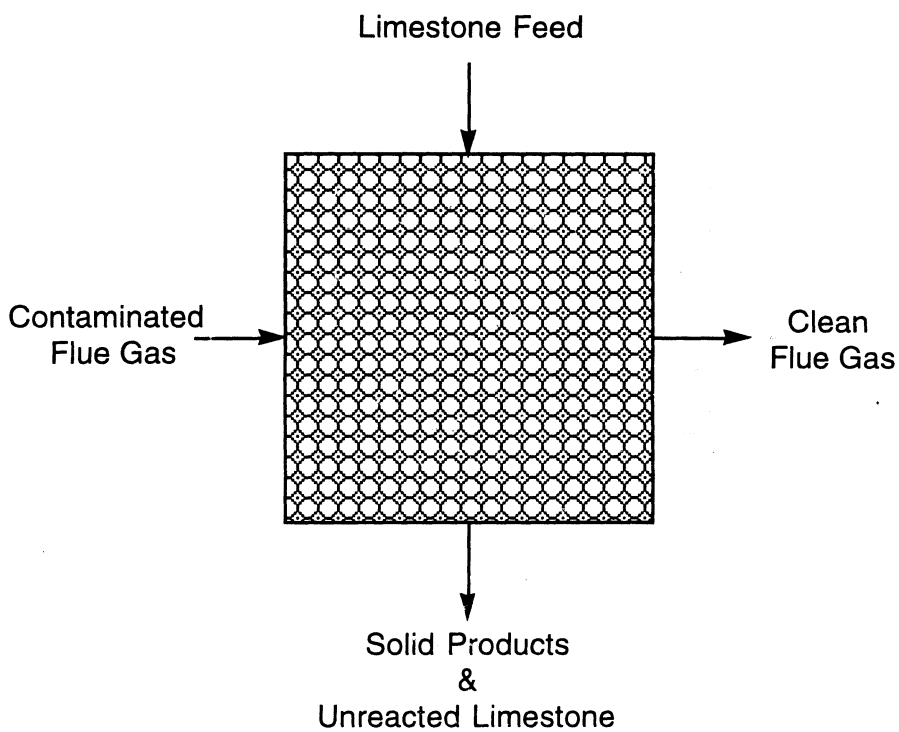

Figure 2-5: Moving Bed Configuration of the LEC Process.

Over a range of surface areas between 10 and 50 m^2/g, the percent calcium utilization increased almost proportionally from 12 to 45% as shown in Figure 2-6. Other low temperature studies performed by Borgwardt and Bruce [1986] showed similar behavior. Hydrated limes evaluated by Jorgensen et al. [1987] over a temperature range between 130 and 166 °F showed an exponential increase in conversion with gas relative humidity.

Raw limestones have also been used to study SO_2 capture reactivity under dry conditions (i.e. when the water has evaporated from the particle surface). Klingspor et al. [1983] performed a kinetic study of the reaction between SO_2 and a technical quality limestone consisting of 85% $CaCO_3$. Their results indicated that the SO_2 capture rate followed a power function with respect to the flue gas relative humidity. This was attributed to the formation of several monolayers (i.e. more than 2.5 monolayers which corresponds to more than 70 % relative humidity) of water vapor adsorbed on the limestone surface. Their work also confirmed the expected strong effect of limestone BET surface area on the SO_2 removal rate.

Sodium-based sorbents that have been tested for SO_2 removal under dry conditions included sodium hydroxide (NaOH), sodium carbonate (Na_2CO_3) and sodium bicarbonate ($NaHCO_3$). Sodium hydroxide and sodium carbonate react with SO_2 to form sodium sulfite/sulfate.

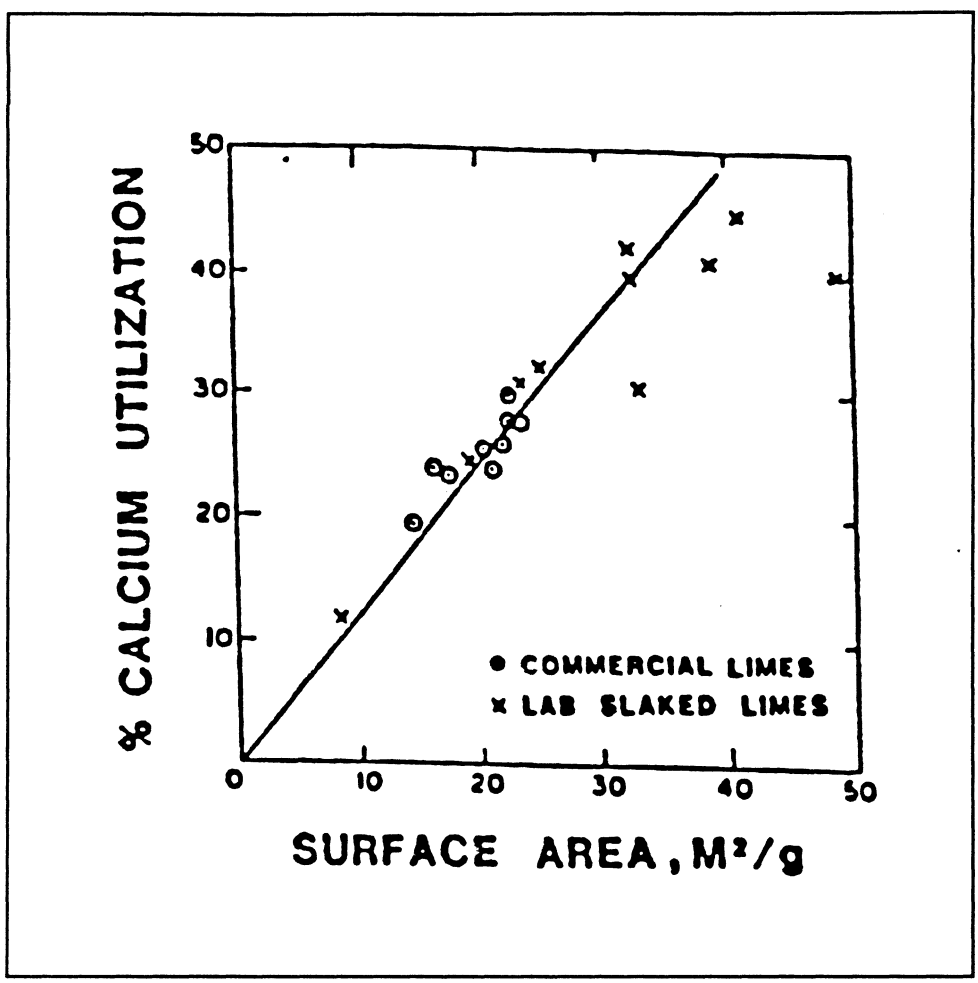

Figure 2-6: Effect of Sorbent Surface Area on Low Temperature SO_2 Capture Performance. 150 °F, 60 % Relative Humidity, 1000 ppm SO_2, 60 minutes [Yoon et al., 1986].

These two compounds have been used as co-sorptive additives to enhance the reactivity of hydrated lime or calcium carbonate. Sodium bicarbonate, $NaHCO_3$, has been extensively studied at temperatures in the range of 300 to 500 °F (Davis, 1982). At this temperature range, $NaHCO_3$ thermally decomposes to anhydrous soda ash which reacts with SO_2 to form Na_2SO_3/Na_2SO_4. Jorgensen et al. [1987] performed bench-scale kinetic studies on $NaHCO_3$ at lower temperatures (i.e. ~ 150 °F), where thermal decomposition effects are believed to be negligible. They observed a steady SO_2 removal rate after a few minutes of sorbent exposure. They did not encounter any sorbent blinding during the course of the reaction. This was attributed to the formation of CO_2 during the reaction with SO_2, creating sufficient fresh active sorbent surface for the reaction to proceed. Their test results using sodium carbonate, Na_2CO_3, as the sorbent showed lower SO_2 removal rates than those observed when using $NaHCO_3$ even at high gas relative humidities. This indicated that the reaction between $NaHCO_3$ and SO_2 proceeds without the formation of an intermediate Na_2CO_3. Another result of their study was that the gas relative humidity was less critical for SO_2 removal by these sodium-based compounds than by calcium hydroxide.

2.2.2 Chemical Additives

The importance of using additives to promote sorbent reactivity and to improve SO_2 removal is suggested by several chemical and physical aspects. By incorporating an additive during hydration, the sorbent's physical properties

such as surface area and porosity can be increased, which would improve sorbent utilization. Some additives have the potential of enhancing the basicity of the sorbent, which would promote the reaction between SO_2 and sorbent. Since the presence of water is essential to the SO_2/sorbent reaction, some additives may help retain enough moisture on the sorbent surface so that the rate and degree of reaction would be enhanced.

The types of additives investigated for promoting sorbent reactivity include deliquescent inorganic salts, organic compounds and oxidation catalysts.

In general, inorganic deliquescents were found to be more effective than organic compounds. The inorganic salts include calcium chloride ($CaCl_2$), sodium chloride and bromide (NaCl and NaBr), sodium hydroxide (NaOH), sodium nitrate ($NaNO_3$), and sodium carbonate (Na_2CO_3). These additives could be mixed in a dry procedure or by the procedure of water dissolution followed by drying. All of these additives were found to shift the ultimate SO_2 absorption [Jorgensen et al., 1987]. The most notable result was a significant increase in SO_2 removal using $CaCl_2$ as an additive. Relating to water adsorption on the sorbent particles, $CaCl_2$ has a high water affinity (i.e. hygroscopic salt). This would increase the water adsorbed by the particles, reduce the SO_2 ash blinding effect, and result in more SO_2 absorption. Yoon et al. [1986] evaluated several additives which included co-sorptive compounds (such as NaOH, Na_2CO_3, $NaNO_3$, NaCl and Na_2SO_3) and non-cosorptive compounds (such as

$CaCl_2$, KCl, $FeCl_3$, and $MgCl_2$). Their results showed that both types of additives were highly effective in promoting SO_2 removal and hydrated lime utilization. According to these results, calcium utilization could be improved by 50 to 100% with the use of additives.

Organic compounds such as adipic acid, glycerin, and sugar have also been evaluated by Yoon et al. [1986] at dry scrubbing conditions. Both adipic acid and sugar showed significant reductions in sorbent utilization ranging from 15 to 25%. Glycerin, on the other hand, showed a slight increase (i.e. about 10%) in calcium utilization. For wet FGD systems, organic acid and buffer additives such as adipic acid, citric acid, and sodium formate helped promoting the SO_2 removal by about 15%.

2.3 Modeling of Noncatalytic Gas-Solid Reactions

In many gas-solid reactions, like the one between SO_2 and calcium hydroxide or limestone, solid products are formed. For the case of SO_2 and limestone (i.e. $CaCO_3$ is the active portion) in the presence of water, the following reaction scheme is proposed:

$$SO_2\,(g) + CaCO_3\,(s) \rightarrow CO_2\,(g) + \{CaSO_3\,(s),\ CaSO_3.2H_2O\,(s),\ CaSO_4\,(s),\ CaSO_4.1/2H_2O\,(s),\ CaSO_4.2H_2O\,(s)\} \quad (2\text{-}9)$$

This can be represented more simply by:

$$SO_2\,(g) + CaCO_3\,(s) \rightarrow CO_2\,(g) + \text{products} \quad (2\text{-}10)$$

or in a general form by:

$$A\,(g) + bB\,(s) \rightarrow cC\,(g) + dD\,(s) \quad (2\text{-}11)$$

The overall volume of solid may increase or decrease depending on the relative density of the solid product compared with that of the solid reactant. In general, the change is very small and the overall size may be regarded as constant (which is true in our case, ρ_c = 4.230 and ρ_p = 4.647 lbmole of Ca^{2+}/ft^3). For this case, two simple idealized models (the continuous-reaction-model and the unreacted-core-model) have been used to develop kinetic equations. The continuous-reaction-model, as shown in Figure 2-7, assumes that the gas reacts continuously throughout the particles with different rates at different locations within the solid reactant. The unreacted-core-model, as shown in Figure 2-8, assumes that the gas reacts first at the outer surface of the solid, and then that the reaction front moves into the particle. In this case, a completely converted outer layer and an unreacted core of solid material exist at any time during the reaction. As the reaction progresses, the unreacted core gradually shrinks in size until the entire sorbent becomes unreactive. The unreacted-core-model was shown to fit a wide range of situations better than the continuous-reaction-model. Klingspor et al. [1983] were able to fit their kinetic data of the low temperature dry SO_2/limestone reaction using a chemical reaction control unreacted-core-model. The continuous-reaction-model proved to fit experimental data better than the unreacted-core-model for slow reactions in a very porous solid such as the slow poisoning of a catalyst pellet [Levenspiel, 1978].

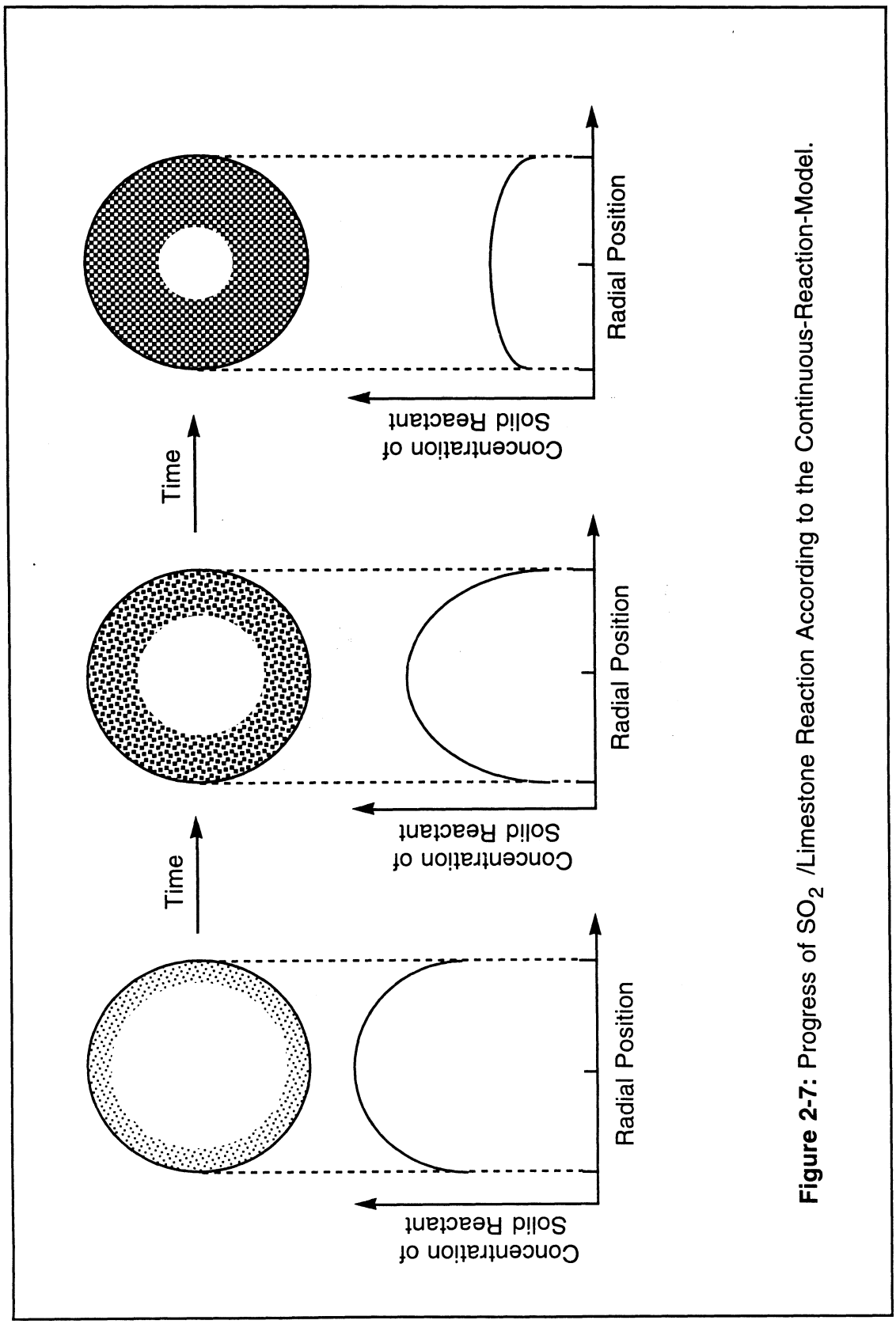

Figure 2-7: Progress of SO_2 /Limestone Reaction According to the Continuous-Reaction-Model.

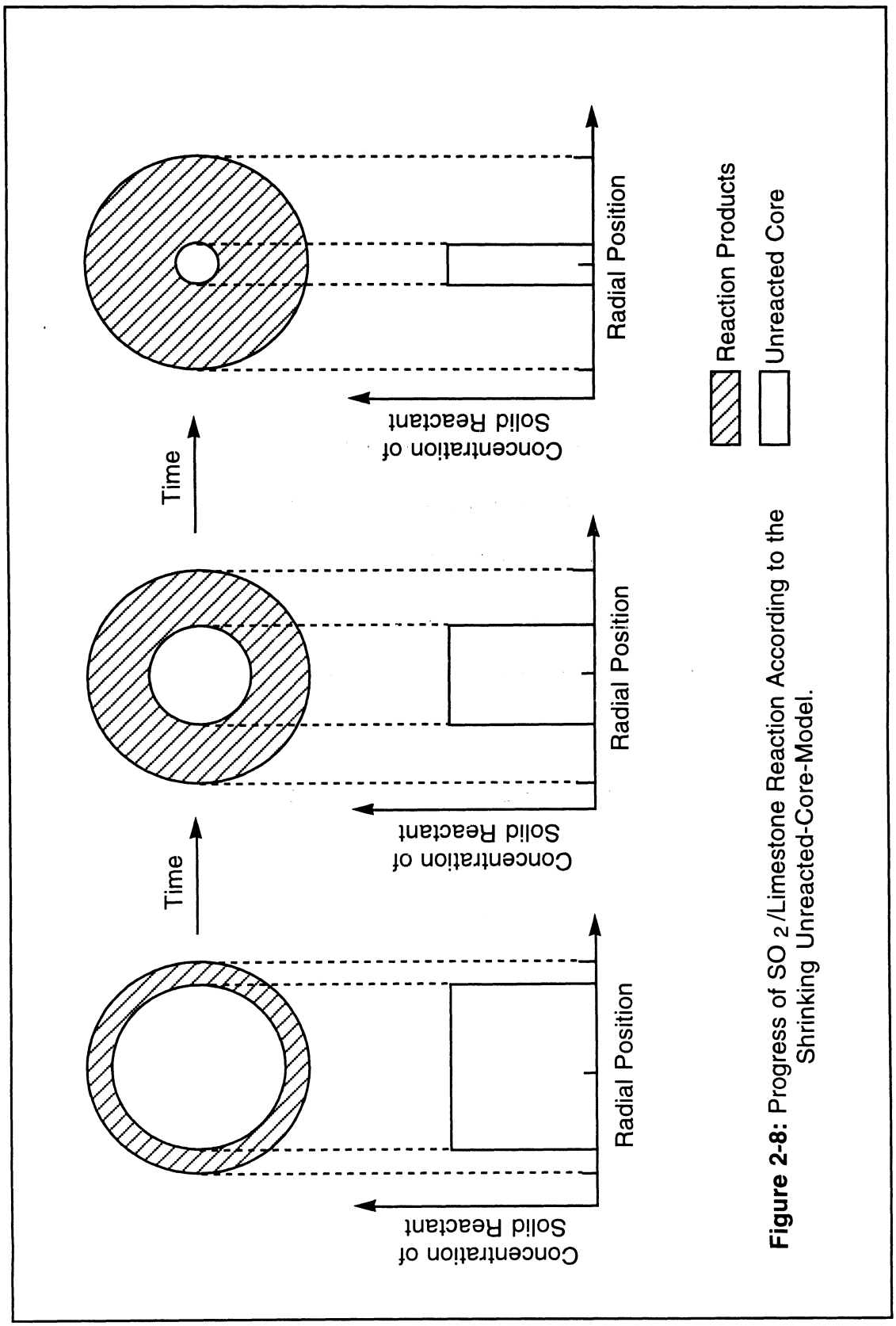

Figure 2-8: Progress of SO_2/Limestone Reaction According to the Shrinking Unreacted-Core-Model.

Since the shrinking unreacted-core-model seems to represent the case studied more realistically, its kinetic equations will be developed as follows:

Assumptions used in the unreacted-core-model are summarized in the following five steps:

a. Diffusion of the gaseous reactant (i.e. SO_2) through the gaseous film surrounding the solid particles (i.e. limestone).
b. Diffusion of gaseous reactant through the product layer to the surface of the unreacted core (i.e. to the reaction front).
c. Chemical reaction of gaseous reactant with the solid.
d. Diffusion of the gaseous products through the product layer back to the outer surface of the solid.
e. Diffusion of gaseous products through the bulk gas surrounding the solid particles.

The above five steps are schematically represented in Figure 2-9. These steps occur simultaneously during the reaction, and the model is considered a resistance-in-series model. Depending on the experimental conditions, one of these steps could be made the major resistance, and therefore the rate-controlling step. For example, by using small particle sizes, small sample size, and high gas velocity, all transport resistances are eliminated other than those associated with the reaction at individual particle surfaces.

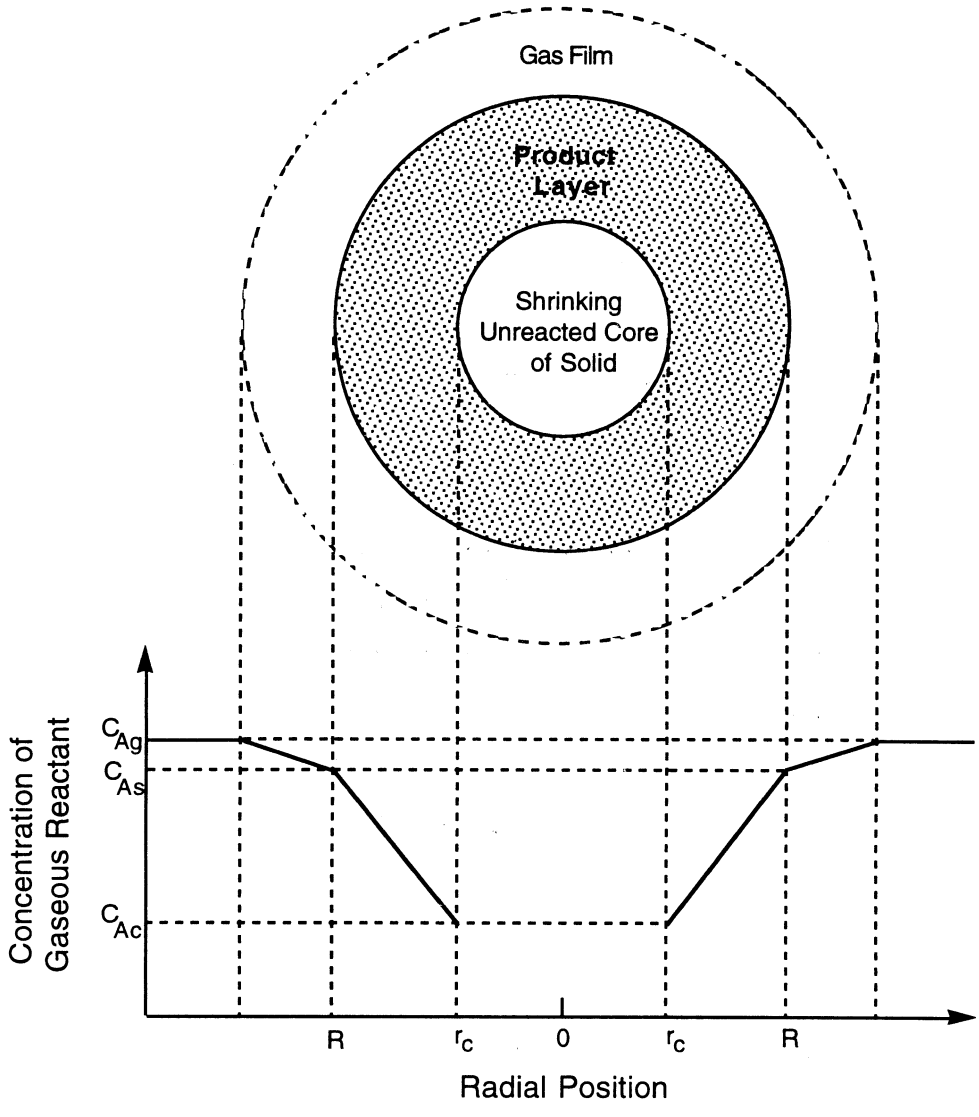

Figure 2-9: Various Steps Occurring in a Shrinking Unreacted-Core-Model.

2.3.1 Gas Film Diffusion Control

If the major resistance occurs in the gas film surrounding the solid particles, the overall process will be gas film diffusion controlled. In this case, the concentration profile of the reacting gas will be as shown in Figure 2-10 (A). The reaction rate can be written as follows:

$$-\frac{1}{S_{ex}}\frac{dN_B}{dt}=-\frac{b}{S_{ex}}\frac{dN_A}{dt}=bk_g(C_{Ag}-C_{As}) \qquad (2\text{-}12)$$

Where: N_B: Amount of solid B (moles).

N_A: Amount of gas A (moles).

t: Time.

S_{ex}: Available external surface area of solid particles ($4\pi R^2$, R: particle radius).

b: Stoichiometric coefficient as shown in Equation (4-11).

k_g: Gas phase mass transfer coefficient.

C_{Ag}: Concentration of reactant A in the bulk gas.

C_{As}: Concentration of reactant A at particle surface (i.e. in this case $C_{As}=0$).

The amount of solid B can be expressed in terms of the molar density, ρ_B, and the volume of the particle, V, as:

$$N_B=\rho_B V=\frac{4\pi}{3}\rho_B r_C^3 \qquad (2\text{-}13)$$

Where: r_C: Radius of unreacted core.

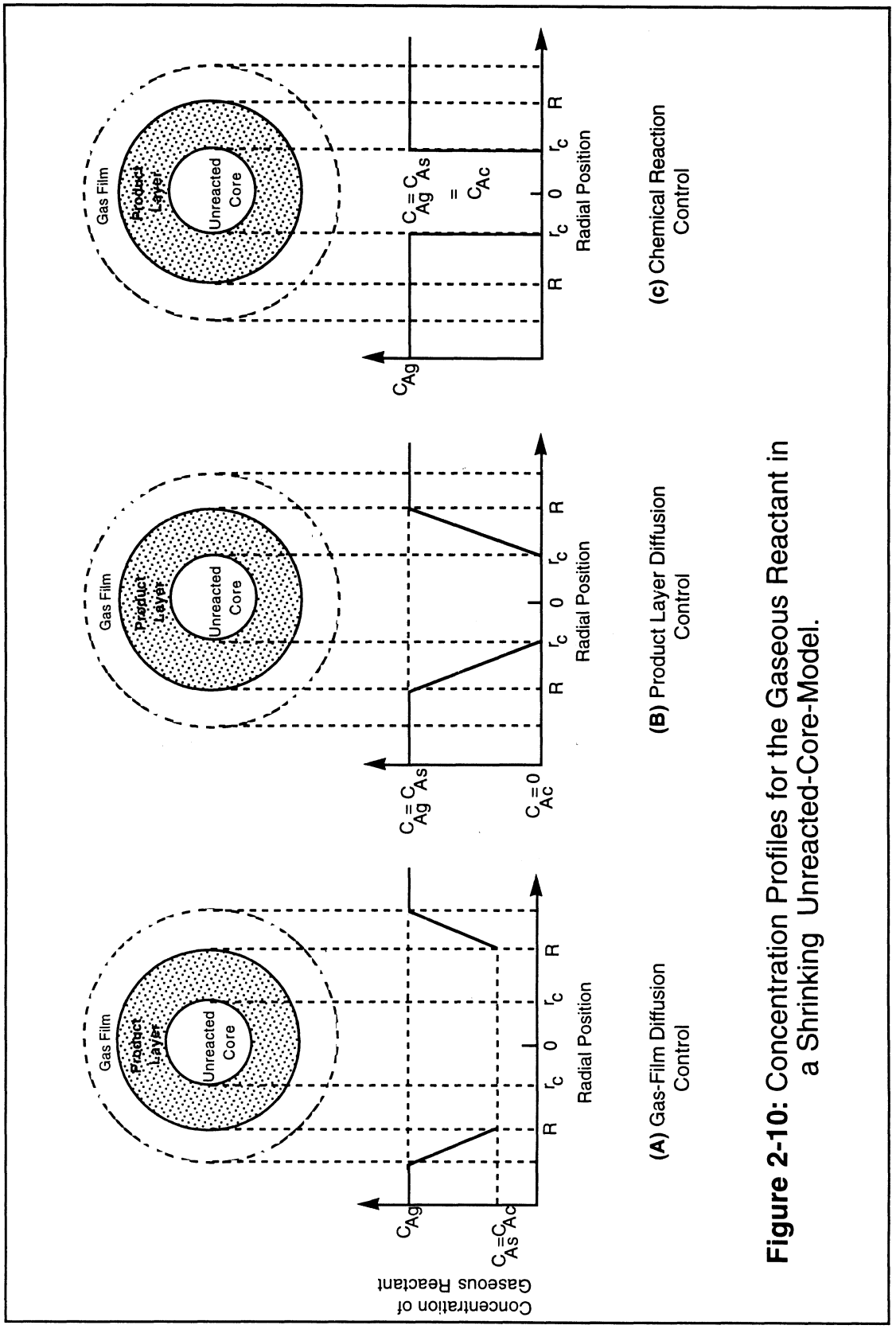

Figure 2-10: Concentration Profiles for the Gaseous Reactant in a Shrinking Unreacted-Core-Model.

As the reaction progresses, the unreacted core of the solid shrinks in size. The rate of disappearance of solid reactant can be related to the rate of shrinkage of the unreacted core by the following equation:

$$-\frac{1}{4\pi R^2}dN_B=-\frac{1}{4\pi R^2}\rho_B dV=-\frac{1}{4\pi R^2}d\left(\frac{4\pi}{3}r_c^3\right)$$

$$=-\rho_B\left(\frac{r_C}{R}\right)^2\frac{dr_C}{dt}=bk_gC_{Ag} \qquad (2\text{-}14)$$

By integrating Equation (2-14), the radius of the unreacted core can be given as a function of time by:

$$1-\left(\frac{r_C}{R}\right)^3=\frac{3bk_gC_{Ag}}{\rho_B R}t \qquad (2\text{-}15)$$

The fractional conversion of the solid reactant is given by:

$$x_B=\frac{\text{Amount of B reacted}}{\text{Total initial amount of B}}$$

$$=\frac{\rho_B(\text{Volume of reacted B})}{\rho_B(\text{Total volume of particle})} \qquad (2\text{-}16)$$

or:

$$x_B=\frac{\frac{4}{3}\pi R^3-\frac{4}{3}\pi r_c^3}{\frac{4}{3}\pi R^3}=1-\left(\frac{r_c}{R}\right)^3 \qquad (2\text{-}17)$$

Combining Equations (2-15) and (2-17), the fractional conversion of the solid reactant as a function of time for the case of gas film diffusion control is given by:

$$X_B = \left(\frac{3bk_gC_{Ag}}{\rho_B R}\right)t \qquad (2\text{-}18)$$

In this case, through a linear plot of the experimental conversion versus time data, the mass transfer coefficient (k_g) can be obtained from the slope of the line.

2.3.2 Product Layer Diffusion Control

If the overall rate of reaction is controlled by the resistance to diffusion through the product layer, the concentration profile for the gas and solid reactants will be represented by Figure 2-10 (B). The reaction rate is given by:

$$-\frac{dN_A}{dt} = -\frac{1}{b}\frac{dN_B}{dt} = 4\pi r^2 D\frac{dC_A}{dr} = \text{Constant} \qquad (2\text{-}19)$$

Where: r: Any radius in the product layer.

D: Diffusion coefficient.

C_A: Concentration of gas reactant.

By integrating this equation from $r = R$ to $r = r_C$ and substituting for N_B as given by Equation (2-13), we get:

$$-\rho_B\left(\frac{1}{r_C} - \frac{1}{R}\right)r_C^2\frac{dr_C}{dt} = bDC_{Ag} \qquad (2\text{-}20)$$

A second integration with respect to time from t=0 to t=t gives the expression for the change of the unreacted core radius with time:

$$1-3\left(\frac{r_C}{R}\right)^2+2\left(\frac{r_C}{R}\right)^3=\frac{6bDC_{Ag}}{\rho_B R^2}t \qquad (2\text{-}21)$$

In terms of fractional conversion, X_B, Equation (2-21) is equivalent to the following equation:

$$1-3(1-x_B)^{\frac{2}{3}}+2(1-X_B)=\frac{6bDC_{Ag}}{\rho_B R^2}t \qquad (2\text{-}22)$$

Similarly, by plotting the left hand side of Equation (2-22) versus t, a straight line should be expected. The diffusion coefficient, D, is obtained from the slope of the line.

2.3.3 Chemical Reaction Control

If the resistance of the gas film diffusion and the product layer diffusion are negligible, the rate of reaction will be controlled by the chemical reaction at the surface of the unreacted core. In this case, the concentration profiles for the gas and the solid are represented by Figure 2-10 (C). The rate of disappearance of solid is given by:

$$-\frac{dN_B}{dt}=-4\pi\rho_B r_C^2\frac{dr_C}{dt}=4\pi r_C^2 bk_S C_{Ag} \qquad (2\text{-}23)$$

Where: k_s: Reaction rate constant

Integration of this equation with time from 0 to t gives the expression for the decrease in radius of the unreacted core as a function of time:

$$1-\frac{r_c}{R}=\frac{bk_sC_{Ag}}{\rho_B R}t \qquad (2\text{-}24)$$

Substituting for r_c/R in terms of fractional conversion, Equation (2-24) becomes:

$$1-(1-X_B)^{\frac{1}{3}}=\frac{bk_sC_{Ag}}{\rho_B R}t \qquad (2\text{-}25)$$

Using Equation (2-17), the radius of the unreacted core could be expressed as:

$$r_c=R(1-X_B)^{\frac{1}{3}} \qquad (2\text{-}26)$$

Combining Equations (2-23) and (2-26), the reaction rate in terms of fractional conversion is given by the following equation:

$$\Re=-\frac{dN_B}{dt}=4\pi bR^2k_sC_{Ag}(1-X_B)^{\frac{2}{3}} \qquad (2\text{-}27)$$

Where:

$\Re$: Reaction rate

The kinetic model developed above attributed a first-order dependency to the gas reactant on the reaction rate. Other empirical kinetic models reported in the literature used other forms of gas reactant dependency on the reaction rate along with a shrinking unreacted-core-model. Irabien et al. [1990] performed a low temperature kinetic study on the $SO_2/Ca(OH)_2$ reaction using a laboratory-

scale fixed-bed reactor. Through differential analysis of their experimental data, they were able to fit their results using a shrinking-core-model with a hyperbolic expression for the influence of gas concentration on the reaction rate. Their reaction rate equation is given by the following:

$$\Re = \frac{k\epsilon C_A}{1 - k_A C_A}\left(1 - \frac{X_B}{X_M}\right)^{\frac{2}{3}} \qquad (2\text{-}28)$$

Where: k: Kinetic constant(min^{-1})

ϵ: Porosity of the bed

k_A: Adsorption parameter (l/mole)

C_A: SO_2 concentration (mole/l)

X_B: Solid conversion

X_M: Maximum solid conversion

2.4 Resistance-in-Series Kinetic Model

The resistance-in-series model has been used by several researchers in wet and dry scrubbing for modeling the reaction between SO_2 and lime/limestone. Uchida et al. [1975] applied this mechanistic model for the absorption of SO_2 in a limestone slurry by assuming the gas-phase resistance to be negligible. Hariott and Kinzey [1986] considered gas and liquid phase resistances in modeling the dry capture of SO_2 by lime, neglecting the resistance to lime dissolution. Appell [1989] assumed gas-phase resistance control in modeling a fixed-bed Limestone Emission Control (LEC) process and considered evaporation and condensation of water. This model was extended by Visneski et al. [1990] to include liquid phase as well as solid dissolution

resistances. Other researchers have adopted this model usually neglecting one or more of the resistances according to the experimental conditions they have used. During the course of the reaction between SO_2 and limestone in the presence of water, the controlling mechanism may change from one resistance to another depending on the experimental conditions.

An extended version of the resistance-in-series model used by Visneski et al. [1990] was developed and it includes the following mass and heat transfer effects:

a. The diffusion of SO_2 from the bulk gas through the flue gas film surrounding the limestone particles. The rate of transport in this step is controlled by the resistance of the gas film surrounding the liquid film.
b. Dissolution of SO_2 through the liquid bulk and transfer of dissolved SO_2 to the reaction plane. The rate of transfer in this step is controlled by the resistance of the liquid film.
c. Dissolution of sorbent and transfer of the dissolved sorbent through the liquid bulk to the reaction plane.
d. Condensation of water vapor from the flue gas on the sorbent surface.
e. Drying of the sorbent particles.
f. Sorbent surface blinding caused by the deposition of reaction products (i.e. $CaSO_3/CaSO_4$)
g. Dry sorbent capture. This is used for the dry portion of the limestone bed (i.e. where no bulk of liquid water is present on the limestone surface) contacted by humidified gas.

A schematic representation of the various steps occurring in the SO_2 removal process is shown if Figure 2-11.

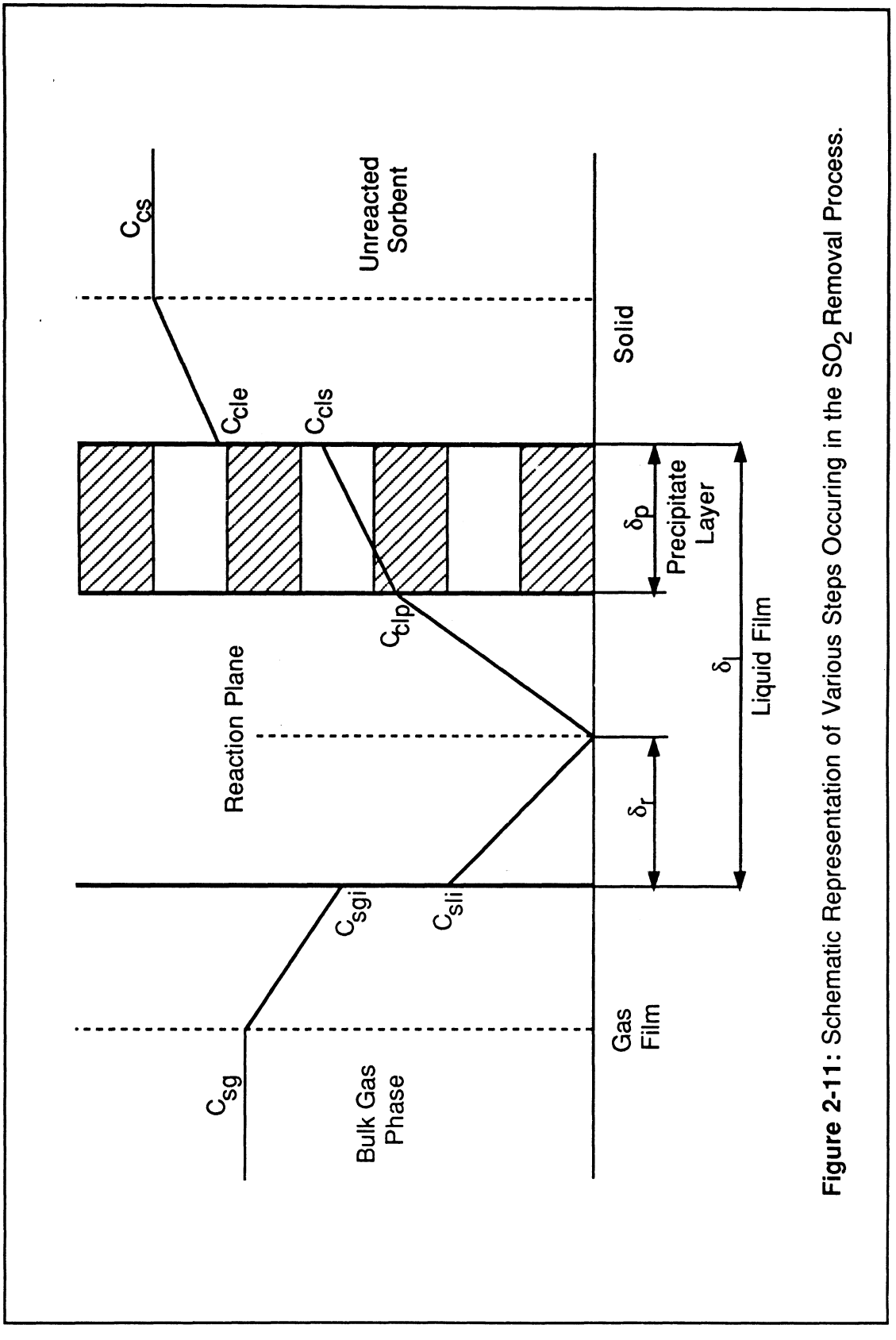

Figure 2-11: Schematic Representation of Various Steps Occuring in the SO_2 Removal Process.

2.4.1 Gas Phase Material Balances

2.4.1.1 SO_2 Material Balance

IN - OUT + GENERATION = ACCUMULATION

$$A_Z f_{sg}|_Z - A_Z f_{sg}|_{Z+\Delta Z} - A_Z \Delta Z g_s = A_Z \Delta Z \frac{\partial N_{sg}}{\partial t} \qquad (2\text{-}29)$$

Where: A_Z: Cross sectional area of bed perpendicular to Z direction (ft^2).

f_{sg}: Flux of SO_2 in gas phase in direction of gas flow (lbmole SO_2/ft^2 sec.).

g_s: Rate of transport of SO_2 from gas to solid phase (lbmole SO_2/ft^3 sec).

N_{sg}: Concentration of SO_2 in the reactor (lbmole SO_2/ft^3 of reactor).

Dividing by $A_Z \Delta Z$ and taking the limit as $\Delta Z \rightarrow 0$, Equation (2-29) becomes:

$$-\frac{\partial f_{sg}}{\partial Z} - g_s = \frac{\partial N_{sg}}{\partial t} \qquad (2\text{-}30)$$

In terms of concentration of SO_2 in the gas phase, C_{sg}, the flux, f_{sg}, and the concentration of SO_2 in the reactor, N_{sg}, are given as:

$$f_{sg} = U_g C_{sg} \qquad (2\text{-}31)$$

U_g: Superficial gas velocity (ft/sec).

$$N_{sg} = \epsilon_g C_{sg} \qquad (2\text{-}32)$$

ϵ_g: Fraction of bed occupied by the gas.

Taking the derivatives for f_{sg} with respect to Z and N_{sg} with respect to t and replacing them in Equation (2-30), we get:

$$U_g\frac{\partial C_{sg}}{\partial Z}+\epsilon_g\frac{\partial C_{sg}}{\partial t}=-C_{sg}\frac{\partial U_g}{\partial Z}-C_{sg}\frac{\partial \epsilon_g}{\partial t}-g_s \qquad (2\text{-}33)$$

Explicit expressions for U_g and $\partial U_g/\partial Z$ are required. These could be obtained through a material balance of the total gas, including non-condensables and water vapor:

$$-\frac{\partial f_g}{\partial Z}-g_W=\frac{\partial N_g}{\partial t} \qquad (2\text{-}34)$$

Where: f_g : Flux of total gas in direction of gas flow (lbmole/ft^2 sec).

N_g: Concentration of total gas (lbmole/ft^3 of reactor).

g_W: Rate of transport of water from gas phase to liquid phase (lbmole/sec ft^3 of reactor).

But, f_g and N_g can be expressed in terms of the gas temperature, T_g, and the system pressure, P, using the ideal gas law:

$$f_g=U_g\rho_g=U_g\frac{P}{RT_g} \qquad (2\text{-}35)$$

$$N_g=\epsilon_g\rho_g=\epsilon_g\frac{P}{RT_g} \qquad (2\text{-}36)$$

Taking the derivatives for f_g with respect to Z and N_g with respect to t and replacing these terms in Equation (2-34), we get:

$$\frac{\partial\left(\frac{U_g}{T_g}\right)}{\partial Z} = -g_w\frac{R}{P} - \frac{\partial\left(\frac{\epsilon_g}{T_g}\right)}{\partial t} \qquad (2\text{-}37)$$

or:

$$\frac{\partial U_g}{\partial Z} = -\frac{g_w}{\rho_g} - \frac{\partial \epsilon_g}{\partial t} + \frac{\epsilon_g}{T_g}\frac{\partial T_g}{\partial t} + \frac{U_g}{T_g}\frac{\partial T_g}{\partial Z} \qquad (2\text{-}38)$$

The SO_2 material balance equation becomes:

$$U_g\frac{\partial C_{sg}}{\partial Z} + \epsilon_g\frac{\partial C_{sg}}{\partial t} = C_{sg}\left(\frac{g_w}{\rho_g} - \frac{\epsilon_g}{T_g}\frac{\partial T_g}{\partial t} - \frac{U_g}{T_g}\frac{\partial T_g}{\partial Z}\right) - g_s \qquad (2\text{-}39)$$

2.4.1.2 H_2O Material Balance

The key H_2O gas phase material balance is similar to Equation (2-30) and is given by:

$$-\frac{\partial f_{wg}}{\partial Z} - g_w = \frac{\partial N_{wg}}{\partial t} \qquad (2\text{-}40)$$

Where: f_{wg}: Flux of H_2O in gas phase in direction of gas flow (lbmole H_2O/ft^2 sec.)

N_{wg}: Concentration of water in reactor (lbmole/ft^3 of reactor).

Similar manipulation and development as in the case of the SO_2 material balance yields the following final form for the H_2O gas material balance in terms of concentration (i.e. C_{wg}):

$$U_g\frac{\partial C_{wg}}{\partial Z}+\epsilon_g\frac{\partial C_{wg}}{\partial t}=C_{wg}\left(\frac{g_w}{\rho_g}-\frac{\epsilon_g}{T_g}\frac{\partial T_g}{\partial t}-\frac{U_g}{T_g}\frac{\partial T_g}{\partial Z}\right)-g_w \qquad (2\text{-}41)$$

2.4.2 Liquid Phase Material Balance

The key H_2O liquid phase material balance is given by:

$$-\frac{\partial f_{wl}}{\partial Z}+g_w=\frac{\partial N_{wl}}{\partial t} \qquad (2\text{-}42)$$

Where: f_{wl}: Flux of H_2O in liquid phase in direction of liquid flow (lbmole H_2O/ft^2 sec.)

N_{wl}: Concentration of liquid water in reactor (lbmole/ft^3 of reactor)

But:

$$f_w=U_lC_{wl}=0 \qquad (2\text{-}43)$$

and

$$N_{wl}=\epsilon_l\rho_l=\epsilon_lC_{wl} \qquad (2\text{-}44)$$

Taking the derivatives of f_{wl} with respect to Z and N_{wl} with respect to t and replacing them in Equation (2-42), we get:

$$\frac{\partial \epsilon_l}{\partial t}=\frac{g_w}{\rho_l} \qquad (2\text{-}45)$$

2.4.3 Solid Phase Material Balance

A mass balance on the solids is given by:

$$-\frac{\partial f_{ss}}{\partial Z}+g_s=\frac{\partial N_{ss}}{\partial t} \qquad (2\text{-}46)$$

Where: f_{ss}: Flux of sulfate or sulfite groups in solid phase (lbmole/sec/ft^2 reactor)

N_{ss}: Concentration of sulfate or sulfite groups in reactor (lbmole/ft^3 reactor)

$$f_{ss}=U_s C_{ss}=0 \qquad (2\text{-}47)$$

$$N_{ss}=\epsilon_s C_{ss}=\epsilon_{so}\left(\frac{\rho_{so}}{\rho_s}\right)C_{ss}=\epsilon_{so}\left(\frac{\rho_c}{\rho_s}\right)C_{ss} \qquad (2\text{-}48)$$

$$\rho_s=\rho_c-C_{ss}\left(\frac{\rho_c}{\rho_p}-1\right) \qquad (2\text{-}49)$$

Taking the derivatives of N_{ss} with respect to t and f_{ss} with respect to Z and replacing them in Equation (2-46), we get:

$$\epsilon_s\frac{\partial C_{ss}}{\partial t}=\left(\frac{\rho_s}{\rho_c}\right)g_s \qquad (2\text{-}50)$$

2.4.4 Heat Balance on the Gas

[Rate of accumulation of heat within the gas]

= [Net convective inflow of heat] - [Rate of heat transfer to solids]

+ [Rate of heat transfer generation due to gas phase reaction]

+ [Heat inflow due to axial dispersion and conduction in the gas]

The heat inflow due to axial dispersion and conduction in the gas could be neglected. The key enthalpy balance for the gas is as follows:

$$N_{Ng}\frac{\partial N_{Ng}}{\partial t}+N_{wg}\frac{\partial H_{wg}}{\partial t}=-f_{Ng}\frac{\partial H_{Ng}}{\partial Z}-f_{wg}\frac{\partial H_{wg}}{\partial Z}-g_g \qquad (2\text{-}51)$$

Where: $N_{Ng}=\epsilon_g C_{Ng}$: Concentration of condensables (lbmole/ft^3 reactor)

H_{Ng}: Enthalpy of condensables (Btu/lbmole)

$N_{wg}=\epsilon_g C_{wg}$:Concentration of water vapor in reactor (lbmole/ft^3 reactor)

H_{wg}: Enthalpy of water vapor (Btu/lbmole)

$f_{Ng}=U_g C_{Ng}$:Flux of noncondensables in gas phase in direction of gas flow (lbmole/sec/ft^2 reactor)

$f_{wg}=U_g C_{wg}$: Flux of water in gas phase in direction of gas flow (lbmole/sec/ft^2 reactor)

g_g:Heat transfer rate from gas phase to liquid phase (Btu/sec/ft^3 reactor)

By using $dH = C_p dT$, Equation (2-51) is expressed in terms of temperature and explicit variables as:

$$\epsilon_g \frac{\partial T_g}{\partial t} + U_g \frac{\partial T_g}{\partial Z} = -\frac{g_g}{C_{Ng} C_{pNg} + C_{wg} C_{pwg}} \qquad (2\text{-}52)$$

2.4.5 Heat Balance on the Solids/Liquids

If the water phase is lumped into a combined liquid/solid phase, the heat balance on the liquid/solid phase is given by the following equation:

$$N_{Cs} \frac{\partial H_{Cs}}{\partial t} + N_{wl} \frac{\partial H_{wl}}{\partial t} = -f_{Cs} \frac{\partial H_{Cs}}{\partial Z} - f_{wl} \frac{\partial H_{wl}}{\partial Z} + g_g + g_w [H_{wg} - H_{wl}] \qquad (2\text{-}53)$$

Where: $N_{Cs} = \epsilon_s \rho_s$: Concentration of calcium ions (includes sulfate, sulfite and carbonate) in solid (lbmole/ft^3 reactor)

H_{Cs}: Enthalpy of sorbent (includes sulfate, sulfite and carbonate) (Btu/lbmole of calcium ion)

$N_{wl} = \epsilon_l C_{wl} = \epsilon_l \rho_l$: Concentration of liquid water in reactor (lbmole/ft^3 reactor)

H_{wl}: Enthalpy of liquid water (Btu/lbmole)

$f_{Cs} = U_s C_s = 0$: Flux of calcium ions in solid phase in direction of solid flow (lbmole/sec/ft^2 reactor)

$f_{wl} = U_l C_{wl} = 0$: Flux of water in liquid phase in direction of liquid flow (lbmole/sec/ft^2 reactor)

$T_s = T_l$: Temperature of solid/liquid phase (°R)

Using $dH = C_p dT$, Equation (2-53) is expressed in terms of temperature and explicit variables as:

$$\frac{\partial T_l}{\partial t} = \frac{1}{\epsilon_s \rho_s C_{pcs} + \epsilon_l \rho_l C_{pwl}} [g_g + g_w (H_{wg} - H_{wl})] \qquad (2\text{-}54)$$

3.0 EXPERIMENTAL METHODS AND MATERIALS

Both bench-scale integral and differential reactor setups were used for the collection of kinetic data for the reaction between SO_2 gas and various raw limestones. The two sets of experiments were designed to promote better understanding of the mechanisms of the low temperature dry scrubbing process. In this section, detailed descriptions of both experimental setups are presented. Materials used as well as experimental procedures are discussed.

3.1 Integral Reactor Studies

This part of the experimental study was directed at collecting integral kinetic data using a fixed-bed integral reactor. The main purpose of these experiments was to confirm the kinetic SO_2 capture model and to enable us to evaluate the strengths and weaknesses of the model. The key parameters being considered included the SO_2 concentration in the inlet gas, the gas relative humidity, and the limestone particle size.

3.1.1 Apparatus and Procedure

A schematic representation of the experimental system is shown in Figure 3-1. The reactor is basically a 2 inch diameter and 6 inch length plexiglass tube packed with raw limestone and immersed in a constant temperature water bath.

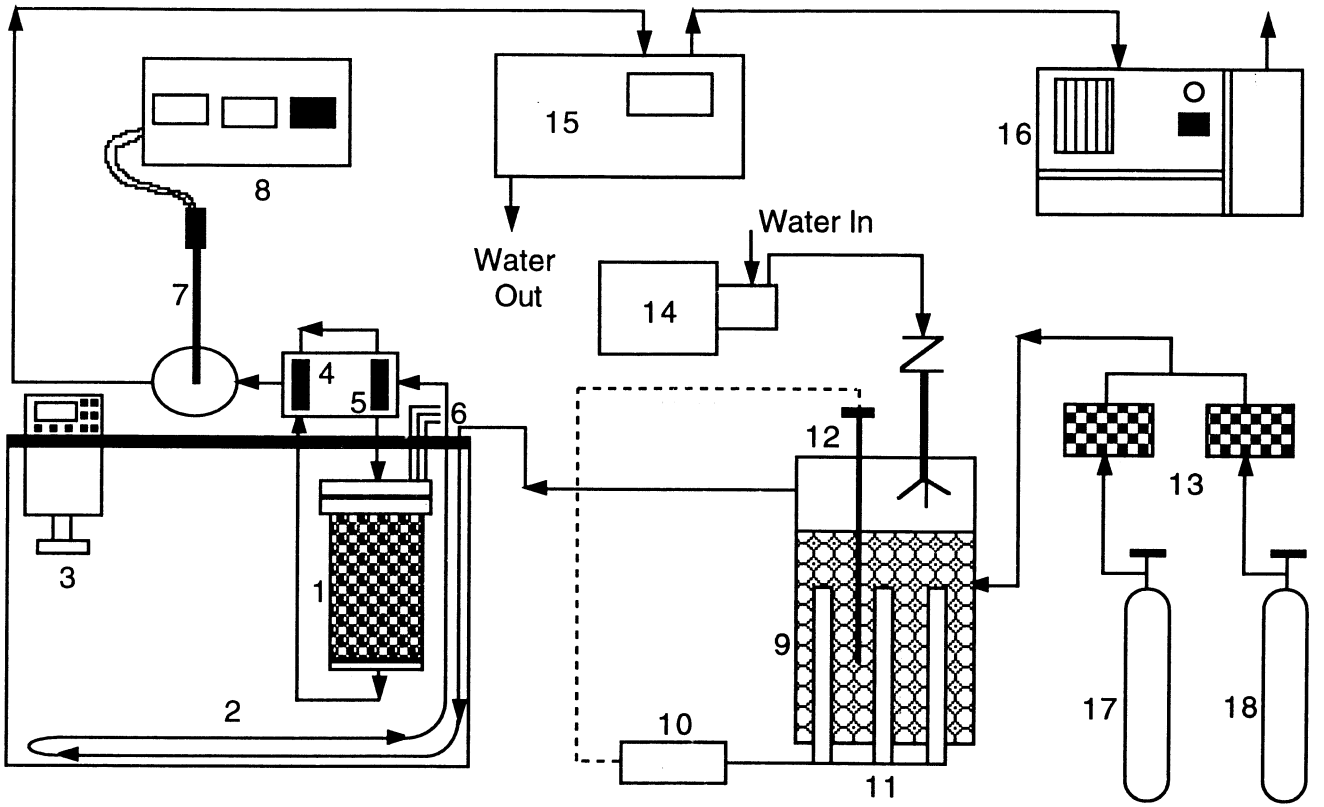

1: Reactor, 2: Constant Temperature Water Bath, 3: Heating Circulator, 4 & 5: Switching Valves from By-Pass to Reactor, 6: Thermocouples, 7: Humidity & Temperature Probe, 8: Humidity & Temperature Display, 9: Evaporation Chamber, 10: Controller, 11: Heaters, 12: Thermocouple, 13: Mass Flow Meters, 14: Peristaltic Pump, 15: Sample Conditioner, 16: SO_2 Analyzer, 17 & 18: Air & SO_2 Sources..

Figure 3-1: Fixed-Bed Integral Reactor System.

The simulated flue gas, which is a mixture of SO_2 and air, was passed through the limestone bed at a superficial velocity of 1.0 ft/sec. This gas was generated by mixing gases from compressed SO_2 and air lines in appropriate amounts by using calibrated mass flow meters in combination with a mass flow controller. To facilitate the use of the mass flow meters and to get the appropriate gas flow rates and SO_2 concentrations, a FORTRAN program was written. By inputting the reactor superficial gas velocity, the temperature, the desired inlet SO_2 concentration, the gas relative humidity, and the concentration of the SO_2 source, the program returned and printed out the flow meter settings. The source code and a more detailed description of the program are available in Appendix A. Prior to the introduction of gas into the reactor, the gas was passed through a humidification system where the gas mixes with water vapor produced by the injection of water into the evaporation chamber. A peristaltic pump (Manufacturer: Cole-Parmer Instrument Co., Model No. 7520-35) was used to accurately measure the amount of water injected. The pump was equipped with a potentiometer reading a range from 0 to 10 turns. A calibration curve that gives the water flow rate as a function of potentiometer reading is available in Appendix B. The FORTRAN program listed in Appendix A also was used to calculate the flow rate of water necessary to obtain the desired gas relative humidity. Therefore, the water pump calibration equation has been added to the program to directly obtain the potentiometer setting. Upon exiting the evaporation chamber, the humidified gas passed through a coil of stainless

steel tubing located in the bottom of the water bath to bring the gas temperature to that of the bath. Through a reactor by-pass, the gas could be diverted around or passed through the reactor. At the exit of the reactor, the gas entered a sampling section where the humidity of the gas was monitored by a humidity and temperature indicator (Manufacturer: Vaisala Inc., Model No. HMI 32) equipped with a humidity and temperature probe (Manufacturer: Vaisala Inc., Model No. HMP 36). Part of the exiting gas was vented and the remaining was sent for SO_2 analysis. Before the gas entered the SO_2 analyzer it was conditioned to remove as much water as possible. This was achieved by passing the humidified gas through a sample conditioner (Manufacturer: KWW DEPA.VIA, Model No. MAK 2), where the water was condensed and collected in a bucket. The gas was then introduced into a pulsed fluorescent SO_2 analyzer (Manufacturer: Thermo Environmental Instruments Inc., Model No. 40). A strip chart recorder was used to record the change of SO_2 concentration with time.

3.1.2 Materials

Sorbent selection for this part of the research study was based on preliminary results obtained by Prudich et al. [1988]. Three Ohio limestones covering the full range of Ohio limestone compositions were used by Prudich et al. [1988] in their LEC pilot unit tests: Vanport, Maxville, and Carey limestones. The test results indicated that the SO_2 removal capacity of Maxville stone was much greater than that of Vanport and Carey stones. The average

SO_2 removal capacity of Maxville stone was almost three times that of Vanport stone. Because of its higher performance over other stones, Maxville limestone was chosen for conducting our bench-scale experimental runs.

Maxville limestone was provided by Maxville Quarries Inc. located in Logan, Ohio. It consists of 70.0 % $CaCO_3$, 12.87 % $MgCO_3$, 0.87 % K_2CO_3, 0.14 % Na_2CO_3, and 16.12 % combined SiO_2, Al_2O_3 and Fe_2O_3. In all experimental runs, except those where particle size effects were studied, the mass mean diameter of the limestone particles was about 8×10^{-3} ft (i.e. 2.48 mm). This corresponds to a specific surface area of about 1150 ft^2/ft^3, calculated using Equation (5-6). A screen size analysis for this Maxville limestone # LS890118A is shown in Table 3-1. Figure 3-2 shows a fractional distribution plot for the screen analysis of Table 3-1.

Size Range (U.S. Standard Screen mesh)	Average Diameter (mm)	Weight %
+ 1/4	6.3000	1.71
- 1/4 + 4	5.2550	2.56
-4 + 5	4.3750	5.85
-5 + 6	3.6750	13.69
-6 + 7	3.0750	15.63
-7 +8	2.5800	14.05
- 8 + 10	2.1800	3.57
- 10 + 12	1.8500	9.20
- 12 + 14	1.5500	10.21
- 14 + 16	1.2900	5.61
- 16 + 18	1.0900	6.46
- 18 + 20	0.9250	4.14
- 20 + 25	0.7800	2.66
- 25 + 30	0.6550	1.43
- 30 + 35	0.5500	1.22
- 35 + 40	0.4625	0.82
- 40 + 45	0.3900	0.16
- 45 + 50	0.3275	0.04
- 50	0.3000	0.99

Table 3-1: Screen Analysis for Maxville Limestone # 9 (LS890118A).

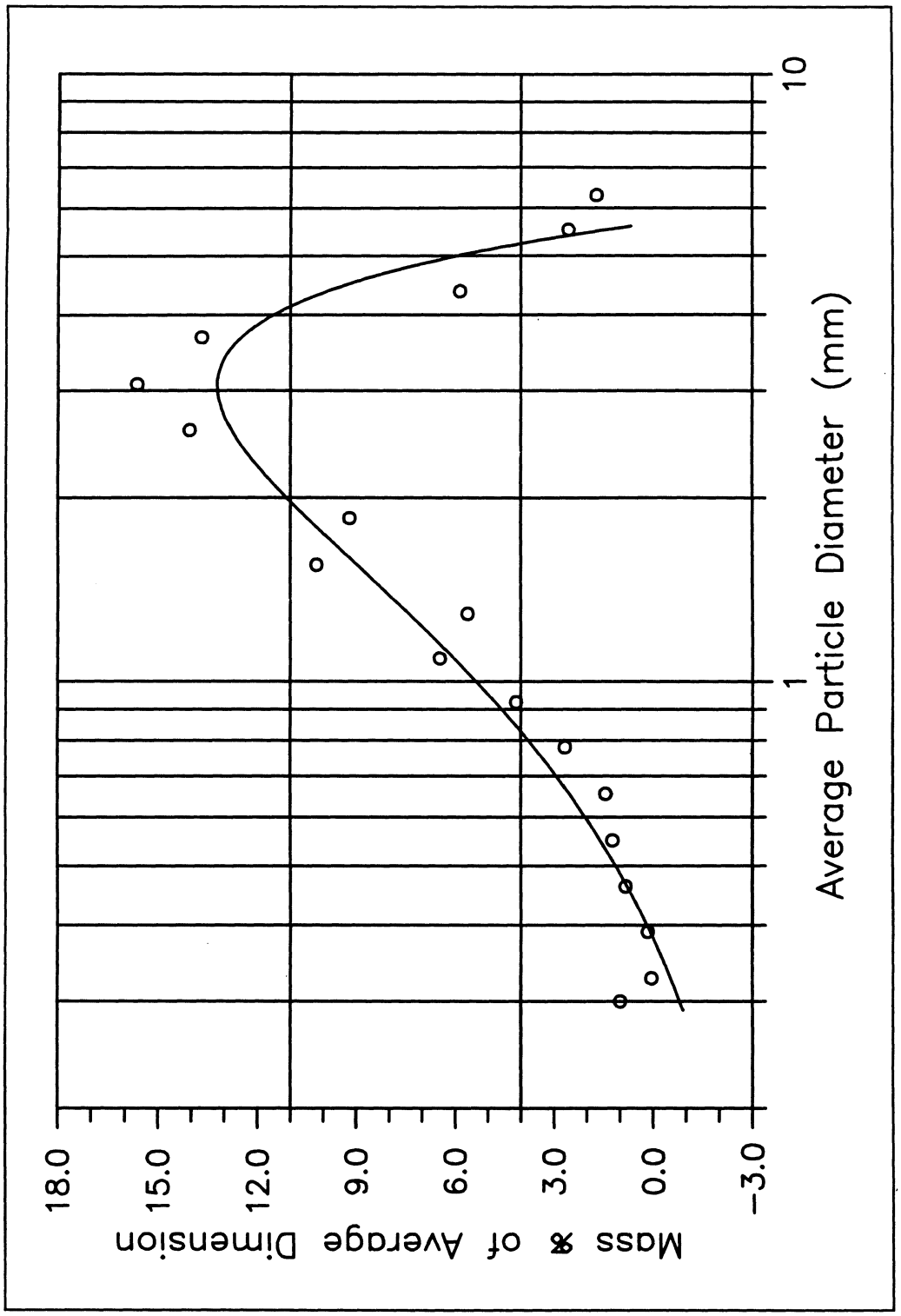

Figure 3-2: Fractional Distribution Plot for Screen Analysis of Maxville Limestone #9 (LS890118A).

3.1.3 Experimental Conditions

Different experimental conditions were used to gain insight into the physical and chemical phenomena that are taking place in the SO_2 capture process. These conditions, shown in Table 3-2, were chosen to reflect the influence of various key parameters that include inlet SO_2 concentration, gas relative humidity, and limestone particle size.

Reaction Temperature	140 °F
Superficial Gas Velocity	1.0 ft/sec
Gas Relative Humidity	25 - 75 %
Inlet SO_2 Concentration	500 - 1750 ppm
Limestone Particle Size	$5x10^{-4}$ - $23x10^{-4}$ m

Table 3-2: Experimental Conditions in Fixed-Bed Integral Reactor.

3.2 Differential Reactor Studies

In addition to the bench-scale integral reactor, a bench-scale differential reactor system was used to collect kinetic and rate data. The system was more appropriate for the evaluation of fine powder sorbents. This reactor used small amounts of sorbents (i.e. 1.0 g) and was used to screen a wide range of limestones. This part of the research program mainly focused on the

humidified/dry capture operating regime, in which humidified SO_2 gas was contacted with dry limestone samples. The key parameters investigated in this kinetic study were limestone type (i.e. limestones with different chemical properties), gas relative humidity, and limestone particle size. The experimental results were used to determine parameters of the extended dry and product layer blinding models.

3.2.1 Apparatus and Procedure

The fixed-bed differential reactor system, as shown in Figure 3-3, was similar overall to the integral reactor system. The main difference was that the reactor unit is a stainless steel filter holder (Manufacturer: Gelman Sciences, Model No. 2220) in which about 1.0 g of limestone particles was evenly dispersed across a filter. The reactor unit was mounted in a constant temperature electric oven. A detailed description of the reactor unit is shown in Figure 3-4. The other equipment, which included mass flow meters, evaporation chamber, and humidity and temperature devices, were the same as the equipment used in the integral reactor system.

Initially, humidified air with the same relative humidity as the reacting SO_2 gas was passed over the limestone sample for about 15 minutes to bring the reactor and reaction medium into thermal and humidity equilibrium with the flue gas and to allow for sorbent pre-conditioning. The reacting gas, consisting of air, SO_2 and vapor water, was mixed, passed through a coil of stainless steel tubing located inside the oven and by-passed to allow this stream to reach

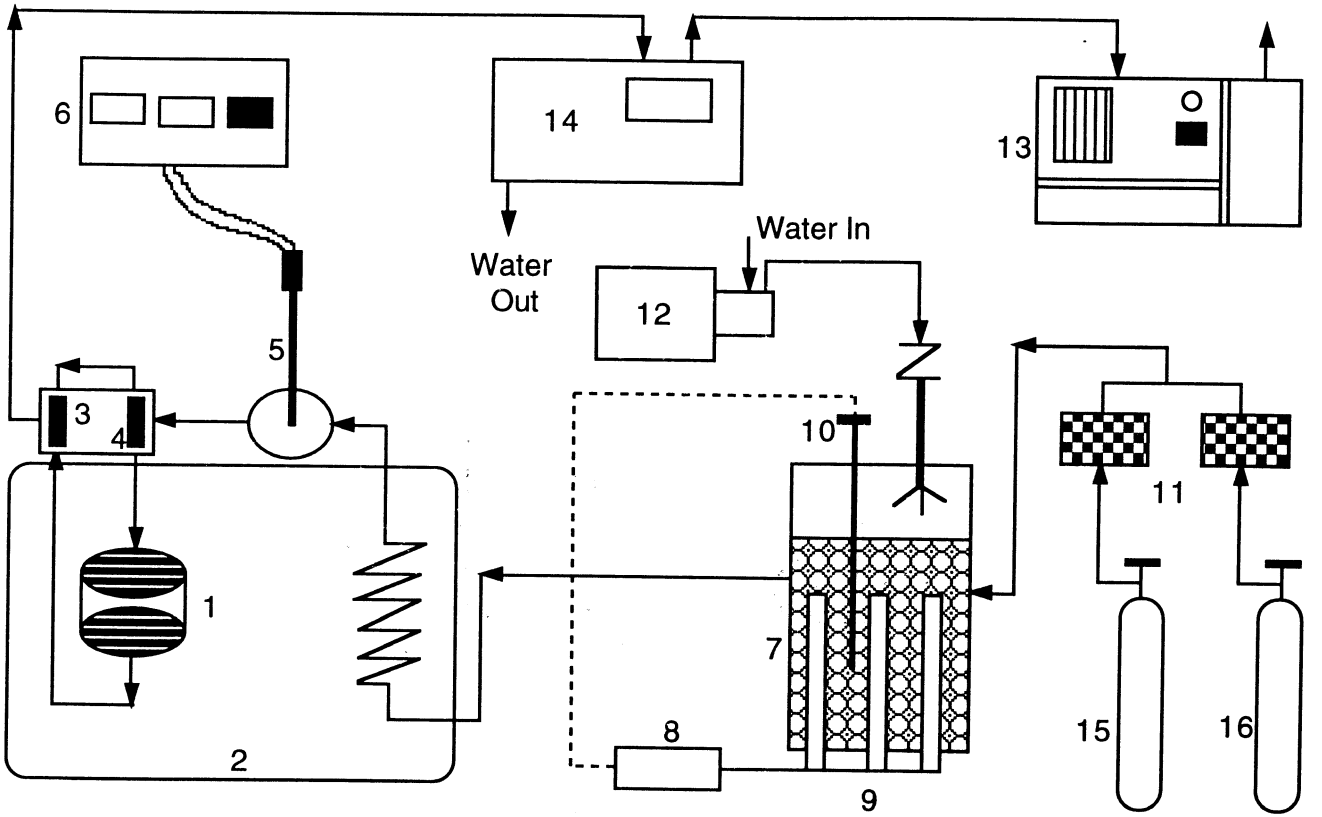

1: Reactor, 2: Constant Temperature Oven, 3 & 4: Switching Valves, 5: Humidity & Temperature Probe, 6: Humidity & Temperature Display, 7: Evaporation Chamber, 8: Controller, 9: Heaters, 10: Thermocouple, 11: Mass Flow Meters, 12: Peristaltic Pump, 13: SO2 Analyzer, 14: Sample Conditioner, 15 & 16: Air & SO2 Sources.

Figure 3-3: Fixed-Bed Differential Reactor System.

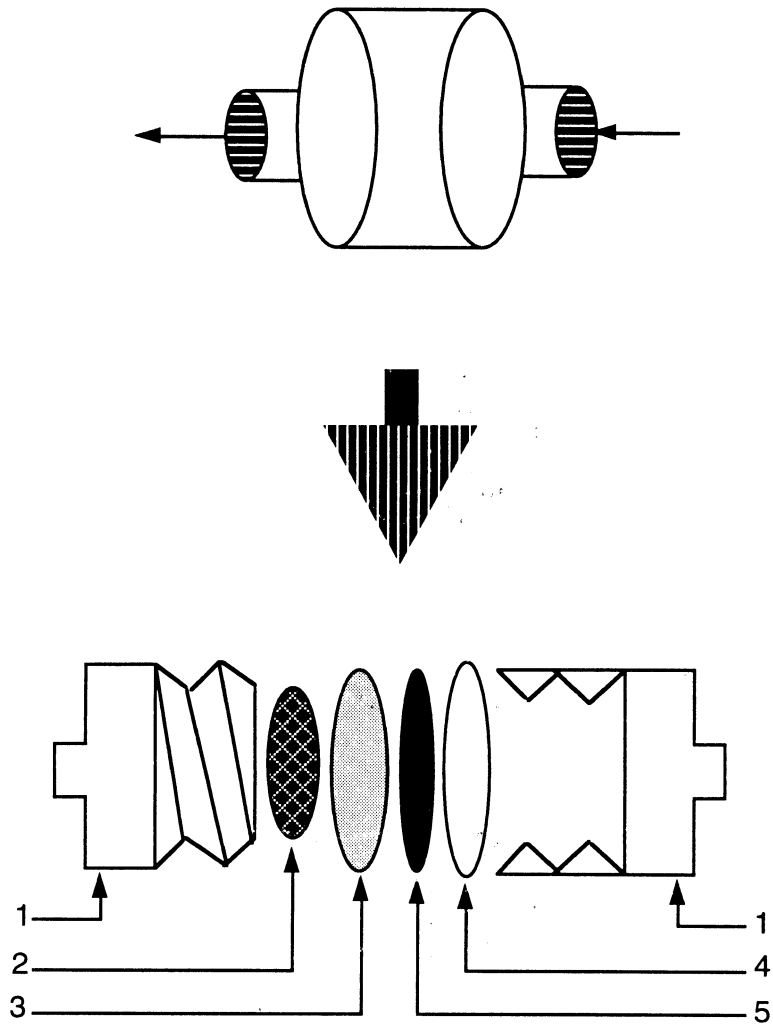

1: Filter Holder, 2: Filter (1.438" dia.), 3: Filter (1.813 " dia.),
4: O-Ring, 5: Solid Sorbent (1.0 g).

Figure 3-4: Detailed Description of Differential Reactor Unit.

reaction temperature. At the start of an experimental run, the switching valves were reversed and the limestone sample was exposed to the reacting gas for a selected periods of time, which were measured using a stop watch. The run was ended by reversing the switching valves. The limestone sample was then removed from the filter and dried at about 110 °C in an electric oven. The sulfur content in the sample was obtained using a LECO-SC-32 sulfur analyzer. The analysis procedure and recipes are presented in Appendix C.

3.2.2 Materials

A total of five different raw limestones, four of them from various locations in Ohio and the other from Missouri, were evaluated. These data are presented in Table 3-3 along with the companies and locations from which they came.

Name	Company	Location
Bucyrus	National Lime & Stone Co.	Bucyrus, Ohio
Carey	National Lime & Stone Co.	Carey, Ohio
Maxville	Maxville Quarries Inc.	Logan, Ohio
Vanport	Waterloo Co.	Jackson, Ohio
Mississippi	Mississippi Lime Co.	Alton, Missouri

Table 3-3: Limestones Used in the Fixed-Bed Differential Reactor.

The four Ohio limestones were selected in an attempt to cover the full range of Ohio limestone compositions. They range from highly calcitic (i.e. high calcium carbonate content) to dolomitic (i.e. roughly equal $CaCO_3/MgCO_3$ contents). Mississippi limestone was selected because it has a very small amount of impurities, consisting of about 98% $CaCO_3$ by weight, and for this reason, as well as the fact that it has been used nationally by other investigators, it was included with the Ohio limestones. Properties of these limestones are presented in Tables 3-4 through 3-8. Characterization of the raw limestones and some of the experimental products were carried out using Scanning Electron Microscopy (SEM) and Energy Dispersive Analysis of X-Rays (EDAX). These data are presented and discussed in the Results and Discussion chapter.

Components	Weight Percent
$CaCO_3$	70.00
$MgCO_3$	12.87
K_2CO_3	0.87
Na_2CO_3	0.14
SiO_2 Al_2O_3 } Fe_2O_3	16.12

TABLE 3-4: Properties of Maxville Limestone.

Components	Weight Percent
$CaCO_3$	98.35
$MgCO_3$	0.68
Others	0.97

TABLE 3-5: Properties of Mississippi Limestone.

Components	Weight Percent
$CaCO_3$	83.56
$MgCO_3$	1.17
K_2CO_3	0.08
Na_2CO_3	0.15
SiO_2 Al_2O_3 } Fe_2O_3	15.03

TABLE 3-6: Properties of Vanport Limestone.

Components	Weight Percent
$CaCO_3$	80.00
$MgCO_3$	17.00
Others	3.00

TABLE 3-7: Properties of Bucyrus Limestone.

Components	Weight Percent
$CaCO_3$	53.89
$MgCO_3$	44.68
K_2CO_3	0.02
Na_2CO_3	0.03
SiO_2 Al_2O_3 } Fe_2O_3	1.38

TABLE 3-8: Properties of Carey Limestone.

3.2.3 Experimental Conditions

For the purpose of modeling, a wide range of gas relative humidity (i.e. 40 to 95%) were used. All experimental runs, except the ones which investigated particle size effects, were performed using a limestone particle size fraction between 53 and 75 microns (i.e. -200+270 mesh). The other experimental conditions were held constant for all runs. The fixed experimental conditions are shown in Table 3-9.

Reaction Temperature	140 °F
SO_2 Concentration	1000 ppm
Superficial Gas Velocity	1.0 ft/sec
Limestone Sample Size	1.0 g

Table 3-9: Fixed Experimental Conditions for Differential Reactor Runs.

4.0 THEORETICAL DEVELOPMENT

4.1 Effects of Sorbent Surface Blinding by Reaction Products

As the reaction between SO_2 and limestone progresses, reaction products (i.e. $CaSO_3/CaSO_4$) gradually build up at the limestone surface. The unreacted-core-model, as discussed previously, assumes that a completely converted outer layer and an unreacted core of solid material exist at any time during the reaction. The unreacted core, in this case, gradually shrinks in size, as the reaction progresses, until the entire limestone particle becomes unreactive. The model being used here idealizes the limestone surface by dividing it into blinded (i.e. non active surface area) and non-blinded (i.e. active surface area) regions as shown in Figure 4-1. The blinded area gradually increases, as shown in Figure 4-2, until the limestone particle becomes entirely unreactive. The model takes the form of an empirical equation which relates the surface area available for mass transfer to the extent of reaction. In deriving such an equation, the following assumptions are made:

a. The precipitate concentration, C_{ss}, reaches its maximum when the reaction stops. This is denoted as $C_{ss,cr}$.
b. At this concentration, the precipitate layer has a uniform thickness over the entire limestone surface area.
c. The blinding area can not exceed the total limestone surface area.
d. The whole surface area of a fresh limestone will be available for mass transfer.

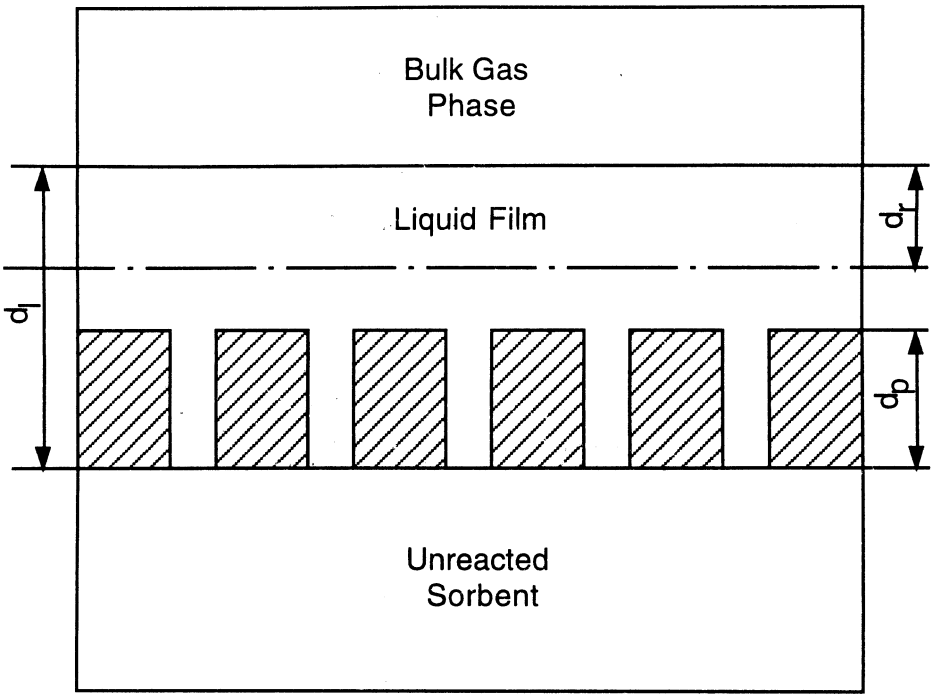

Figure 4-2: Schematic Representation of Blinding Model.

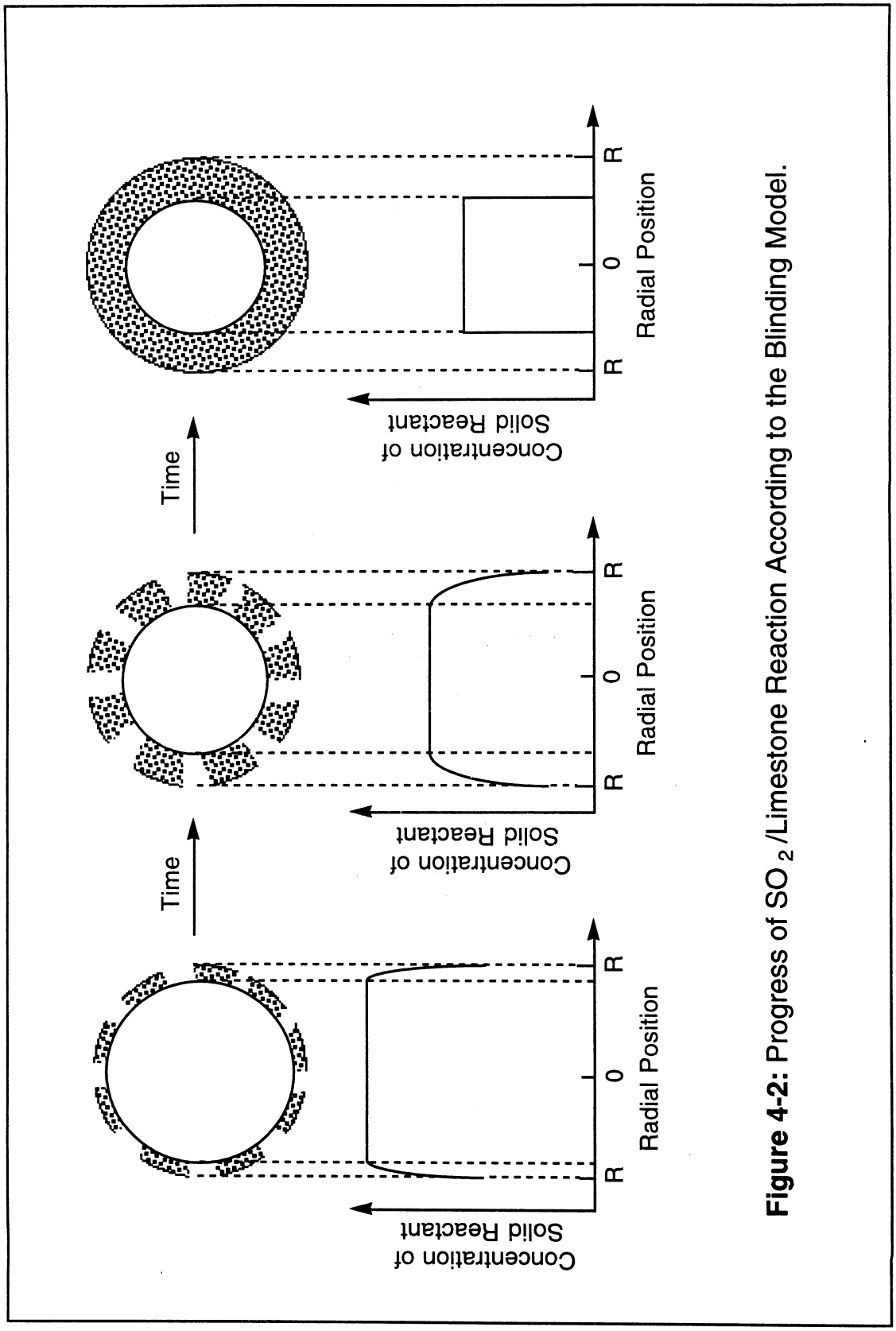

Figure 4-2: Progress of SO_2/Limestone Reaction According to the Blinding Model.

Based on these assumptions, the precipitate layer thickness, δ_p, can be expressed as:

$$\delta_p = k(C_{ss})^{\frac{1}{n}} = \frac{C_{ss}\epsilon_s}{\rho_p A_p} \tag{4-1}$$

Where: k: Rate constant

n: Model parameter

ϵ_s: Volume fraction of solid

ρ_p: Solid density

A_p: Blinded surface area

At the critical precipitate concentration:

$$\delta_{p,cr} = k(C_{ss,cr})^{\frac{1}{n}} = \frac{C_{ss,cr}\epsilon_s}{\rho_p A} \tag{4-2}$$

From Equation (4-2), k is given as:

$$k = \frac{\epsilon_s (C_{ss,cr})^{\frac{n-1}{n}}}{\rho_p A} \tag{4-3}$$

The area of the limestone available for mass transfer, A_{mp}, is given as the difference between the total area, A, and the blinded area, A_p:

$$A_{mp} = A - A_p \tag{4-4}$$

From Equations (4-1), (4-2) and (4-3), the blinded area is given as:

$$A_p = A\left(\frac{C_{ss}}{C_{ss,cr}}\right)^{\frac{n-1}{n}} \tag{4-5}$$

Substituting for A_p as given by Equation (4-5), Equation (4-4) becomes:

$$A_{mp}=A\left[1-\left(\frac{C_{ss}}{C_{ss,cr}}\right)^{\frac{n-1}{n}}\right] \qquad (4\text{-}6)$$

4.2 Dry Sorbent Capture

The model for dry sorbent capture has been developed based on the experimentally observed behavior. The kinetic experimental studies revealed a power function increase in the reaction rate as the gas relative humidity was increased. This can be attributed to the fact that more monolayers of water vapor are adsorbed on the limestone surface. The model being used here aims at reproducing this effect. The model takes the form of an empirical equation which relates the fractional liquid coverage (i.e. ratio of the particle surface area covered with liquid at a given relative humidity to the particle surface area covered with liquid at 100 % relative humidity) to the flue gas relative humidity. This equation is used in the upgraded resistance-in-series model to calculate the sulfur dioxide removal rate in the dry portion of the limestone bed (i.e. where no bulk phase of liquid water is present on the limestone surface). A dry capture correction factor, f, has been defined to represent the ratio of mass transfer area covered by liquid water, A_{ml}, to the total mass transfer area available within the limestone, A_{mp}, as:

$$f=\frac{A_{ml}}{A_{mp}} \qquad (4\text{-}7)$$

The correction factor, f, strongly depends on the gas relative humidity. One of

the forms of the equation that can be used to relate f to the gas relative humidity is a two parameter power equation:

$$f=\alpha_1\left(\frac{Y_r}{100}\right)^{\alpha_2} \qquad (4\text{-}8)$$

α_1, α_2: model parameters and Y_r: % relative humidity

Another form, a Langmuir isotherm equation, has been used by many researchers for the adsorption of gases in multimolecular layers on various substrates [Brunauer et al., 1938]. Klingspor et al. [1983] used a similar form to relate the amount of water vapor adsorbed on limestone and the gas relative humidity. Because the Langmuir equation has been proven to better fit the experimental data, it is used in the overall model.

The general form of the Langmuir isotherm for the adsorption of gases on solid surfaces was developed by Brunauer et al. [1938] and is given as follows:

$$v=\frac{v_m C\left(\frac{P}{P_o}\right)}{1+C\left(\frac{P}{P_o}\right)} \qquad (4\text{-}9)$$

Where: v: Adsorption capacity

v_m: Monolayer capacity

C: Constant

P/P_o: Fractional gas relative humidity (i.e. 100% humidity corresponds to 1.0)

At some reference gas relative humidity, $[P/P_o]^*$:

$$v^* = \frac{v_m C \left(\frac{P}{P_o}\right)^*}{1 + C\left(\frac{P}{P_o}\right)^*} \qquad (4\text{-}10)$$

Dividing Equation (4-9) by Equation (4-10) and letting $Y = v/v^*$, $X = [P/P_o]/[P/P_o]^*$, and $k = C[P/P_o]^*$ gives:

$$Y = \frac{(1+k)X}{1+KX} \qquad (4\text{-}11)$$

If the reference adsorbed capacity is taken to be one at a fractional gas relative humidity of one then Equation (4-11) becomes:

$$f = \frac{(1-k)\,RH}{1-k\,RH} \qquad (4\text{-}12)$$

Where: $f = A_{ml}/A_{mp}$: Substituted for Y

RH: Fractional gas relative humidity

k: Model parameter

4.3 Removal Rate of Sulfur Dioxide

Three main situations need to be considered for evaluating the sulfur dioxide removal rate. These are:

a. When the liquid water extends above the precipitate layer ($\delta_l > \delta_p$).

b. When the liquid water gets below the precipitate layer ($\delta_l < \delta_p$).

c. When there is no bulk liquid water on the limestone surface ($\delta_l = 0$).

The last case corresponds to the dry sorbent capture regime.

4.3.1 Case 1: $\delta_l > \delta_p$ (liquid water extends above precipitate layer)

When the reaction front is located between the gas-liquid interface and the precipitate layer, g_s can take the following expressions:

$$g_s = k_{ms} a_{mg} (C_{sg} - C_{sgi}) = \frac{D_{sl} a_{ml} C_{sli}}{\delta_r} = \frac{D_{cl} a_{ml} C_{clp}}{\delta_l - \delta_p - \delta_r}$$

$$= \frac{D_{cl} a_{mp} (C_{cls} - C_{clp})}{\delta_p} = k_{mc} a_{mp} (C_{cle} - C_{cls}) \qquad (4\text{-}13)$$

When substituting for interfacial concentration $C_{sgi} = C_{sli} H_s / (RT_g)$, the location of the reaction front can be expressed as:

$$\delta_r = \frac{\dfrac{\delta_l - \delta_p}{D_{cl} a_{ml} C_{cle}} + \dfrac{\delta_p}{D_{cl} a_{mp} C_{cle}} + \dfrac{1}{k_{mc} a_{mp} C_{cle}} - \dfrac{1}{k_{ms} a_{mg} C_{sg}}}{\dfrac{1}{D_{sl} a_{ml} C_{sg} \left(\dfrac{RT_g}{H_s} \right)} + \dfrac{1}{D_{cl} a_{ml} C_{cle}}} \qquad (4\text{-}14)$$

If $\delta_r \leq 0$, then the reaction is gas-phase control and g_s is given by:

$$g_s = k_{ms} a_{mg} C_{sg} \qquad \text{(Gas-phase Control)} \qquad (4\text{-}15)$$

k_{ms}: Mass transfer coefficient for Ca^{2+} in dissolution zone (ft/sec)
a_{mg}: Mass transfer area in gas phase boundary layer (ft^2/ft^3 reactor)

If $0 < \delta_r < \delta_l - \delta_p$, then the reaction is liquid-phase control and g_s is given by:

$$g_s = \frac{C_{sg}}{\dfrac{1}{k_{ms} a_{mg}} + \dfrac{\delta_r}{D_{sl} a_{ml} \left(\dfrac{RT_g}{H_s} \right)}} \qquad \text{(Liquid-phase control)} \qquad (4\text{-}16)$$

If $\delta_r \geq \delta_l - \delta_p$, then the reaction is dissolution control and g_s is given by:

$$g_s = k_{mc} a_{mp} C_{cle} \qquad \text{(Dissolution control)} \qquad (4\text{-}17)$$

4.3.2 Case 2: $\delta_l < \delta_p$ (liquid water is below precipitate layer)

In this case, g_s takes the following expressions:

$$g_s = k_{ms} a_{mg} (C_{sg} - C_{sp}) = \frac{D_{sg} a_{mp} (C_{sp} - C_{sgi})}{\delta_p - \delta_l} = \frac{D_{sl} a_{mp} C_{sli}}{\delta_r}$$

$$= \frac{D_{cl} a_{mp} C_{cls}}{\delta_l - \delta_r} = k_{mc} a_{mp} (C_{cle} - C_{cls}) \qquad (4\text{-}18)$$

When substituting for interfacial concentration $C_{sgi} = C_{sli} H_s / [RT_g]$, the location of the reaction front can be expressed as:

$$\delta_r = \frac{\dfrac{\delta_l}{D_{cl} a_{ml} C_{cle}} + \dfrac{1}{k_{mc} a_{mp} C_{cle}} - \dfrac{1}{k_{ms} a_{mg} C_{sg}} - \dfrac{\delta_p - \delta_l}{D_{sg} a_{mp} C_{sg}}}{\dfrac{1}{D_{sl} a_{mp} \left(\dfrac{RT_g}{H_s} \right)} + \dfrac{1}{D_{cl} a_{mp} C_{cle}}} \qquad (4\text{-}19)$$

If $\delta_r \leq 0$, then the reaction is gas-phase control and g_s is given by:

$$g_s = \frac{C_{sg}}{\dfrac{1}{k_{ms} a_{mg}} + \dfrac{\delta_p - \delta_l}{D_{sg} a_{mp}}} \quad \text{(Gas-phase control)} \qquad (4\text{-}20)$$

If $0 < \delta_r < \delta_l$, then the reaction is liquid-phase control and g_s is given by:

$$g_s = \frac{C_{sg}}{\frac{1}{k_{ms}a_{mg}} + \frac{\delta_p - \delta_l}{D_{sg}a_{mp}} + \frac{\delta_r}{D_{sl}a_{mp}\left(\frac{RT_g}{H_s}\right)}} \qquad (4\text{-}21)$$

(Liquid-phase Control)

$$g_s = k_{mc}a_{mp}C_{cle} \qquad \text{(Dissolution control)} \qquad (4\text{-}22)$$

4.3.3 Case 3: $\delta_l = 0$ (Dry scrubbing regime)

In this case, the controlling resistance is either gas-film or dissolution control. The choice of experimental conditions makes one of the resistances negligible and the other controlling. The rate of sulfur dioxide removal is given by Equation (4-23) and Equation (4-24) for gas-phase and dissolution control respectively.

$$g_s = \frac{C_{sg}}{\frac{1}{k_{ms}a_{mg}} + \frac{\delta_p - \delta_l}{D_{sg}a_{ml}}} \qquad \text{(Gas-phase control)} \qquad (4\text{-}23)$$

$$g_s = k_{mc}a_{ml}C_{cle} \qquad \text{(Dissolution control)} \qquad (4\text{-}24)$$

5.0 RESULTS AND DISCUSSION

5.1 Characterization of Limestones Used in this Study

5.1.1 Physical Properties

5.1.1.1 Pore Structure and Surface Morphology

Structure and surface morphology are very important in the reaction between SO_2 and limestone. Since the limestones used in this study came from various geographical locations, they are expected to differ in quality owing to variations in chemical composition, pore structure and surface morphology.

The technique known as Scanning Electron Microscopy (SEM) was used to obtain some information on the pore structure and surface morphology of the limestones. A magnification of 750 times was used to get a general idea about the shapes and the outer surface of the stones. In addition, a higher magnification of 2000 times was used to examine the internal structure of individual stones. Samples of sieved limestones (Maxville, Vanport, Mississippi, Bucyrus and Carey) in the -200+270 mesh size range (53-75 μm) were analyzed and their SEM micrographs are shown in Figures 5-1 through 5-5.

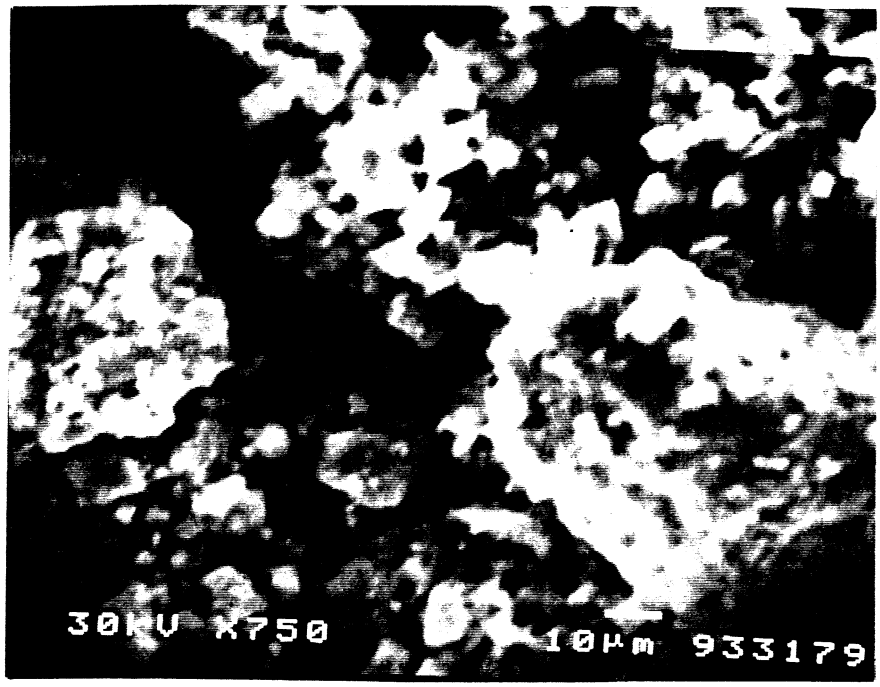

(A)

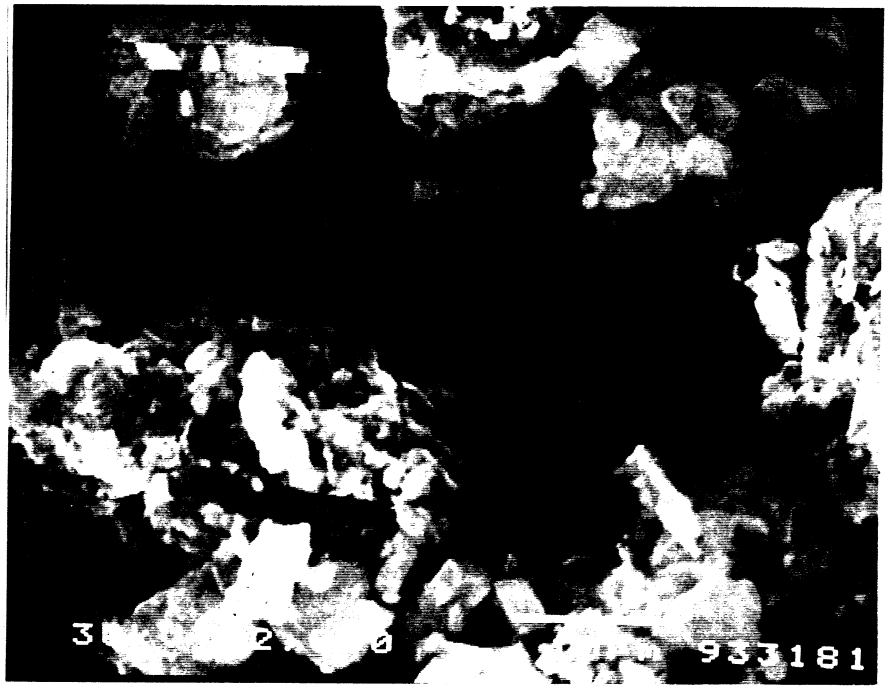

(B)

Figure 5-1: SEM Micrograph of Sieved Maxville Limestone -200+270 U.S. Mesh Size (53-75 μm)

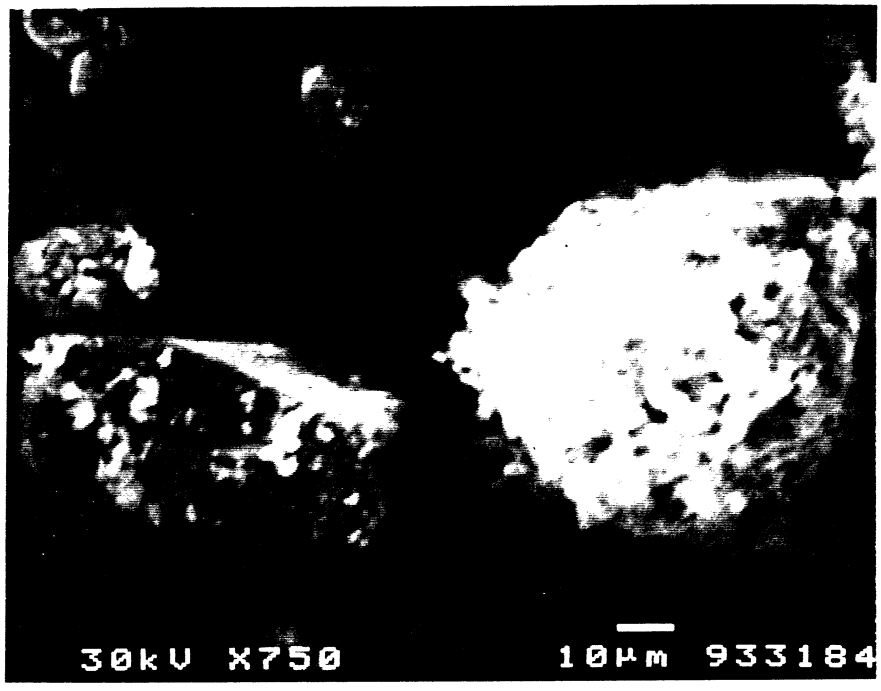

(A)

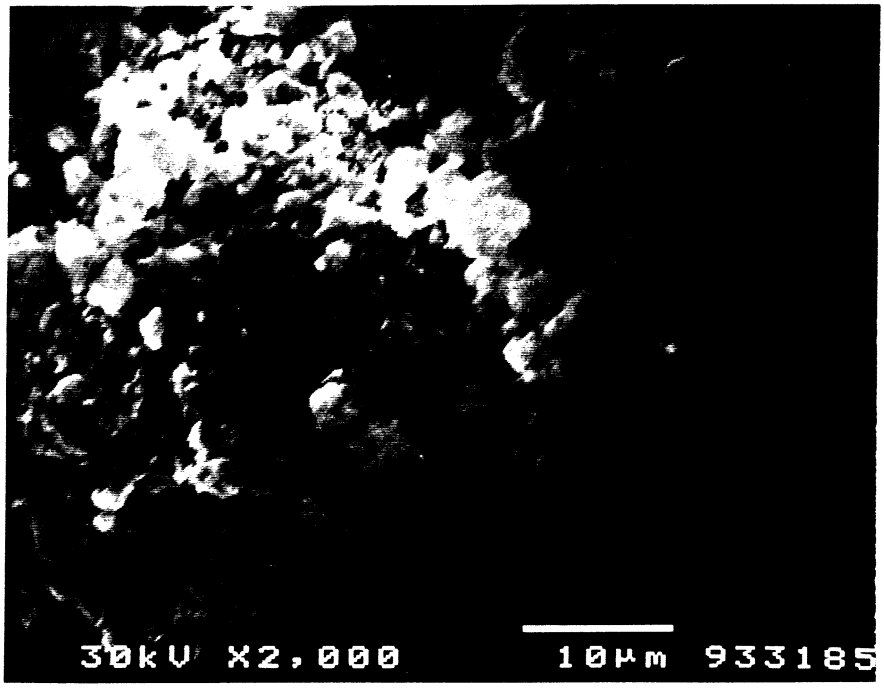

(B)

Figure 5-2: SEM Micrograph of Sieved Mississippi Limestone -200+270 U.S. Mesh Size (53-75 μm)

(A)

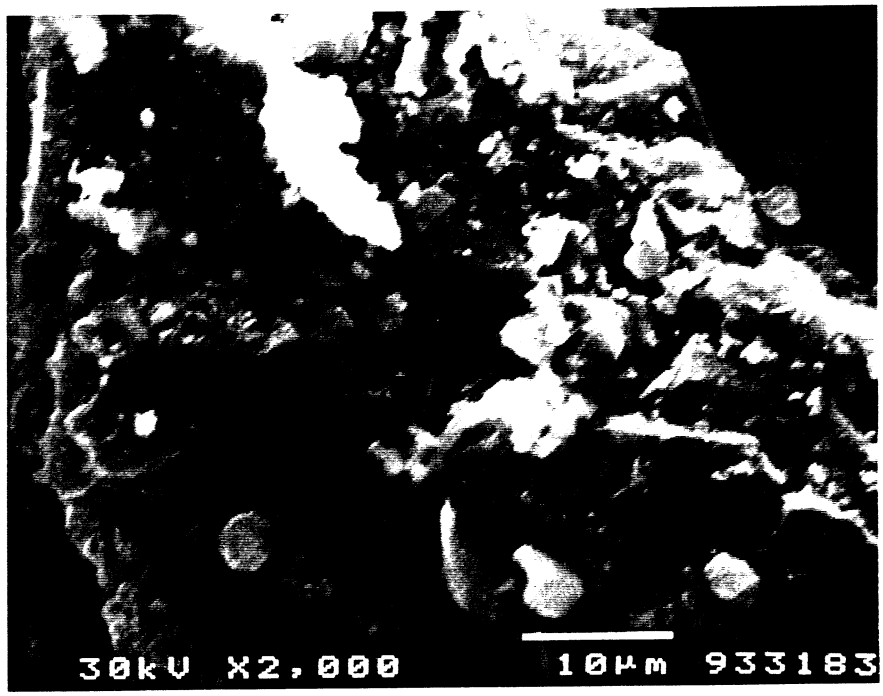

(B)

Figure 5-3: SEM Micrograph of Sieved Vanport Limestone -200+270 U.S. Mesh Size (53-75 μm)

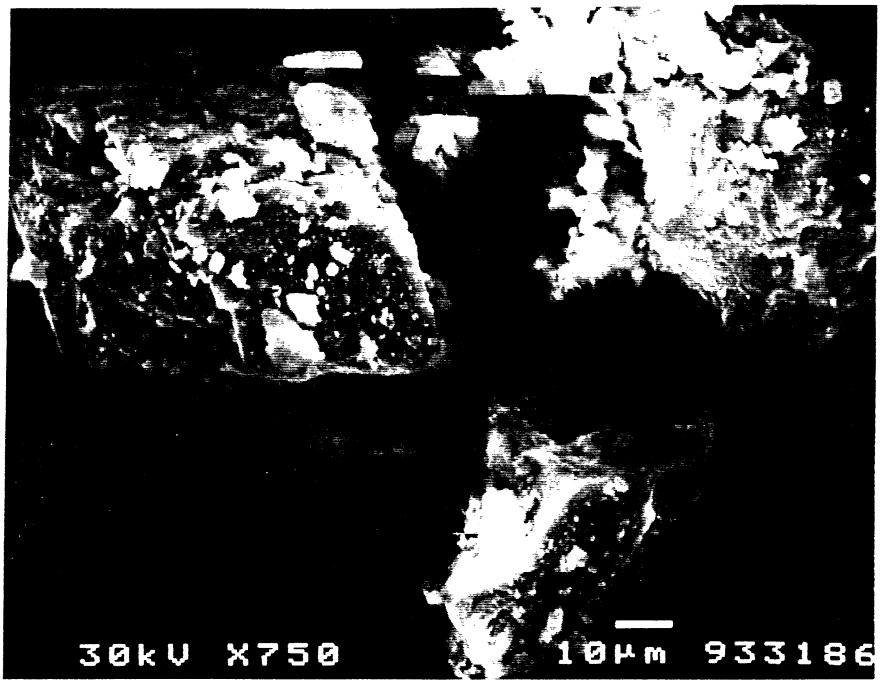

(A)

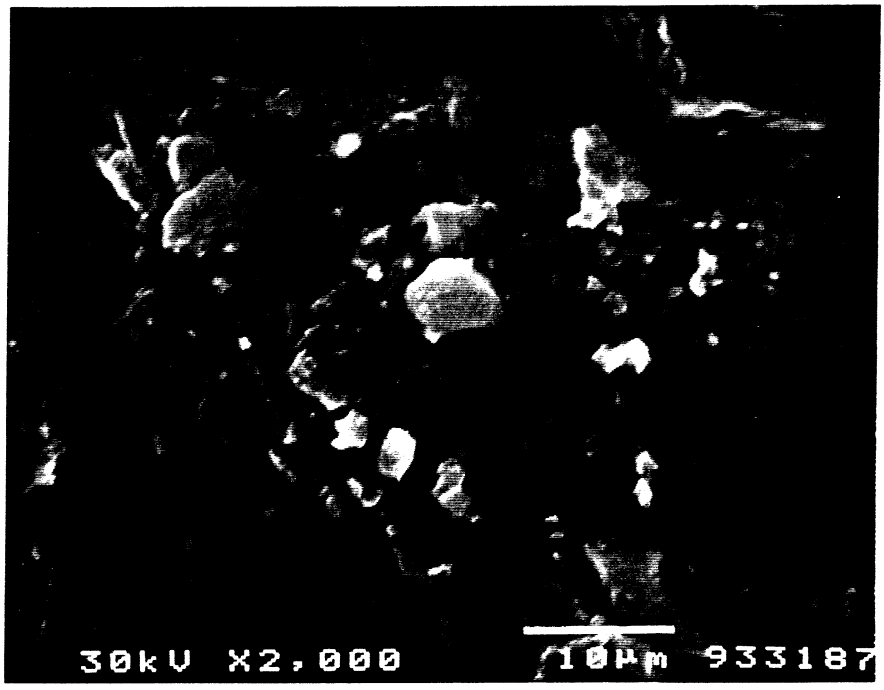

(B)

Figure 5-4: SEM Micrograph of Sieved Bucyrus Limestone -200 + 270 U.S. Mesh Size (53-75 μm)

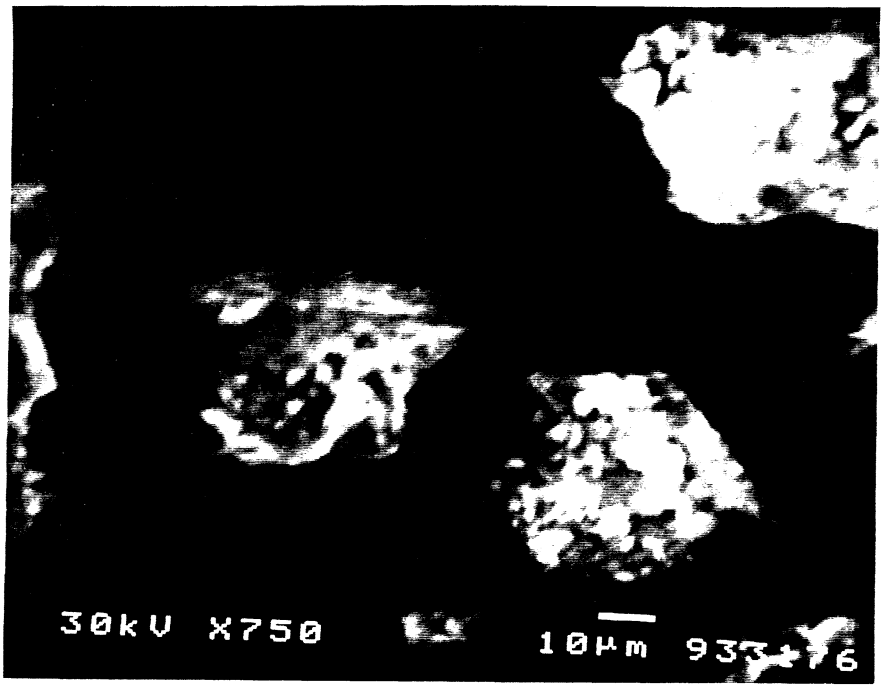

(A)

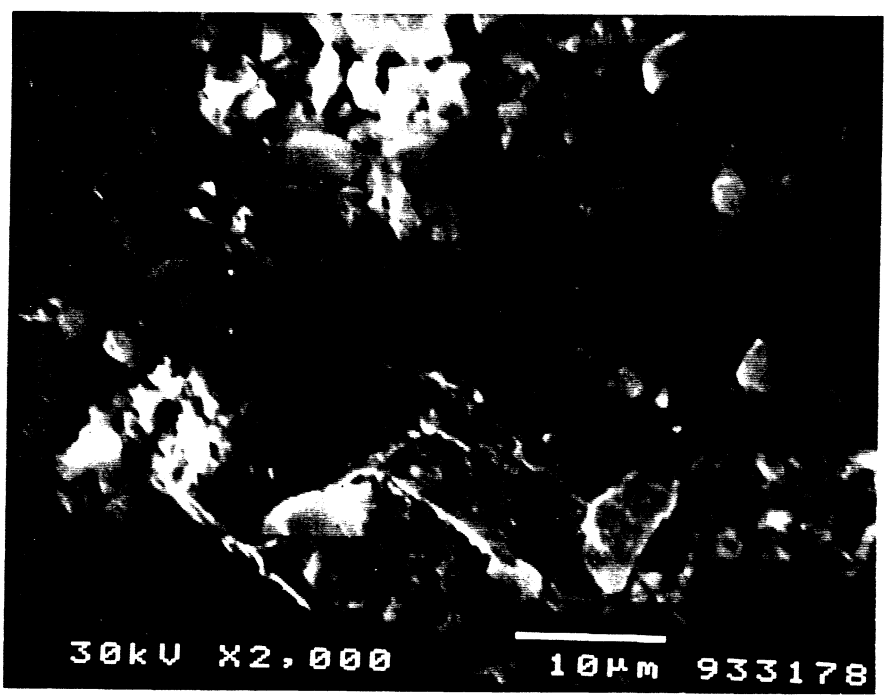

(B)

Figure 5-5: SEM Micrograph of Sieved Carey Limestone -200 + 270 U.S. Mesh Size (53-75 μm)

The SEM analysis, as shown in these figures, gives qualitative results about the pore structure and the surface morphology. Figures 5-1 (A), 5-2 (A), 5-3 (A), 5-4 (A) and 5-5 (A), which were taken at a magnification of 750 times and which were meant to show the external surfaces of the limestones, show that Maxville, Vanport and Bucyrus limestones are less compact than Mississippi and Carey limestones. Maxville and Vanport limestones showed a sponge-like outer surface structure compared to a smooth structure in the case of Mississippi and Carey limestones. Maxville and Vanport limestones showed more "primary" pores along the external surface than Mississippi and Carey stones. These "primary" pores may serve as SO_2 feeder-pores to the interior of the limestone particles and consequently improve sorbent utilization. Cracks along part of the surface of Bucyrus limestone can be seen in Figure 5-4 (A). These cracks may also facilitate the diffusion of SO_2 through the internal limestone pores.

A closer look at individual stones, magnified to 2000 times, gives a better idea about the limestone pore structure. Figures 5-1 (B), 5-2 (B), 5-3 (B), 5-4 (B) and 5-5 (B) represent the SEM micrographs of one individual particle of Maxville, Vanport, Mississippi, Bucyrus and Carey limestones. From these figures, "secondary" pores can be clearly seen and some comparison between the various limestones can be made. Figure 5-1 (B), a high magnified micrograph of a Maxville particle, shows that the "secondary" pores occupy a big portion of the volume of the particle. Vanport and Mississippi limestones,

as shown in Figure 5-2 (B) and Figure 5-3 (B) respectively, show "secondary" pores occupying a much smaller portion of the particle volume when compared to Maxville limestone. The overall structure of these two stones resembles a sponge, with small pores interconnected throughout the particle. Bucyrus limestone, as shown in Figure 5-4 (B), does not appear to have a sponge-like structure. However, thin cracks which extend to the interior of the particle seem to represent the overall pore structure. These cracks may not be as efficient as the pores or holes found in Maxville, Vanport and Mississippi stones in delivering the SO_2 gas through the particle. In addition, stones with a more porous structure have higher surface area available for reaction. Carey limestone, as shown in Figure 5-5 (B), show a less porous structure than Maxville, Vanport and Mississippi stones. In this case, the SO_2/limestone reaction is expected to occur to a lesser extent.

5.1.1.2 Surface Area Determination

Theoretically, the BET surface area is expressed as the sum of the external surface area and the internal surface area. In terms of particle radius, density and surface roughness, Klingspor et al. [1983] suggested the following equation for evaluating the BET surface area:

$$A_S = A_{S0} + \frac{3\sigma}{\rho_p R_p} \qquad (5\text{-}1)$$

Where: A_S: Total BET surface area

A_{S0}: Internal surface area

R_p: Particle radius

ρ_p: Limestone particle density

σ: Correction factor accounting for external surface roughness

A_{SO} and σ are experimentally determined from BET surface area measurements

In terms of the particle shape or sphericity, S_p, the specific surface area based on "external surface area only" is given as:

$$A_S = \frac{3}{S_p R_p}\left(\frac{\rho_S}{\rho_i}\right) \qquad (5\text{-}2)$$

Where: ρ_S: Bulk density of limestone

ρ_i: Inherent density of limestone

S_p: Sphericity of limestone particles

Noting that the ratio of the bulk density to the inherent density is the fraction of the bed occupied by limestone, ϵ_S, Equation (5-2) becomes:

$$A_S = \frac{3\epsilon_S}{S_p R_p} \qquad (5\text{-}3)$$

A typical value for the shape factor or sphericity, S_p, for non-uniform solids is 0.5 (Perry et al., 1987). A value of 0.543 for ϵ_S has been reported and used by Visneski (1991) in modeling the SO_2/limestone reaction in a fixed-bed reactor. A value of 0.5 for ϵ_S has been reported by Yu and Sotirchos (1987).

Taking into consideration the above observations, the limestone surface area can be expressed as a function of particle radius as:

$$A_S = \frac{3.258}{R_p} \qquad (5\text{-}4)$$

According to the screen size analysis for Maxville limestone # LS890118A shown in Table 3-1, the value for the specific area is:

$$A_S = 3.258 \sum \frac{W_{fi}}{R_{p_i}} = 1147 ft^{-1} \qquad (5\text{-}5)$$

The value for the specific surface area for the size range of 53-75 μm is about 31 x 10^3 ft^{-1}.

5.1.2 Chemical Compositions

The chemical compositions for the various limestones used in this study have been reported in Chapter 3. Energy Dispersive Analysis of X-Rays (EDAX) has been conducted to show the different types of elements present in the limestone samples. Through this analysis technique, it is possible to detect the main elements as well as the impurities and get some information about their abundance. Figures 5-6 through 5-8 show the EDAX for Maxville, Vanport and Mississippi limestones, respectively.

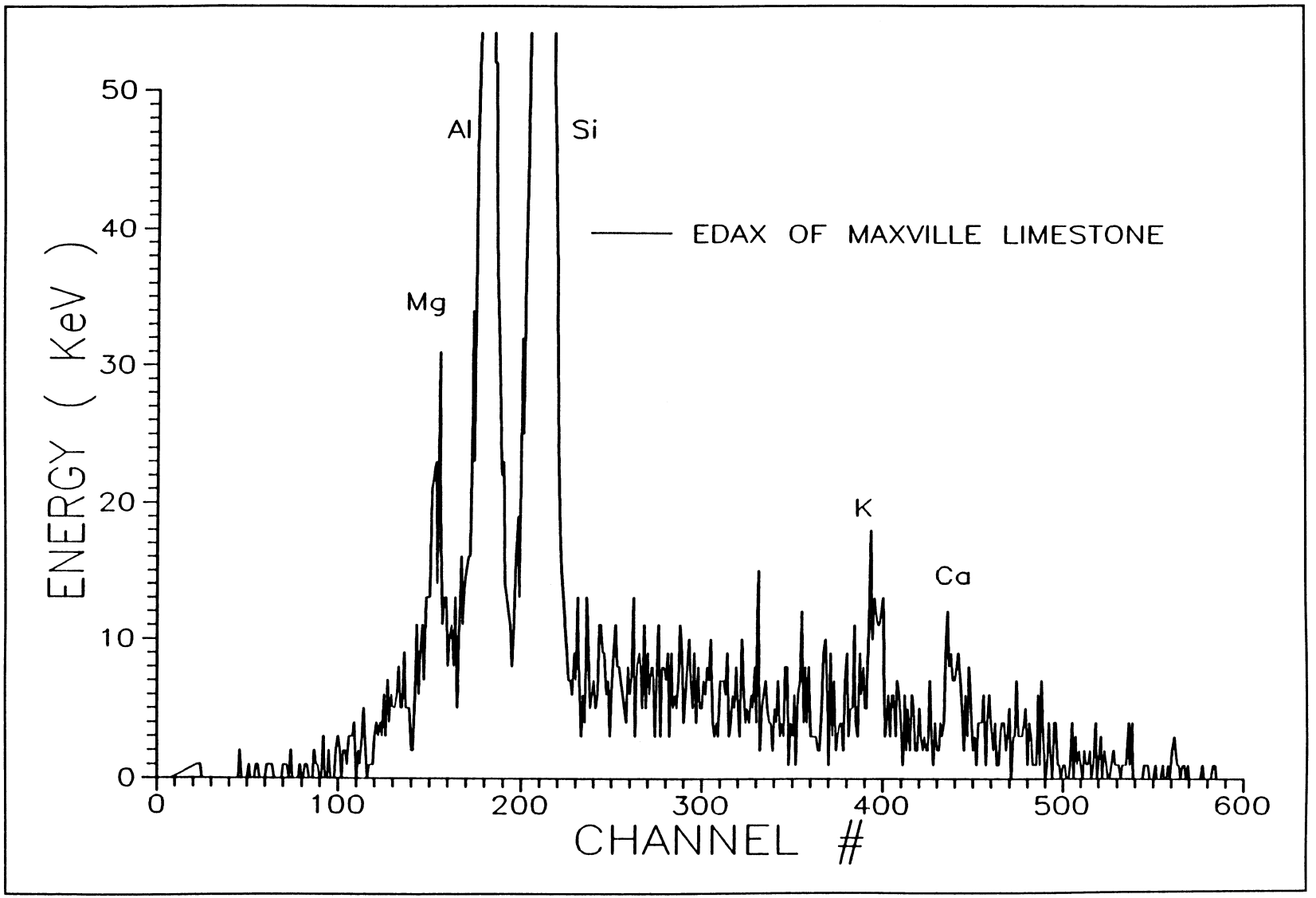

Figure 5-6: EDAX for Maxville Limestone

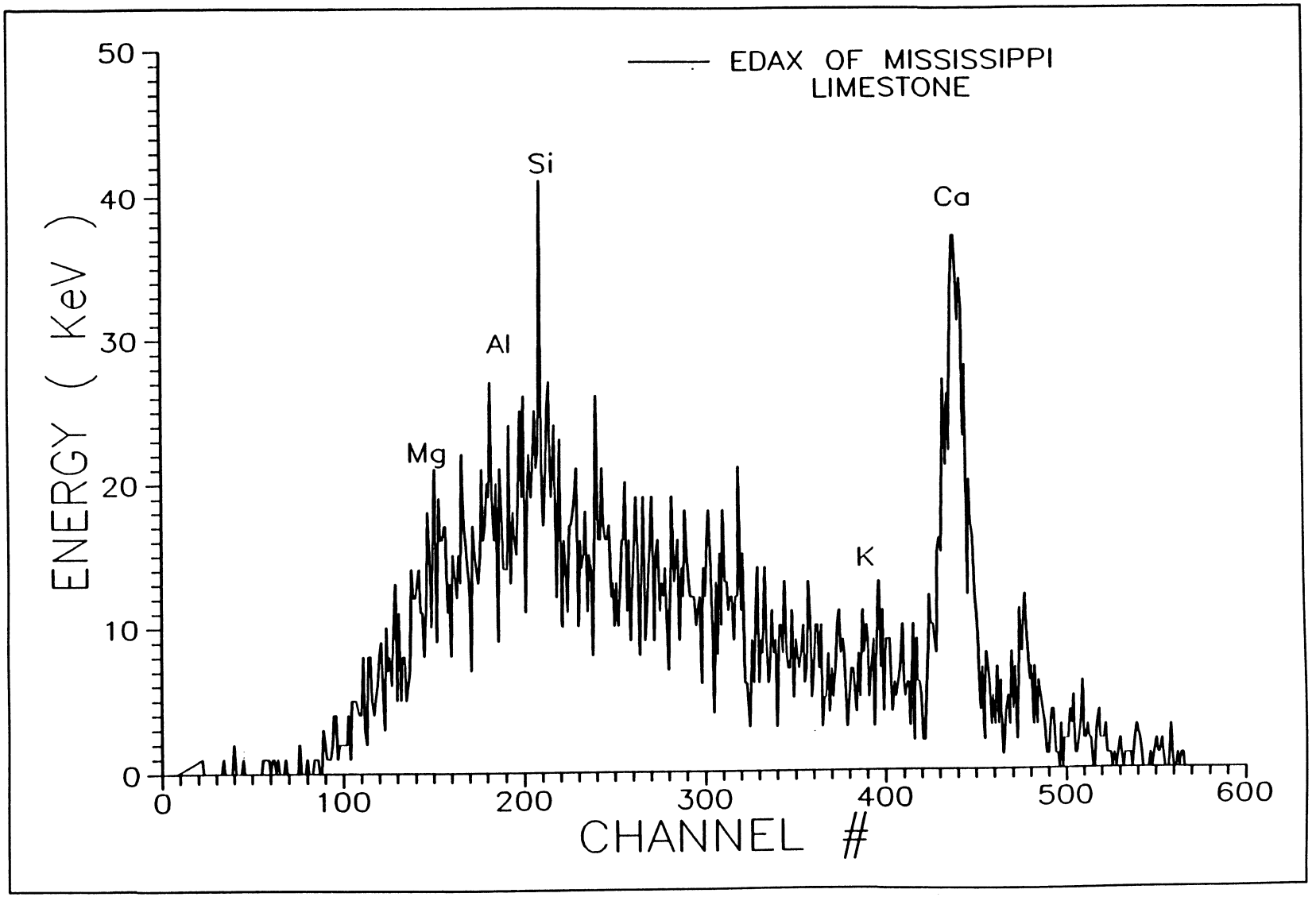

Figure 5-7: EDAX for Mississippi Limestone

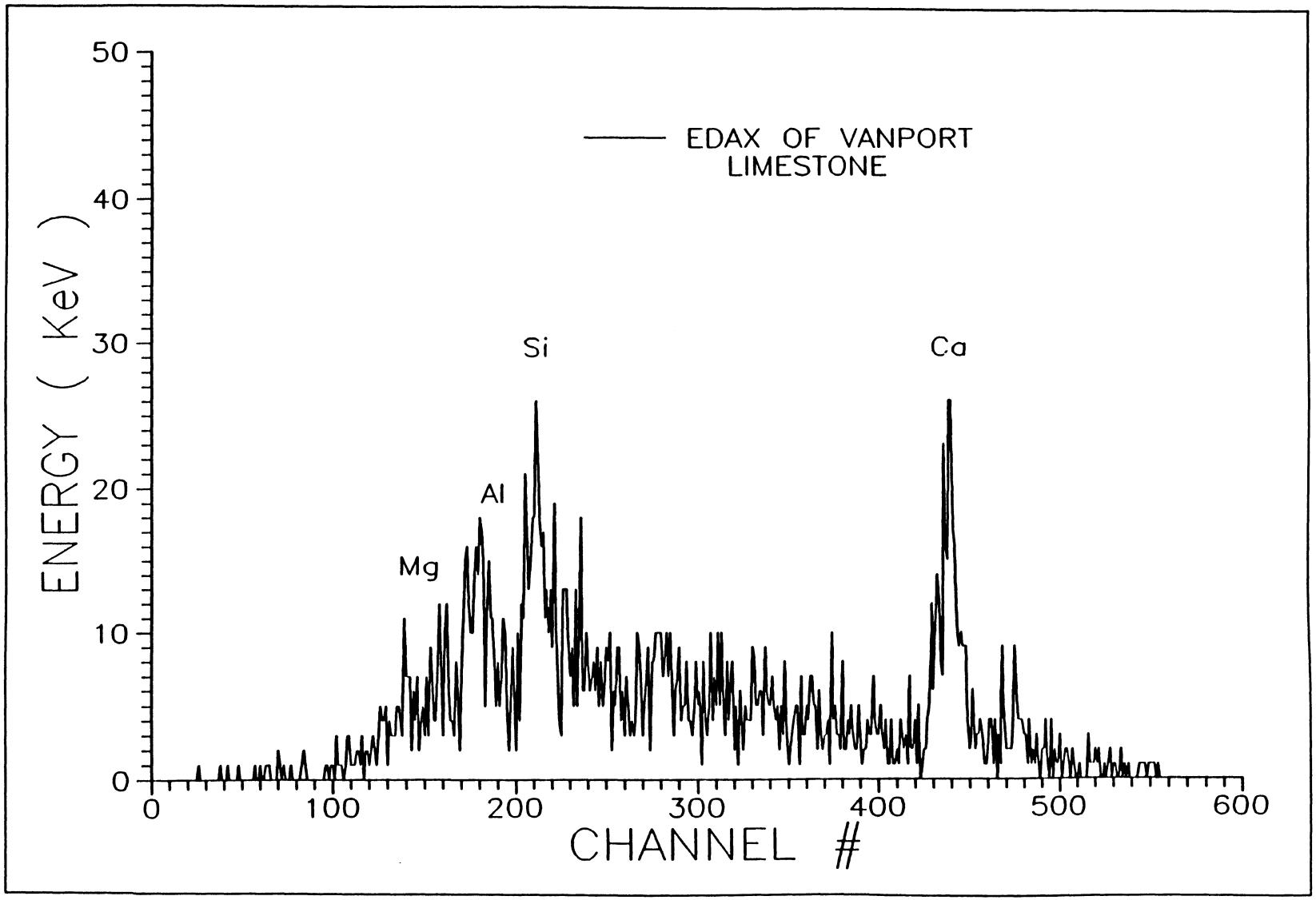

Figure 5-8: EDAX for Vanport Limestone

5.2 Fixed Bed Integral Reactor Experiments

As previously mentioned, Maxville limestone # LS890118A (with size distribution shown in Table 3-1 and plotted in Figure 3-2) was used in this part of the research to investigate the influence of key experimental parameters on the SO_2/limestone reaction. The key controlled conditions were the initial SO_2 concentration, the flue gas relative humidity and the limestone particle size.

Typical results for the outlet SO_2 concentration as a function of time are shown in Figure 5-9. During the initial testing period, the outlet SO_2 concentration was zero, but later it increased and approached that of the inlet gas. To test the reproducibility of the experimental data, two runs at nearly the same inlet SO_2 concentration (i.e. 860 and 825 ppm) with all other variables held constant were performed. Figure 5-9, which is a plot of the data of these two runs, shows a fair correspondence, indicating a degree of reproducibility of the experimental results. Figure 5-10 shows typical percent of SO_2 removal as a function of time.

5.2.1 Influence of Inlet SO_2 Concentration

Figure 5-11 shows the effect of inlet SO_2 concentration on the performance of the limestone bed. Two levels of inlet SO_2 concentration, 850 and 1750 ppm, were used. The results, shown in Figure 5-11, indicate that the SO_2 removal efficiency is decreased as the inlet SO_2 concentration is increased. The operating times at SO_2 removal efficiencies of greater than 90 % were much shorter in the case where high inlet SO_2 concentrations were used. At

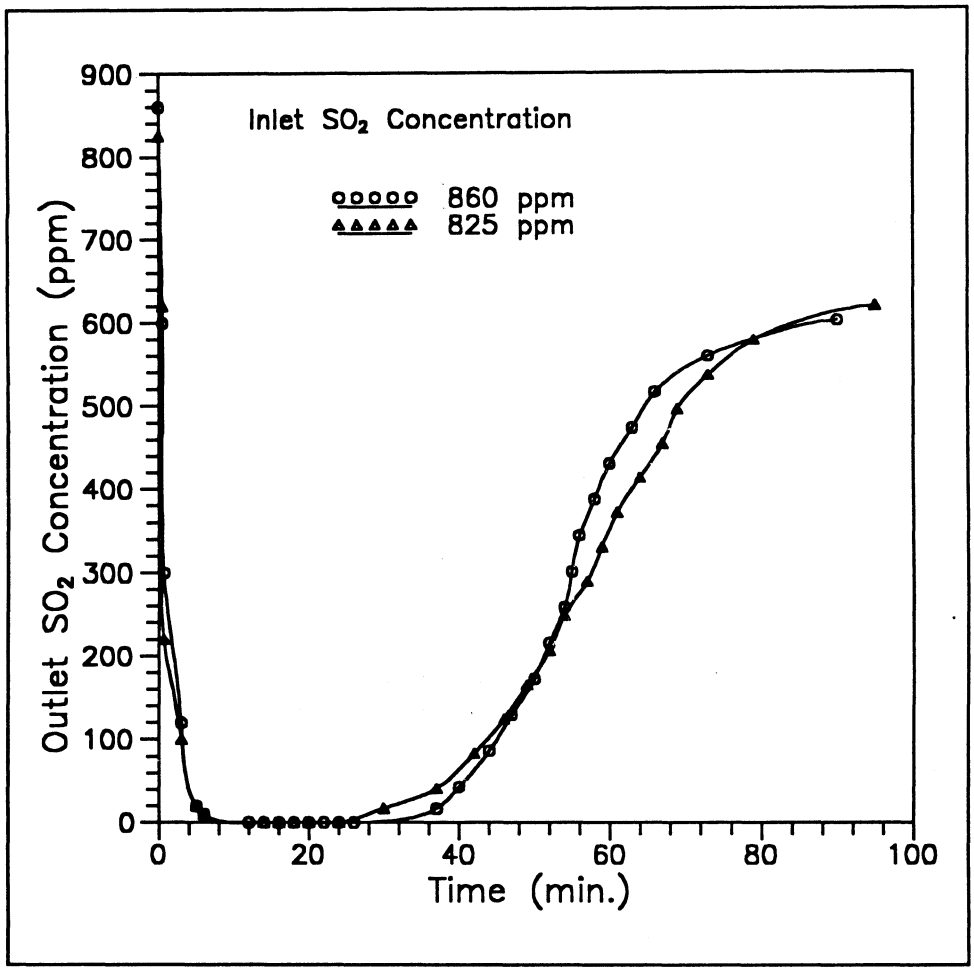

Figure 5-9: Typical Results for Outlet SO_2 Concentration as a Function of Time. Maxville #LS890118A, Flue Gas RH: 75%.

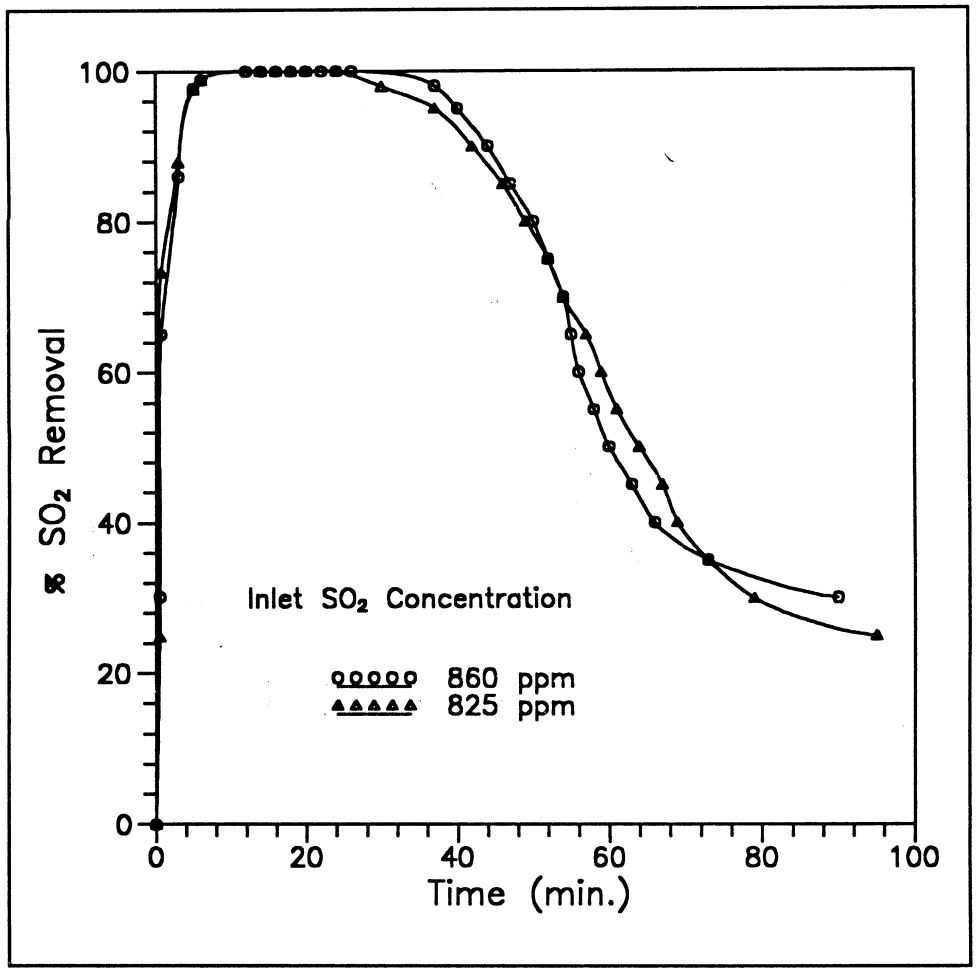

Figure 5-10: Percent of SO_2 Removal as a Function of Time. Maxville #LS890118A, Flue Gas RH: 75%.

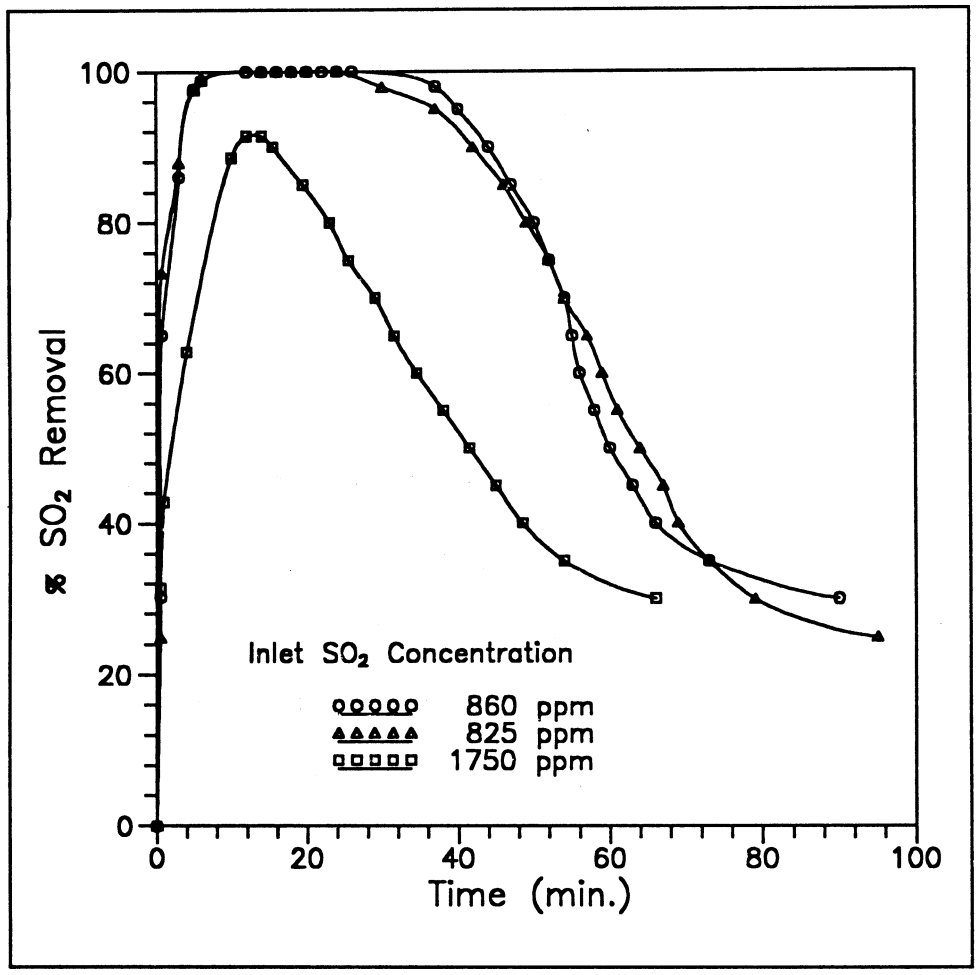

Figure 5-11: Influence of Inlet SO_2 Concentration on Limestone Bed Performance. Maxville #LS890118A, Flue Gas RH: 75%.

low inlet SO_2 concentrations, it was possible to achieve nearly 100 % removal for an initial testing period. Only 90 % SO_2 removal, for a very short operating period, was achieved in the case of high SO_2 concentration.

5.2.2 Influence of Flue Gas Relative Humidity

Figure 5-12 shows the effect of varying the relative humidity of the flue gas introduced into the limestone bed. The data plotted in this figure indicate that the flue gas relative humidity has a profound effect on the SO_2 removal efficiency, which was anticipated because the presence of water is essential for the SO_2/limestone reaction. As the flue gas relative humidity increases, it is expected that the rate of evaporation of water decreases and the limestone takes a longer period of time to dry. This allows the reaction to proceed for a longer period of time, resulting in more SO_2 removal.

An examination of the bench-scale integral experimental data indicated that a significant amount of SO_2 removal, about 5 to 15 %, took place in that part of the limestone bed that is nominally "dry", but humidified. This "dry" effect has also been noticed in the demonstration-scale LEC data (Prudich et al., 1988). Figure 5-13 clearly shows this effect. In the case of a dry limestone bed, the average SO_2 removal efficiency was about 40 % for the first 10 minutes of the testing period, and later it leveled off to about 15 % for an extended period of time. In the case of pre-wet bed, on the other hand, an average SO_2 removal efficiency of 75 % has been achieved over the first 10 minute operating period.

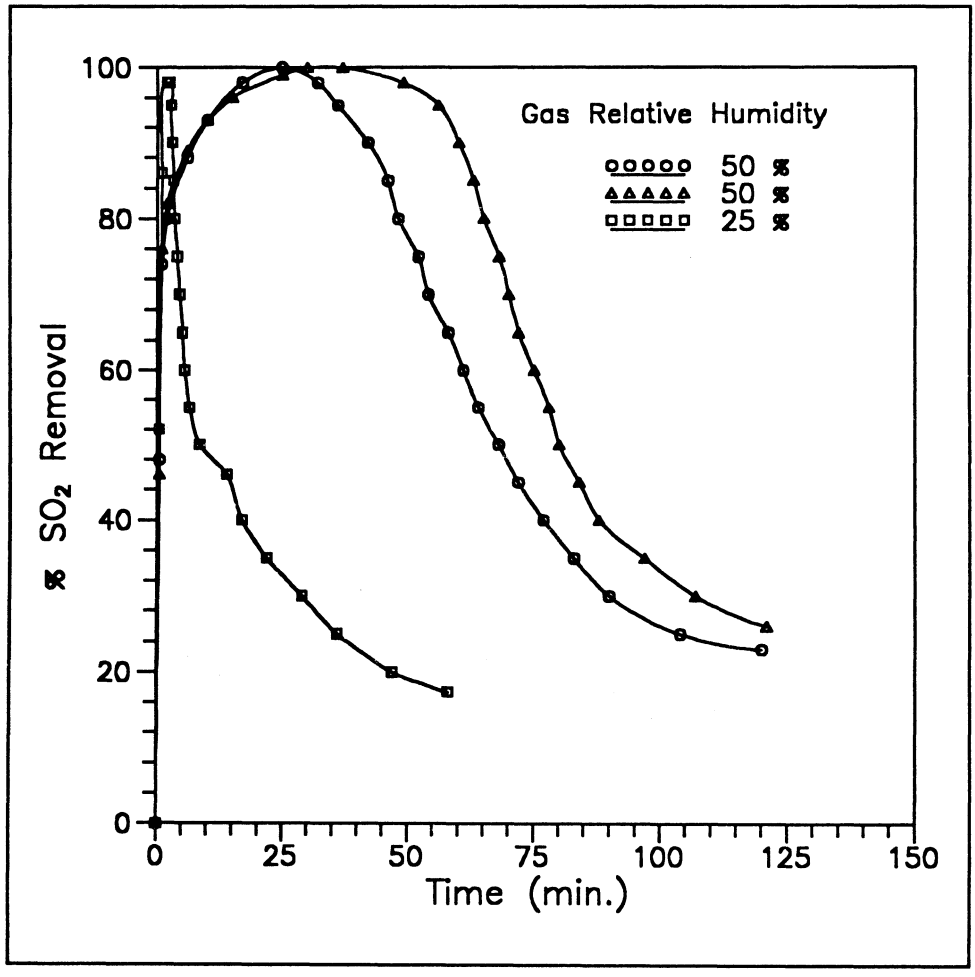

Figure 5-12: Influence of Flue Gas Relative Humidity on Limestone Bed Performance.
Maxville #LS890118A, Inlet SO_2 Conc.: 500 ppm.

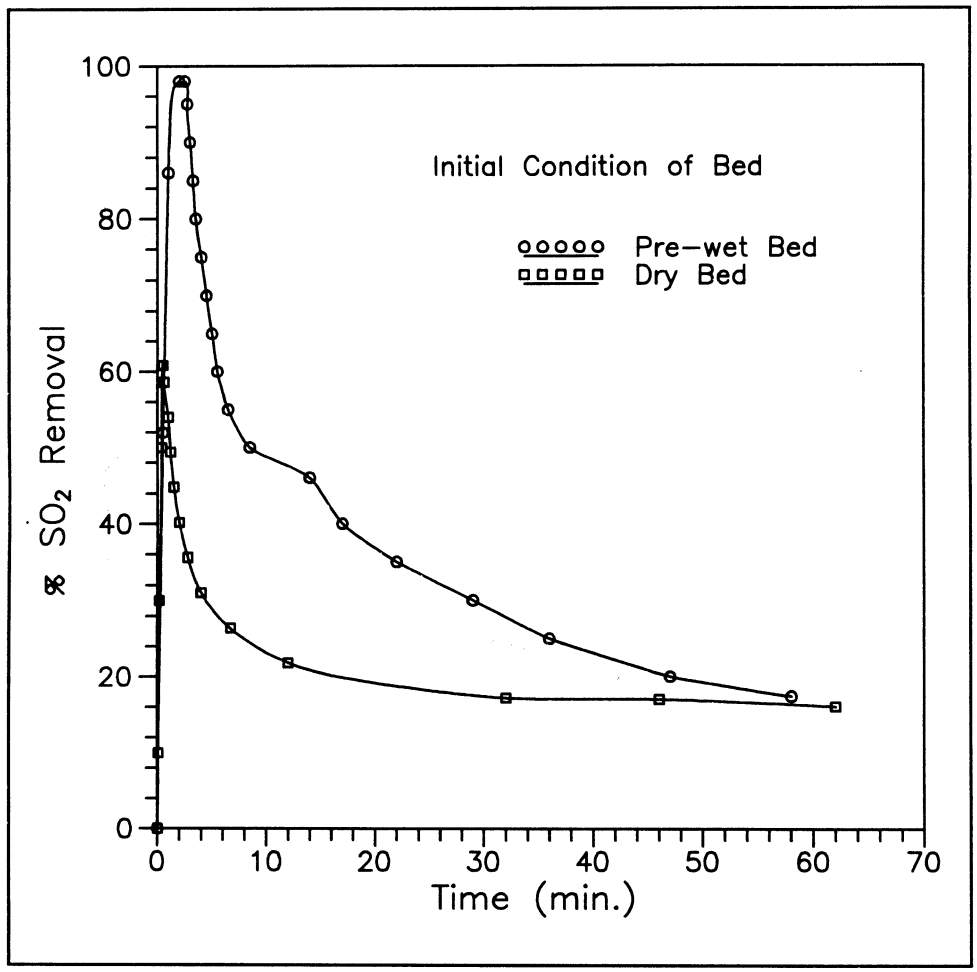

Figure 5-13: Dry Effect in a Fixed Bed of Maxville Limestone # LS890118A. Inlet SO_2 Conc.: 500 ppm, Flue Gas RH: 25 %.

The dry sorbent capture effect was fully investigated using a fixed-bed differential set-up. A mechanistic model was developed for this operating regime. The experimental and modeling results are presented and discussed in a later section.

5.2.3 Influence of Limestone Particle Size

To test the influence of the limestone particle size on the SO_2 removal performance, three size cuts were used. The biggest limestone size range was -8+10 mesh (i.e. 2.00-2.36 mm), with an average particle diameter of 2.18 mm. The middle size range, -16+18 mesh (i.e. 1.00-1.18 mm), was chosen in a way that its average particle diameter (1.09) was half that of the largest size range. The smallest size range, -30+35 mesh (i.e. 0.500-0.600 mm), had an average particle diameter of 0.55 mm, which was half that of the middle size range.

Figure 5-14 shows the SO_2 removal efficiency as a function of time for these three size cuts of Maxville limestone. The smallest limestone size range uniformly shows higher SO_2 removal efficiency than the intermediate and the larger size cuts over the first 30 minutes of the operating period. At a later time, the SO_2 removal efficiency was nearly the same for all these limestone size cuts. This might be explained by the fact that the limestone surface area available for reaction beyond that critical time is nearly the same for the three different size ranges, which was caused by partial surface blinding by the reaction products. This may also be attributable to the drying of the limestone

bed. The average SO_2 removal efficiency over the first 20 minute operating period, as shown in Figure 5-15, was about 60, 87 and 93 % for the largest, intermediate and smallest size cuts, respectively. The higher SO_2 removal performance could be attributed to the increase in the amount of limestone surface area per unit mass.

5.2.4 Characterization of Reacted Limestone

A partially reacted sample of sieved Maxville limestone, -8+10 mesh size, was analyzed using Scanning Electron Microscopy. Figure 5-16 shows the SEM micrograph of limestone particles before and after sulfation.

Visual examination of Figure 5-16 (B) reveals that needle-shaped crystals are formed on the limestone surface, making it partially blinded. These crystals, as shown in Figure 5-17, are 10-50 μm long and 2 μm wide and they are combined (fused) together.

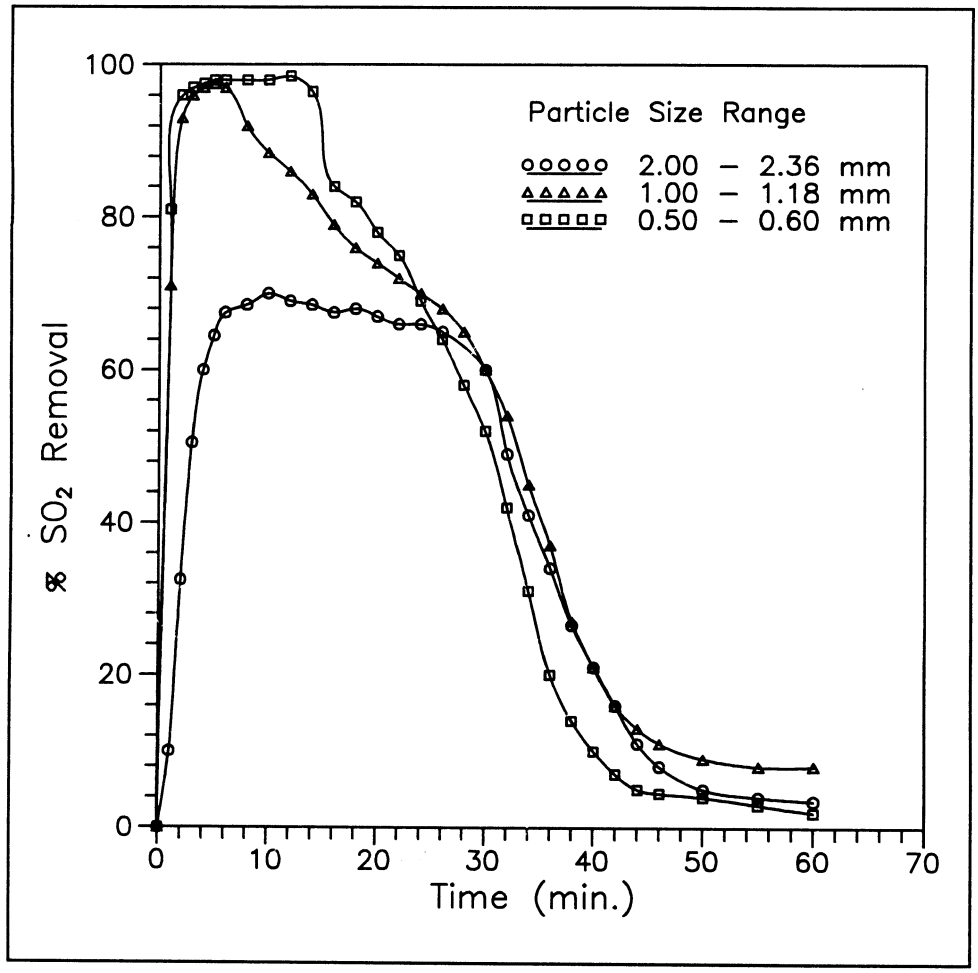

Figure 5-14: Influence of Limestone Particle Size on Bed Performance. Maxville Limestone. Inlet SO_2 Conc.: 500 ppm, Flue Gas RH: 50 %.

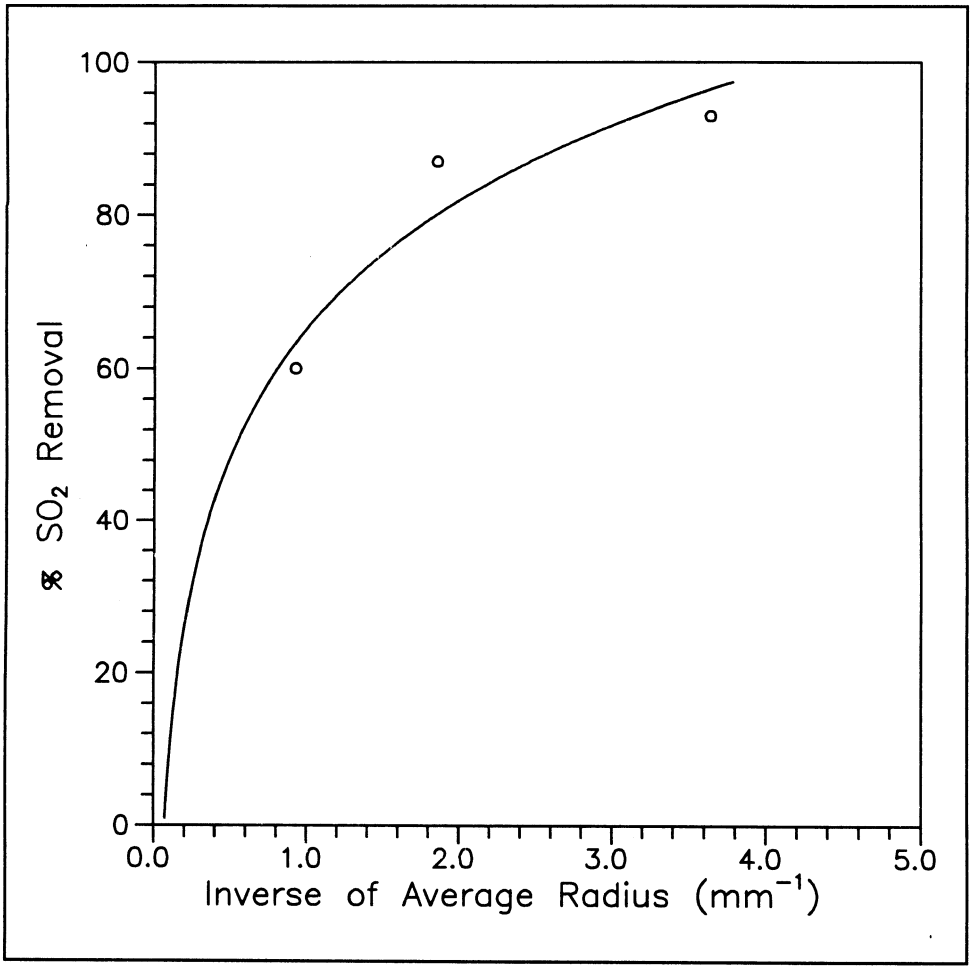

Figure 5-15: Average SO_2 Removal Efficiency over First 20 Minute Operating Period as a Function of Limestone Particle Size.

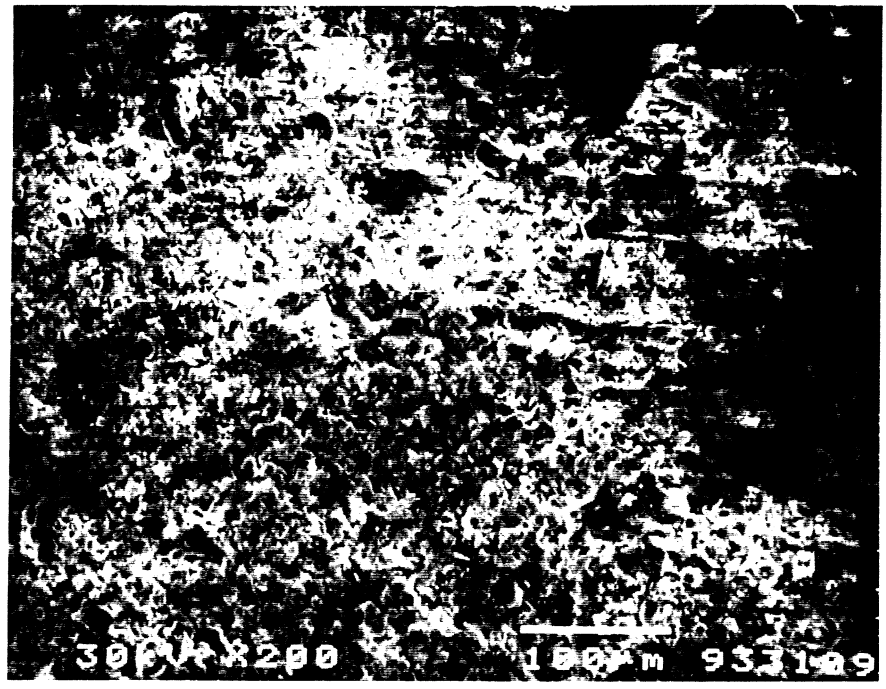

(A)

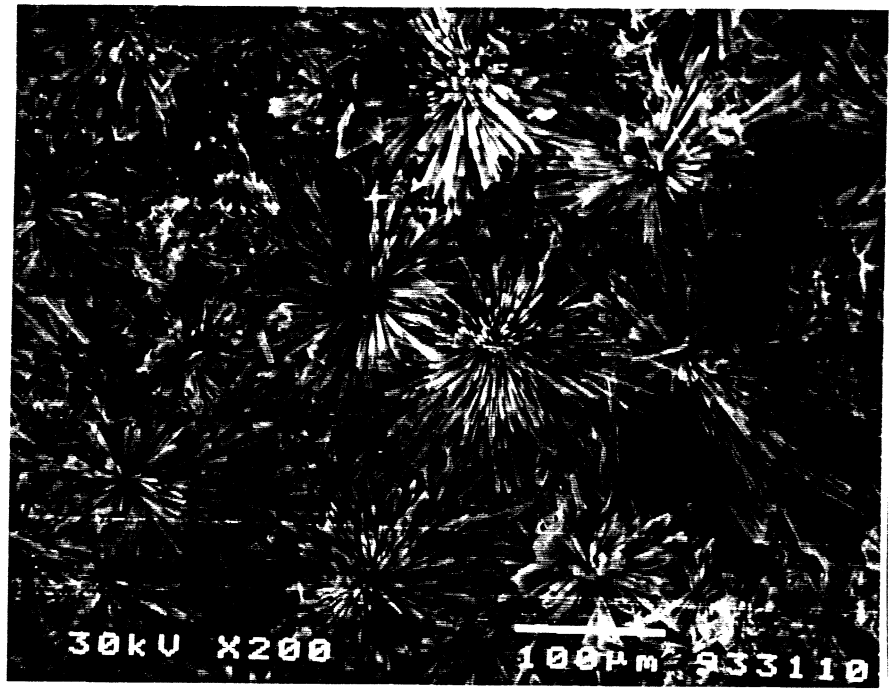

(B)

Figure 5-16: SEM Micrograph of Sieved Maxville Limestone -8+10 U.S. Mesh Size (2.00-2.36 mm) Before and After Sulfation.

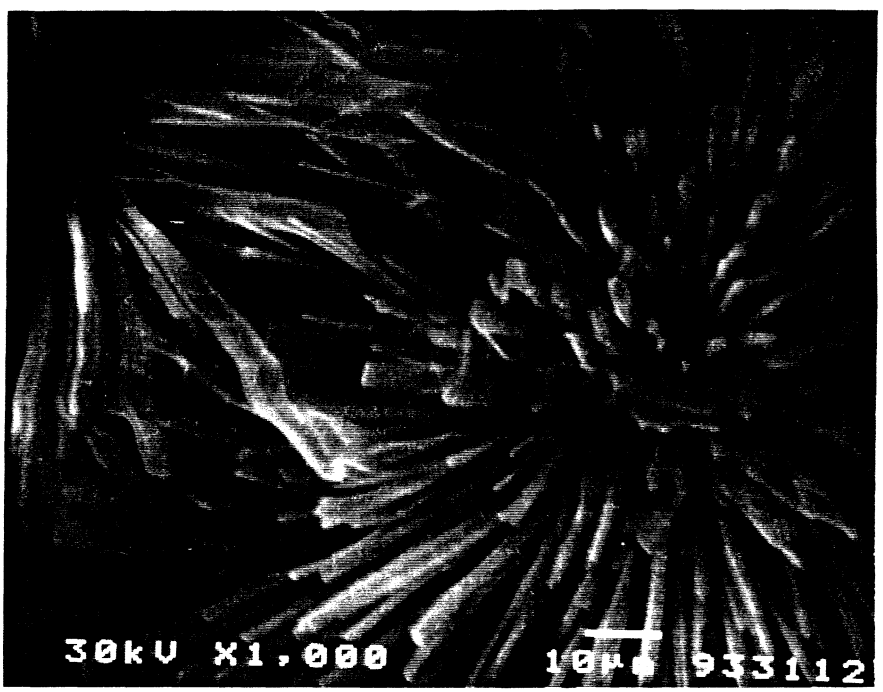

Figure 5-17: SEM Micrograph of Sieved Maxville Limestone -8+10 U.S. Mesh Size (2.00-2.36 mm) Showing Needle Structure.

5.3 Differential Reactor Experiments

As mentioned earlier, this part of the research program mainly focused on the humidified/dry capture operating regime, in which humidified flue gas was contacted with dry limestone samples. The key parameters investigated include limestone type (i.e. having different chemical and physical properties), flue gas relative humidity (40-95 %) and limestone particle size (64-363 μm).

5.3.1 Influence of Gas Relative Humidity on Reaction Rate

Previous studies have demonstrated the importance of water on the limestone reactivity with SO_2 (Seeker et al., 1986; Klingspor et al., 1983; Jorgensen et al., 1987).

Conversion versus time data for Maxville, Mississippi, Vanport, Bucyrus and Carey limestones are presented in Appendix D. Figure 5-18 shows typical conversion versus time results for Maxville limestone at flue gas relative humidities ranging from 40 to 95 %. Conversion versus time results for the other four limestones are shown in Figures D-1 through D-4. Initial reaction rates were obtained from these results and are plotted as a function of flue gas relative humidity in Figures 5-19 through 5-23. As can be seen for all limestones evaluated, the reaction rate was strongly dependent on the flue gas relative humidity. At very low values of flue gas relative humidity (i.e. 0 to 40 %), the reaction rate was nearly zero. The reaction rate followed a power function with respect to flue gas relative humidity. This could be attributed to the fact that more monolayers of water vapor were adsorbed onto the

limestone surface.

Parameters of the dry capture model developed in Chapter 4 were calculated using the reaction rate versus flue gas relative humidity results. The method by which this was done will be presented and discussed in a later section.

An examination of the reaction rate versus flue gas relative humidity data for the different limestones investigated indicated that these sorbents have varying abilities in capturing SO_2 from the flue gas. This difference can be attributed to both chemical and physical properties of the limestones. Carey limestone, which is dolomitic, showed lower reaction rates when compared to calcitic Maxville and Vanport limestones

According to their SEM micrographs, Maxville and Vanport limestones showed more "primary" pores on the external surface than Mississippi and Carey stones. This might have provided more surface area per unit mass available for reaction, resulting in higher reaction rates.

BET surface area data for Maxville, Vanport and Carey limestones obtained for a size range of -80 + 100 mesh (Mandal, 1993), indicated that the reaction rate for limestones may be primarily a function of sorbent surface area available for reaction. Table 5-1 shows the BET surface area data for the -80 + 100 mesh size range and the initial reaction rates at 95% flue gas relative humidity and for the -200 + 270 mesh size range. These results indicate that the reaction rate is nearly proportional to the BET surface area.

Limestone Type	BET Surface Area (m^2/g)*	Initial Reaction Rate (mole/kg.hr)**
Maxville	5.2	15.4
Vanport	3.1	8.4
Carey	2.6	3.8

Table 5-1: Initial Reaction Rate as a Function of BET Surface Area. * -80+100 Mesh Size, ** -200+270 Mesh Size and for 95% Flue Gas Relative Humidity.

Dissolution rate results (Maldei, 1993), as shown in Table 5-2, for the limestones used in this research, indicated that Maxville and Vanport stones had higher dissolution rates than Mississippi, Bucyrus and Carey limestones. This might also have contributed to the higher reaction rates observed in the sulfation process.

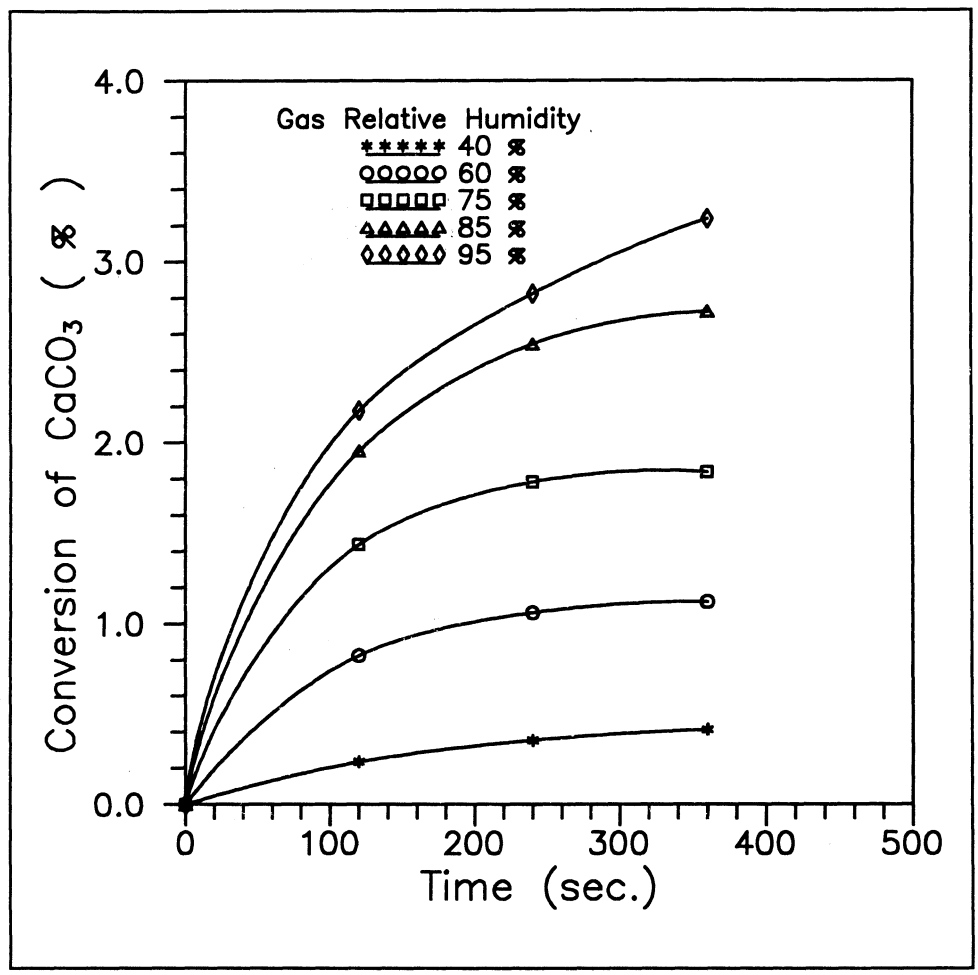

Figure 5-18: Conversion of Maxville Limestone (53-75 μm) as a Function of Time for Various Gas Relative Humidities.

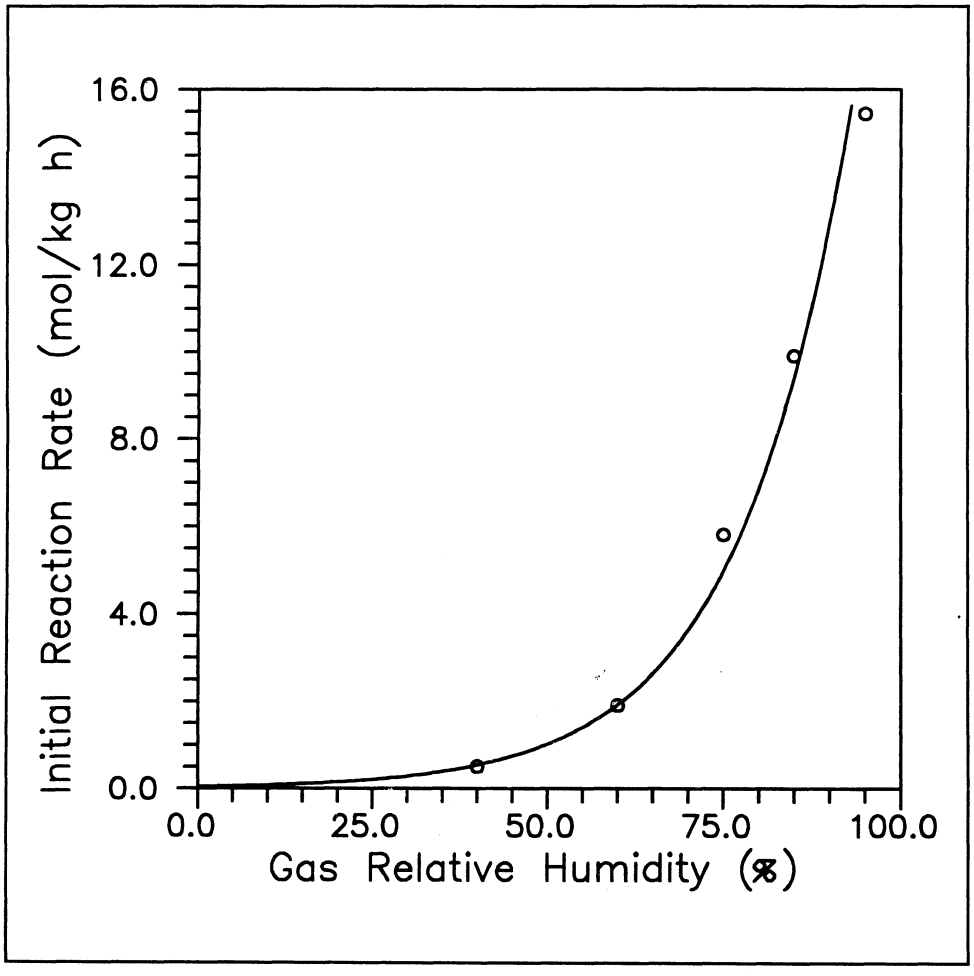

Figure 5-19: Initial Reaction Rate as a Function of Gas Relative Humidity for Maxville Limestone (53-75 μm).

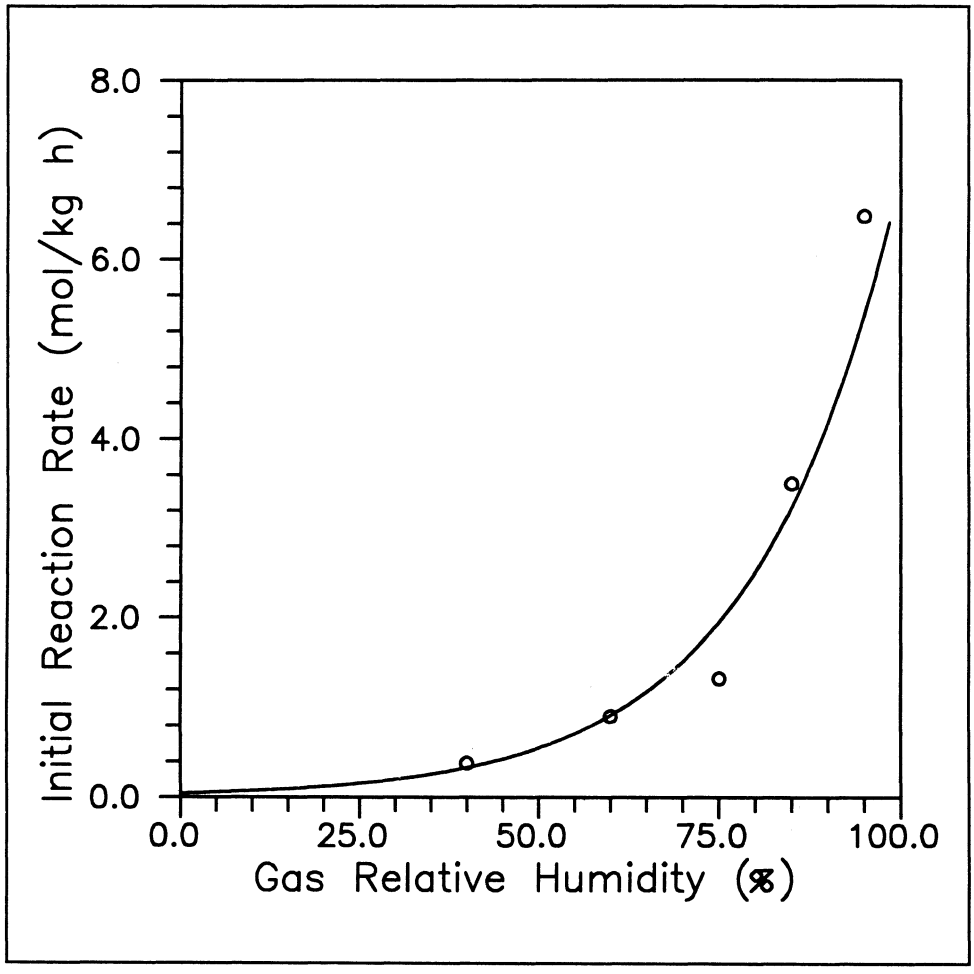

Figure 5-20: Initial Reaction Rate as a Function of Gas Relative Humidity for Mississippi Limestone (53-75 μm).

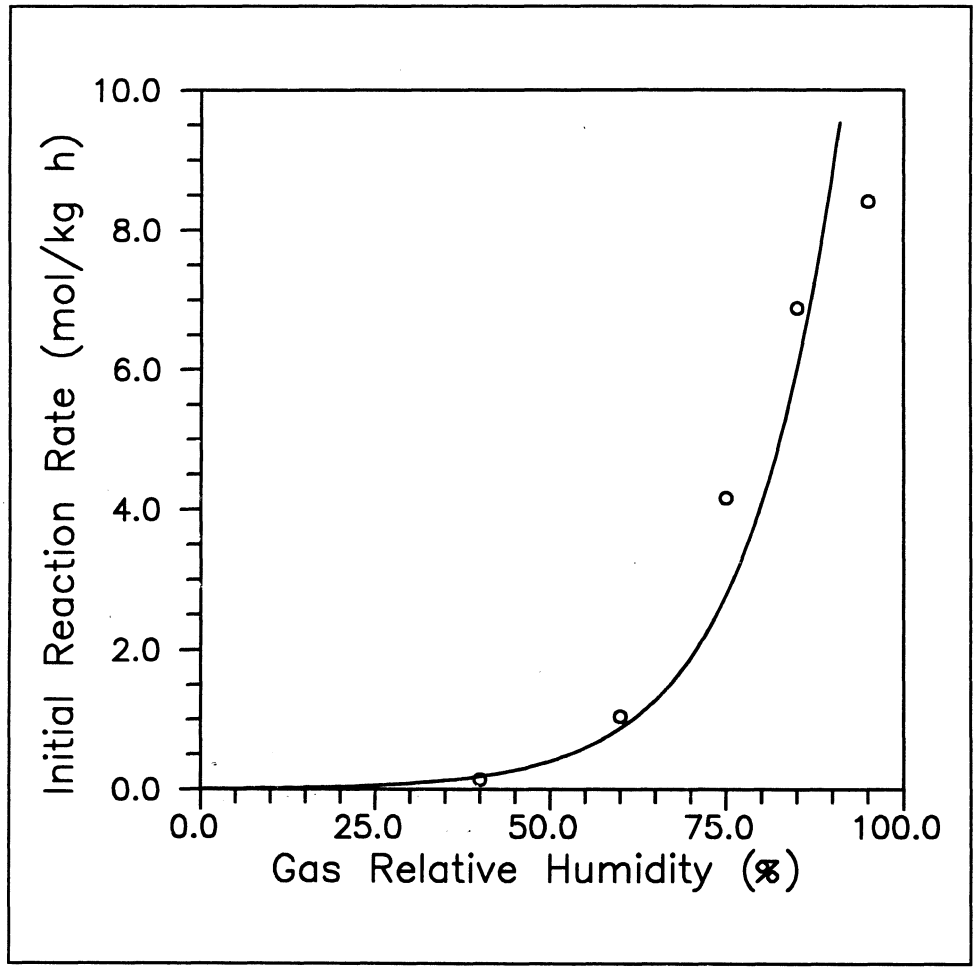

Figure 5-21: Initial Reaction Rate as a Function of Gas Relative Humidity for Vanport Limestone (53-75 μm).

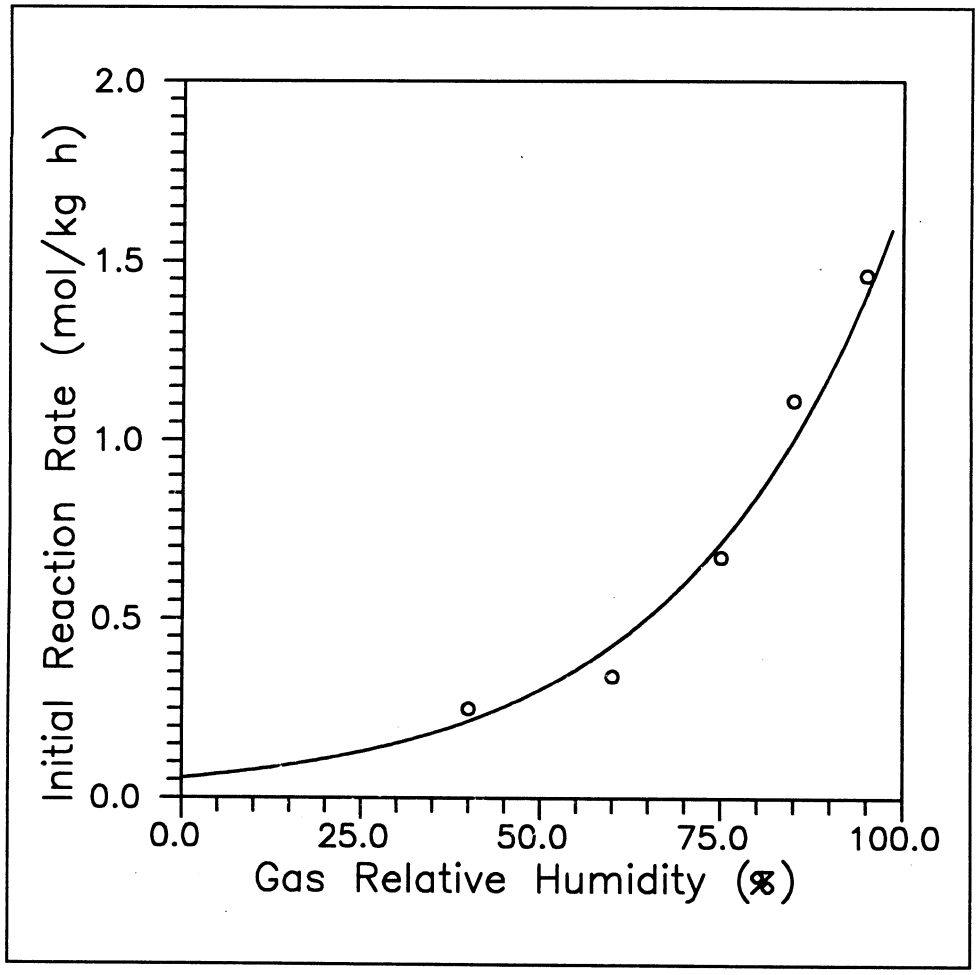

Figure 5-22: Initial Reaction Rate as a Function of Gas Relative Humidity for Bucyrus Limestone (53-75 μm).

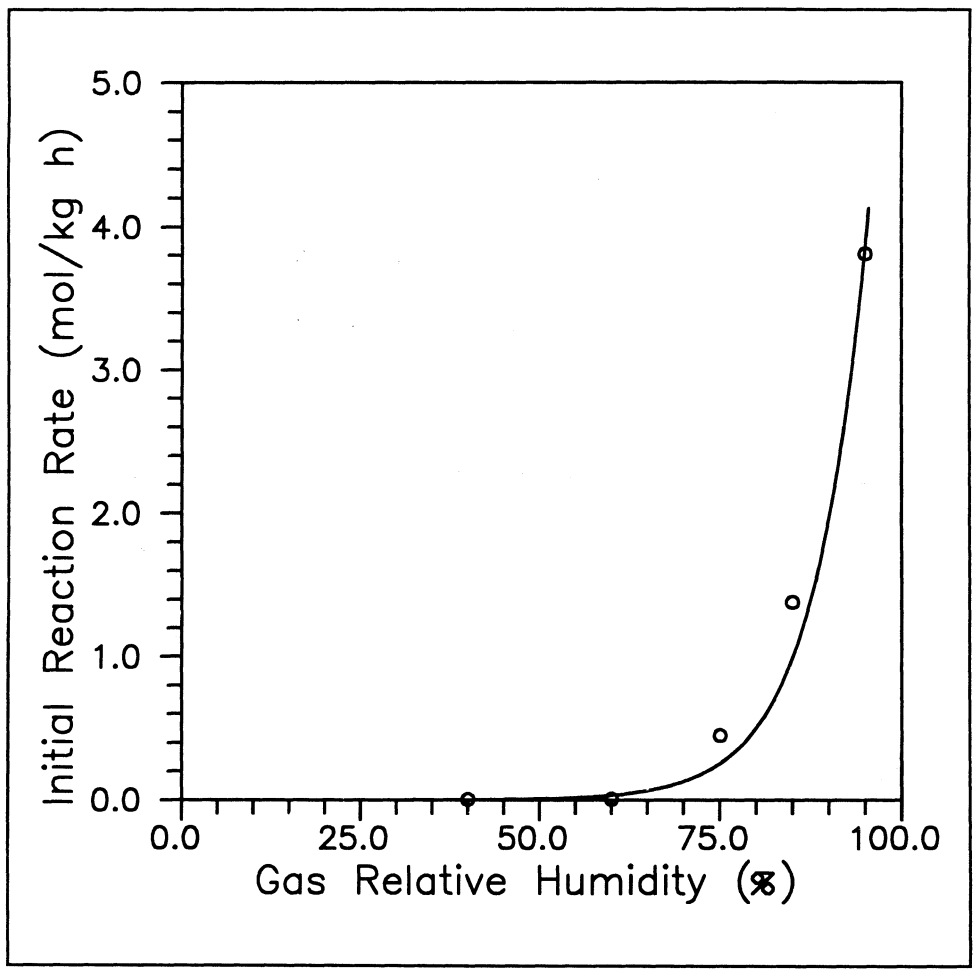

Figure 5-23: Initial Reaction Rate as a Function of Gas Relative Humidity for Carey Limestone (53-75 μm).

5.3.2 Influence of Limestone Particle Size on Reaction Rate

Four particle size cuts were used to study the influence of limestone particle size on the reaction rate. They were : -200+270 mesh (i.e. 53 - 75 μm), -80+100 mesh (i.e. 150 - 180 μm), -50+60 mesh (i.e. 250 - 300 μm), and -40+50 mesh (i.e. 300 - 425 μm), with average particle diameters of 64 μm, 165 μm, 275 μm and 363 μm, respectively. Maxville limestone was chosen for these tests because it showed a better ability to react with SO_2 as compared to the other four limestones.

Figure 5-24 shows a plot of the conversion versus time data for the various sizes of Maxville particles used. Initial reaction rates have been obtained from these results and have been plotted as a function of the inverse particle radius in Figure 5-25. As expected, the reaction rate profoundly increased with decreasing limestone particle size. The rate is linearly proportional to the inverse of the particle radius.

For dry sorbent capture, the controlling resistance is either gas film or dissolution control. Experimental conditions used in this study were intended to eliminate gas film resistance. Small particle sizes, small sample size and high flue gas velocity were used in order to minimize these effects. The rate of transport, g_S, is then given by the following equation :

$$g_S = k_{mc} A_{ml} C_{cle} = k_{mc} f A_{mp} C_{cle} \qquad (5\text{-}6)$$

Where k_{mc}: Mass transfer coefficient for Ca^{2+} in the dissolution zone
C_{cle}: Solubility of limestone
The product $k_{mc}C_{cle}$ is the limestone dissolution rate per unit area.

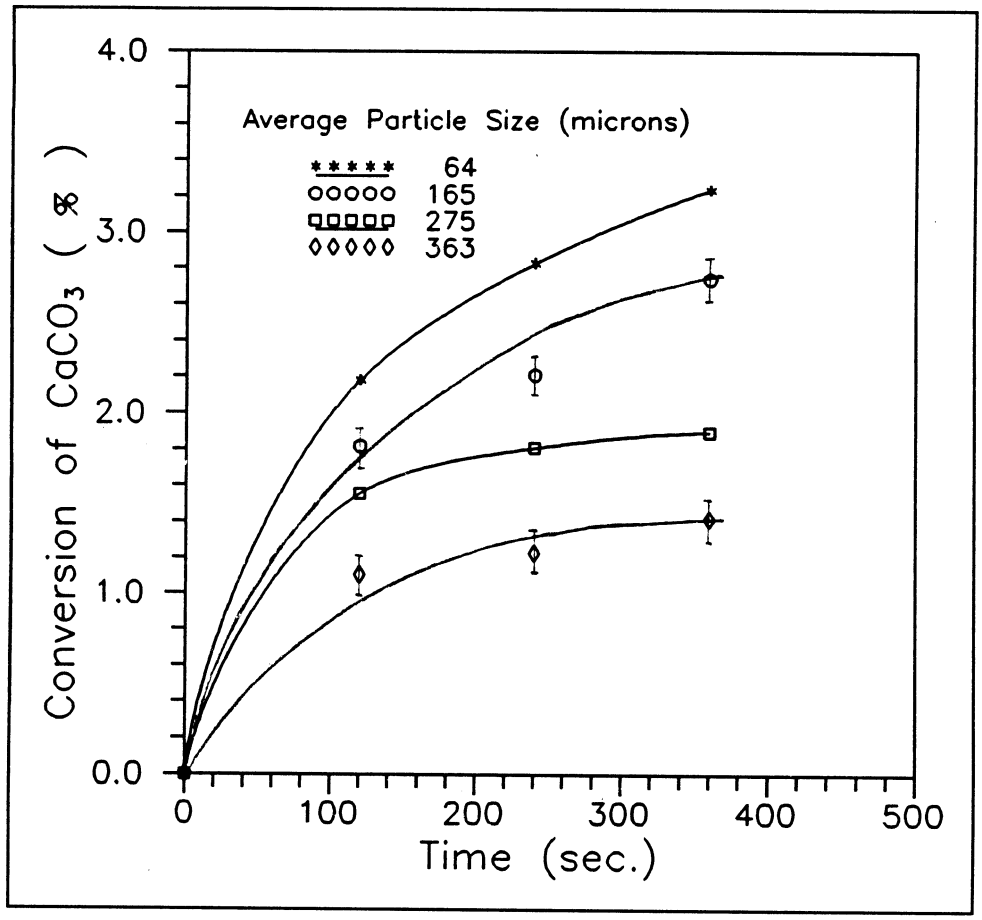

Figure 5-24: Conversion of Maxville Limestone as a Function of Time for Various Particle Size Ranges. Flue Gas Relative Humidity : 95 %. Error Bars: Standard Deviation Error.

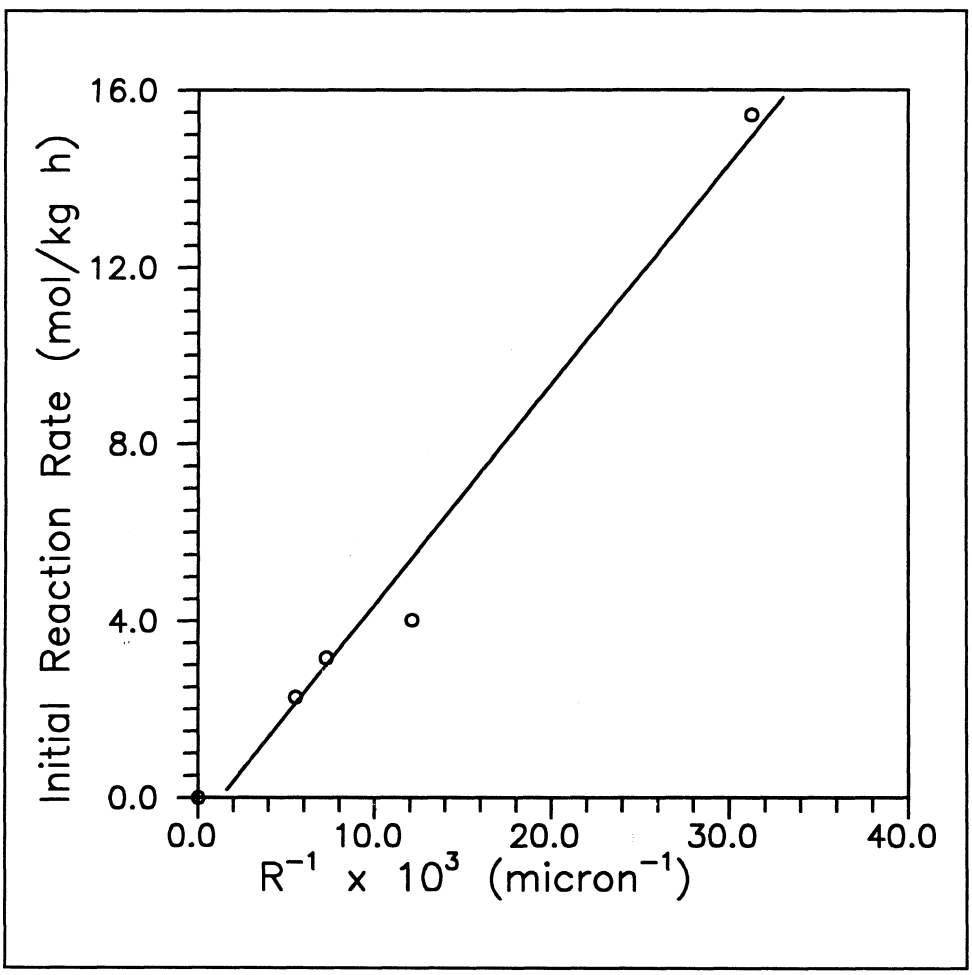

Figure 5-25: Initial Reaction Rate as a Function of Inverse Particle Radius. Flue Gas Relative Humidity : 95 %.

Since initial reaction rates were used, the whole limestone surface area was available for mass transfer (i.e. A_{mp} is equal to A_S, which is the limestone surface area). In this case, g_S will be proportional to A_S :

$$g_S \propto A_S = \frac{3.258}{R_p} \qquad (5\text{-}7)$$

This is in good agreement with the results shown in Figure 5-25.

5.3.3 Dry Sorbent Capture Model Results

The model for dry sorbent capture has been developed in Chapter 4. The dry capture correction factor, f, which represents the ratio of mass transfer area covered by liquid water (A_{ml}) to the total mass transfer area available within the precipitate (A_{mp}), has been related to the flue gas fractional relative humidity in a Langmuir isotherm form as :

$$f = \frac{(1-k)\,RH}{1-k\,RH} \qquad (5\text{-}8)$$

The experimental results, which give the initial reaction rate versus the flue gas relative humidity for Maxville, Mississippi, Vanport, Bucyrus and Carey limestones, were used to determine the model parameter k. It should be noted that initial reaction rates were required for this purpose to eliminate the blinding effects of the product precipitate layer. In this case, the whole limestone surface area will be available for mass transfer. Tables D-39 through D-43 in Appendix D show the experimental initial reaction rates versus flue gas fractional relative humidity data for Maxville, Mississippi, Vanport, Bucyrus and

Carey limestones.

Values for the correction factor, f, were obtained by equating the experimental reaction rate, $g_{S,exp}$, and the calculated rate. The initial reaction rate was calculated using Equation (5-6). The value for the parameter, k, was varied to minimize the least squares error between the experimental and the calculated reaction rates. Dissolution rates for Maxville, Mississippi, Vanport, Bucyrus and Carey limestones at 140 °F and pH = 5.0 obtained by Maldei [1993] were used. These are presented in Table 5-2.

Limestone Type	Dissolution Rate (lbmole/ft^2 sec)
Maxville	1.7×10^{-8}
Mississippi	6.3×10^{-9}
Vanport	1.0×10^{-8}
Bucyrus	1.6×10^{-9}
Carey	3.2×10^{-9}

Table 5-2: Dissolution Rates for Limestones Used at 140 °F and pH = 5.0 [Maldei, 1993].

The best values for the parameter, k, were determined as discussed above and are listed for each limestone in Table 5-3, with an average value of 0.88.

Limestone Type	Dry Capture Model Parameter (k)
Maxville	0.89
Mississippi	0.87
Vanport	0.88
Bucyrus	0.87
Carey	0.89

Table 5-3: Values for Dry Capture Model Parameter, k.

Figures 5-26 through 5-30 show plots of best fit curves along with experimental data for Maxville, Mississippi, Vanport, Bucyrus and Carey limestones, respectively.

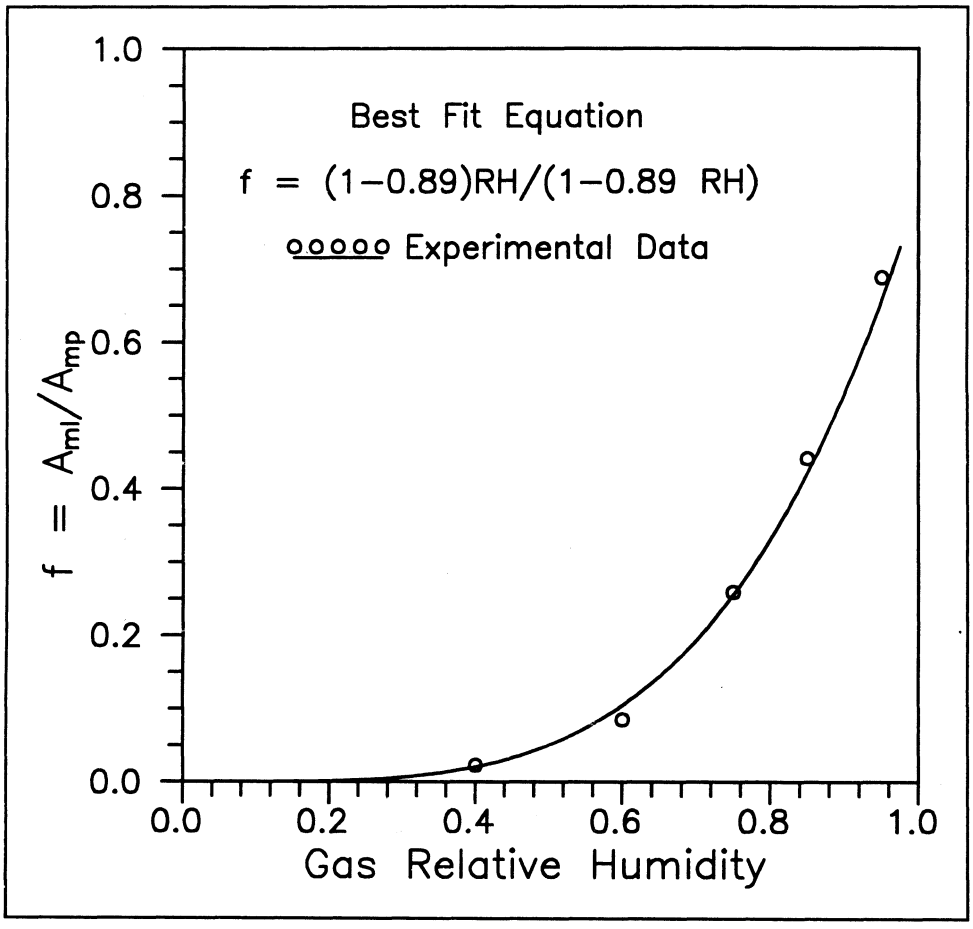

Figure 5-26: Dry Capture Correction Factor as a Function of Gas Fractional Relative Humidity for Maxville Limestone (53-75 μm).

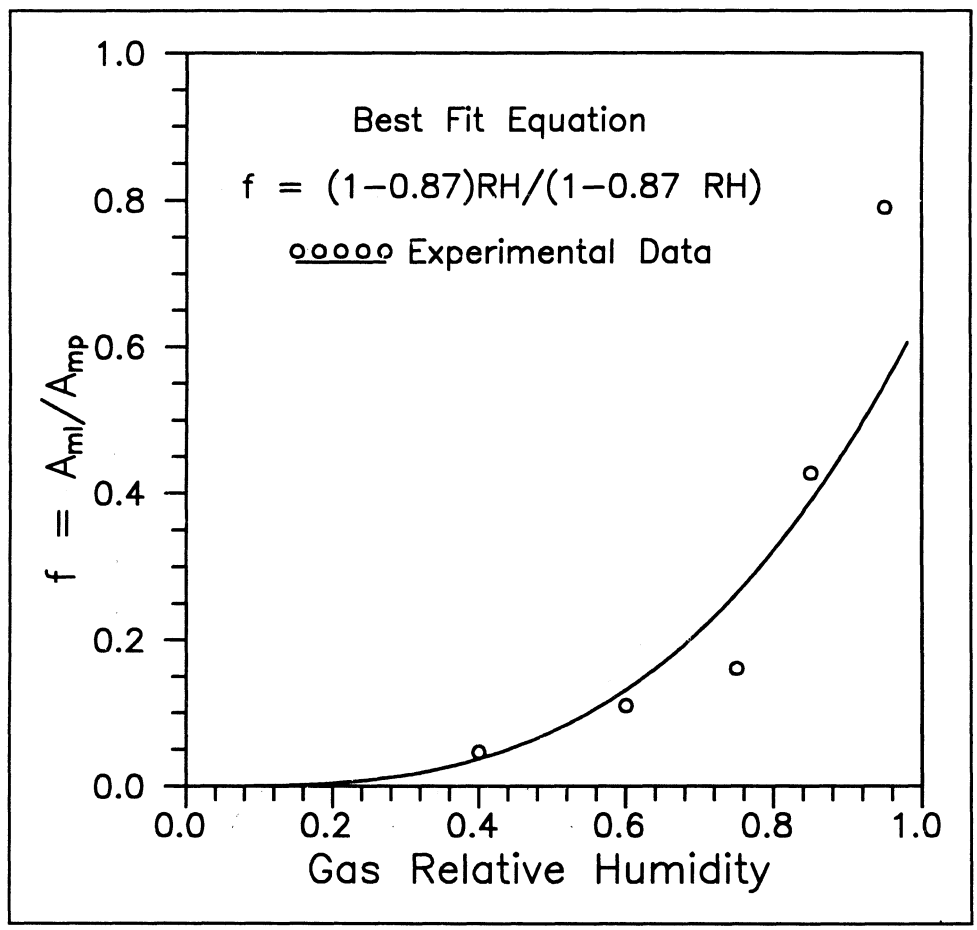

Figure 5-27: Dry Capture Correction Factor as a Function of Gas Fractional Relative Humidity for Mississippi Limestone (53-75 μm).

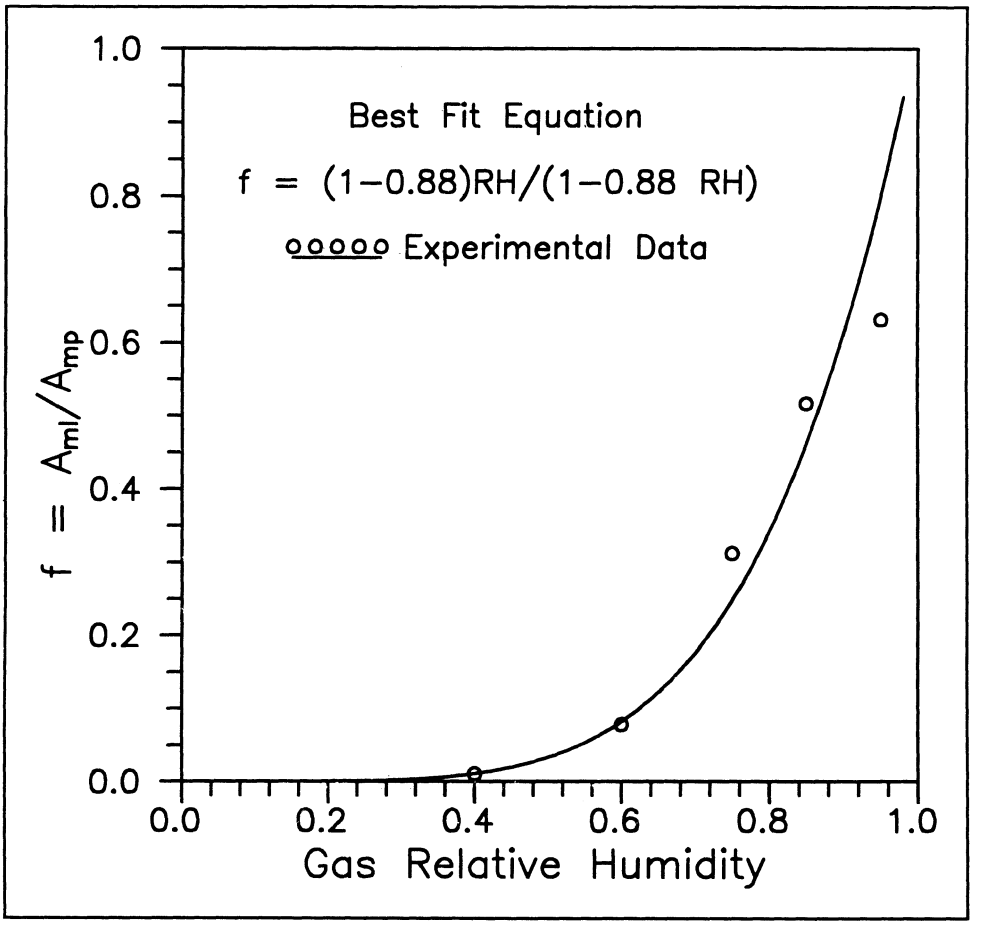

Figure 5-28: Dry Capture Correction Factor as a Function of Gas Fractional Relative Humidity for Vanport Limestone (53-75 μm).

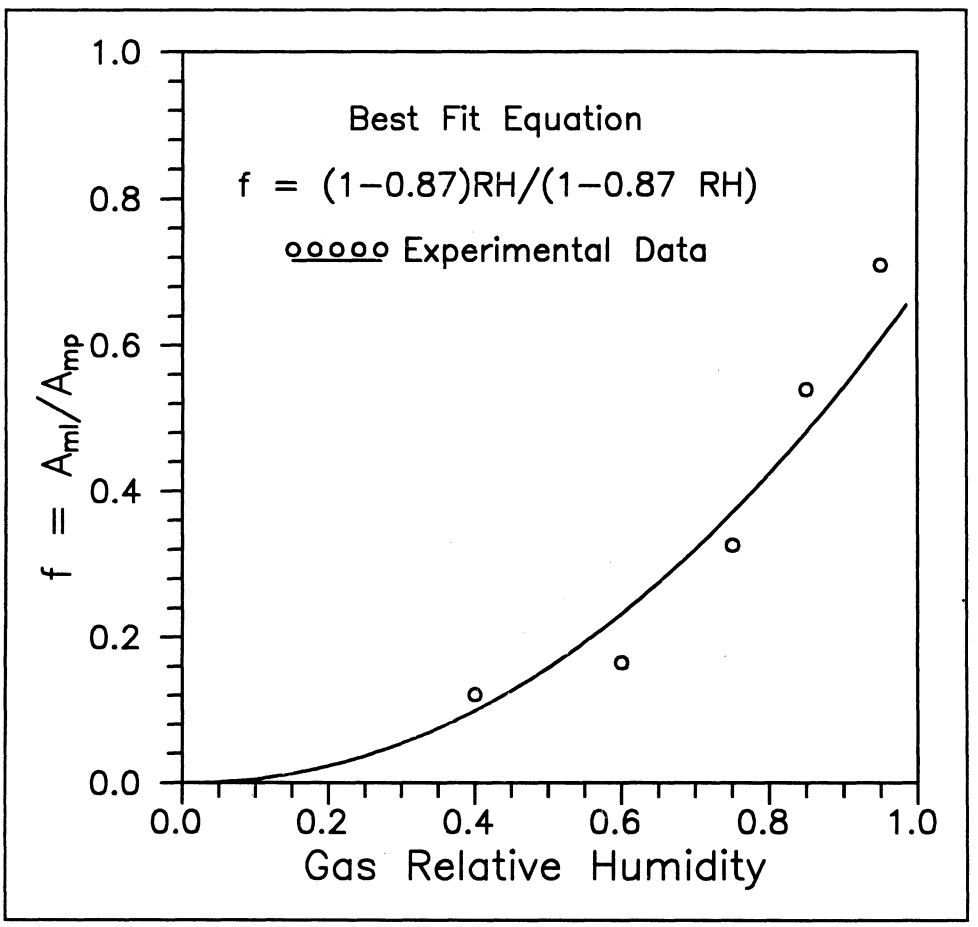

Figure 5-29: Dry Capture Correction Factor as a Function of Gas Fractional Relative Humidity for Bucyrus Limestone (53-75 μm).

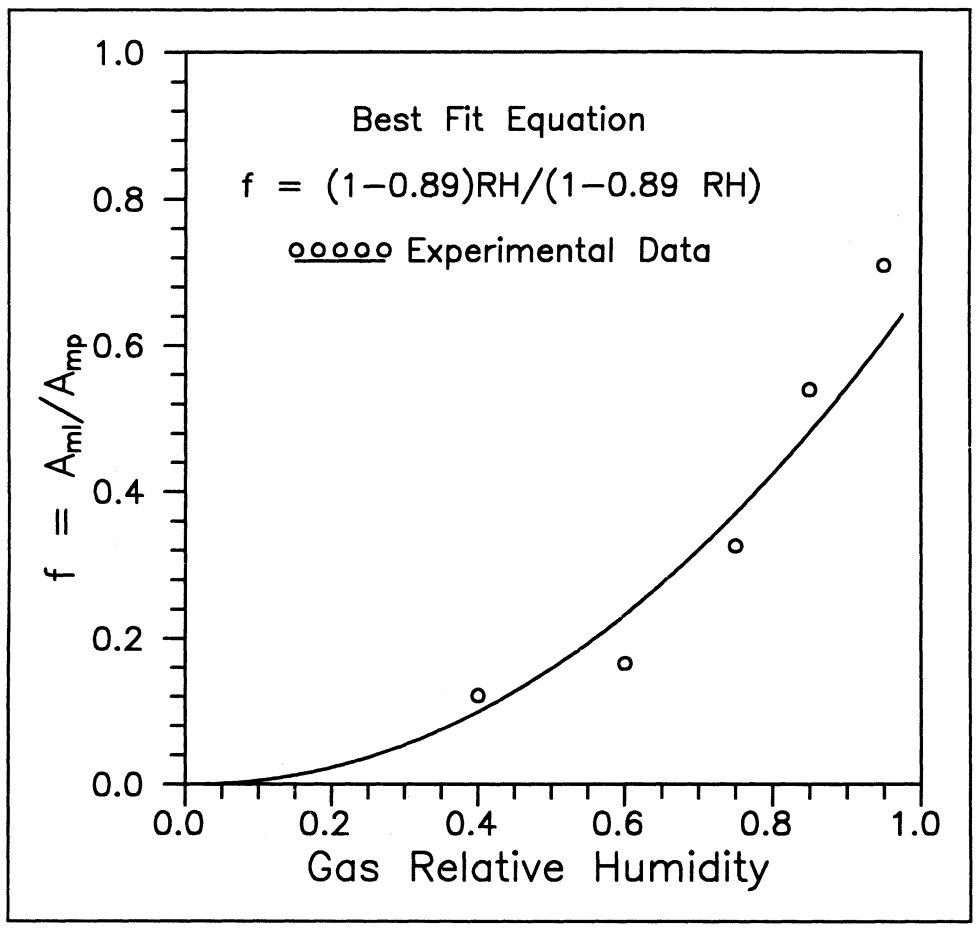

Figure 5-30: Dry Capture Correction Factor as a Function of Gas Fractional Relative Humidity for Carey Limestone (53-75 μm).

5.3.4 Product Layer Blinding Model Results

The model for precipitate layer blinding has been presented in Chapter 4. The surface area of the limestone that is available for mass transfer, A_{mp}, has been related to the extent of reaction according to the following equation :

$$A_{mp} = A\left[1 - \left(\frac{C_{SS}}{C_{SS,cr}}\right)^{\frac{n-1}{n}}\right] \qquad (5\text{-}9)$$

The critical precipitate concentration, $C_{SS,cr}$, which is experimentally determined is the value of C_{SS} at which the reaction stops. Experimental runs at conditions listed in Table 5-4 have been conducted for the purpose of determining $C_{SS,cr}$ and the model parameter n.

Reaction temperature	140 °F
SO_2 Concentration	1000 ppm
Superficial gas velocity	1.0 ft/sec
Gas Relative Humidity	95 %
Limestone Particle Size	53-75 μm

Table 5-4: Experimental Conditions for Product Layer Blinding Runs.

The conversion versus time data for Maxville, Mississippi, Vanport, Bucyrus and Carey limestones at the above experimental conditions are presented in Appendix D. Figures 5-31 through 5-35 show plots of these results. The values for the critical precipitate concentration, $C_{SS,cr}$, are listed in Table 5-5.

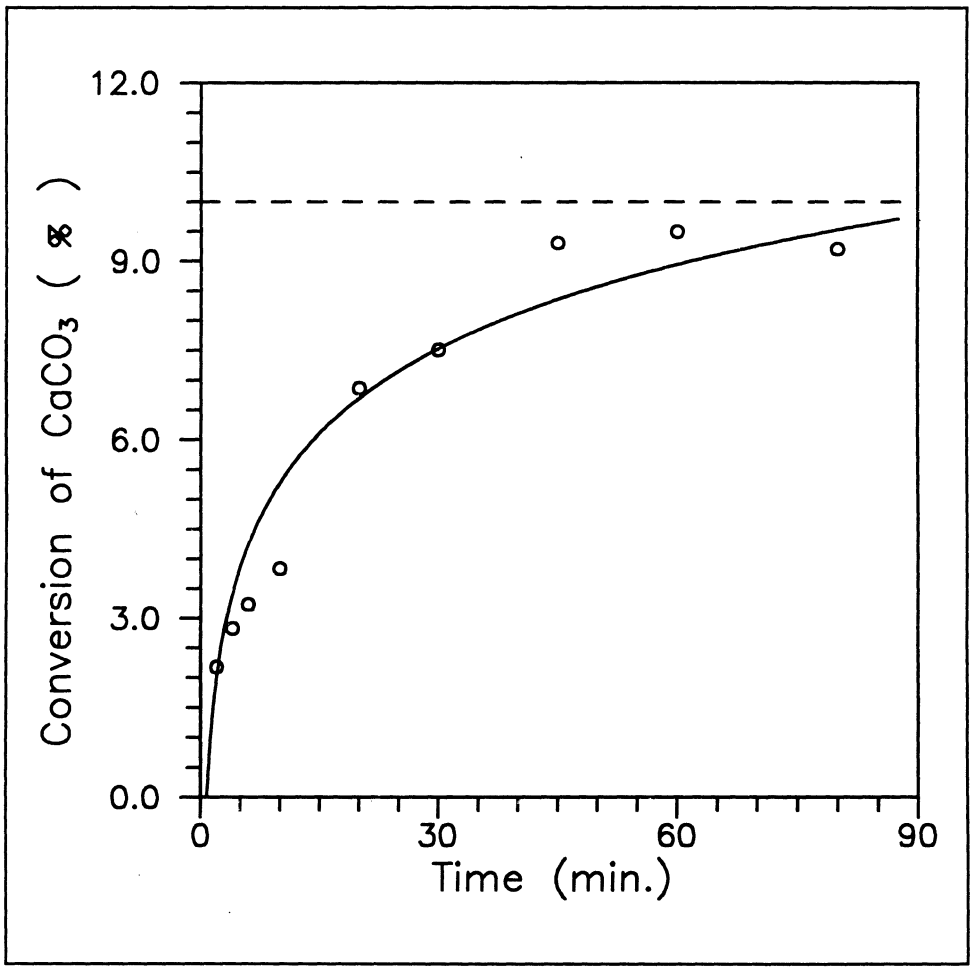

Figure 5-31: Conversion of Maxville Limestone (53-75 μm) as a Function of Time at Flue Gas Relative Humidity = 95 %.

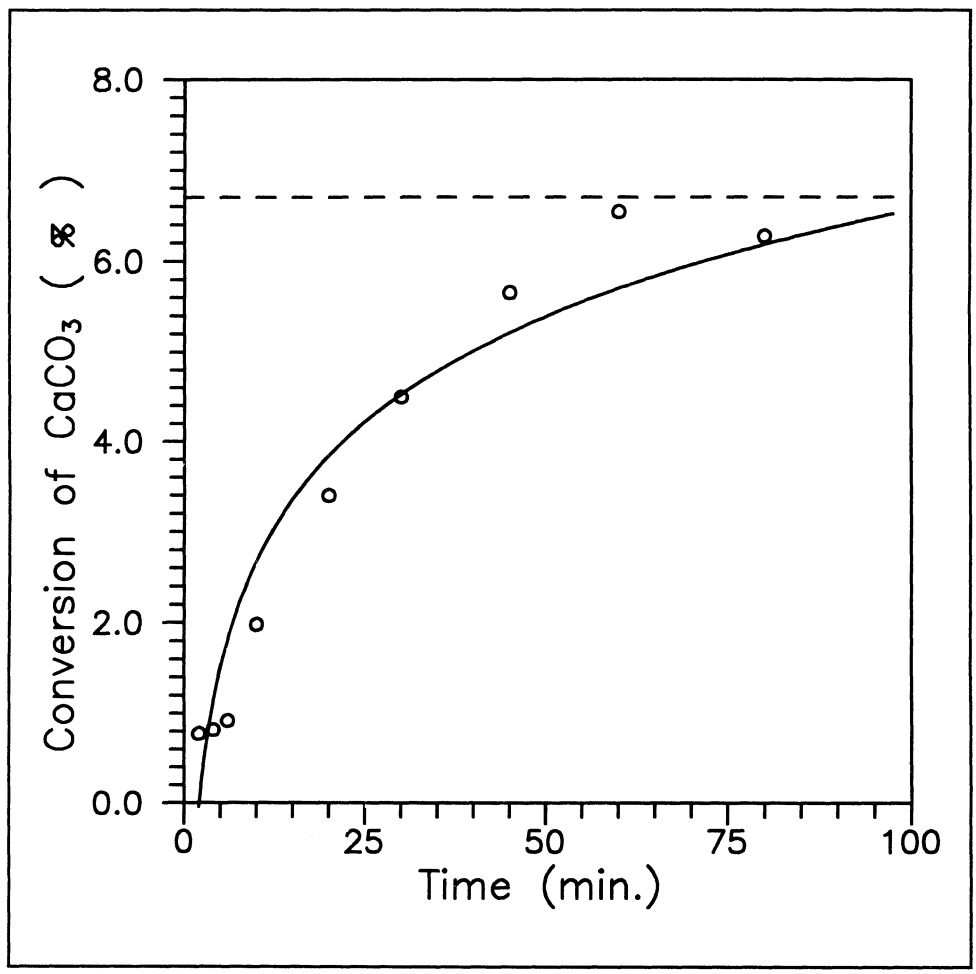

Figure 5-32: Conversion of Mississippi Limestone (53-75 μm) as a Function of Time at Flue Gas Relative Humidity = 95 %.

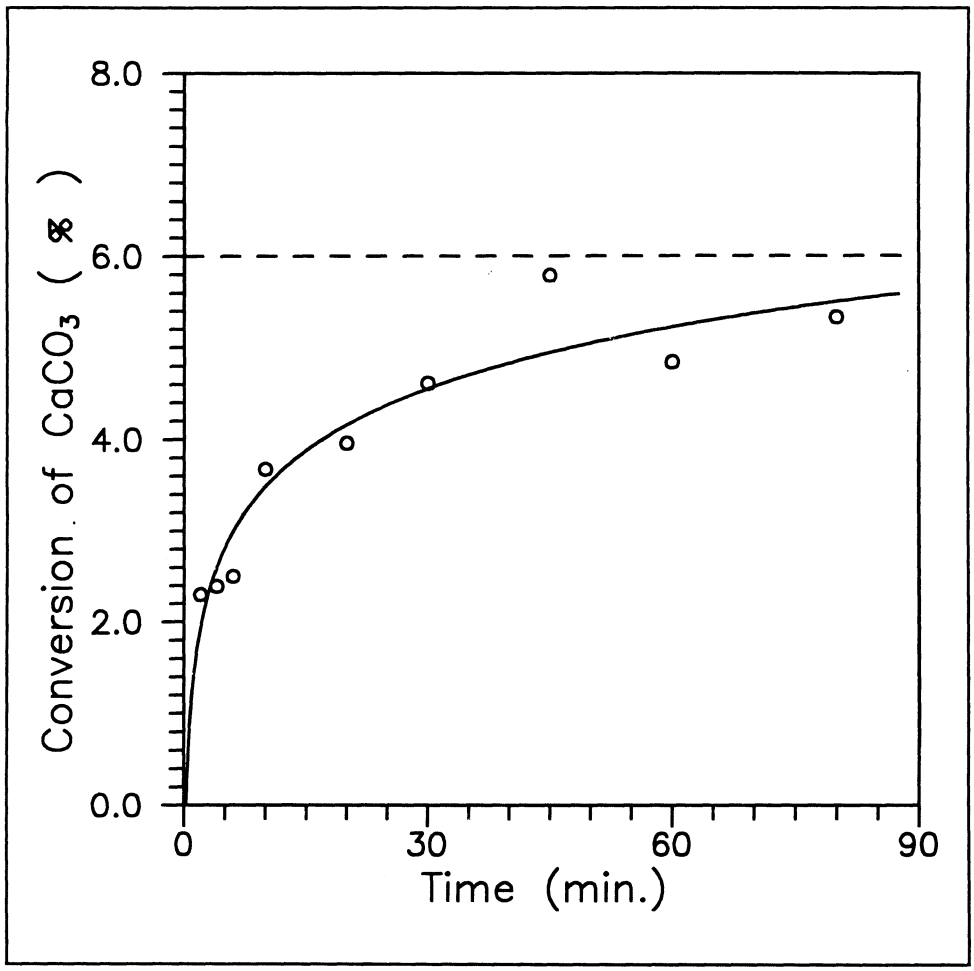

Figure 5-33: Conversion of Vanport Limestone (53-75 μm) as a Function of Time at Flue Gas Relative Humidity = 95 %.

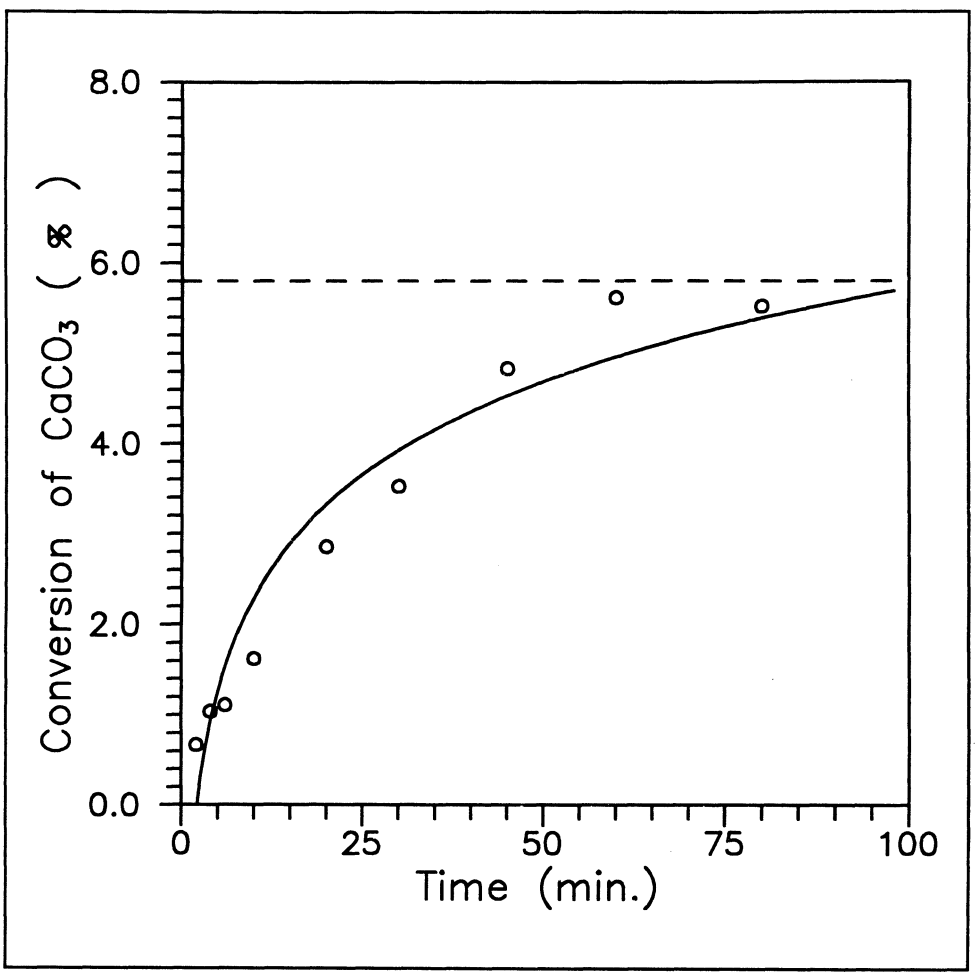

Figure 5-34: Conversion of Bucyrus Limestone (53-75 μm) as a Function of Time at Flue Gas Relative Humidity = 95 %.

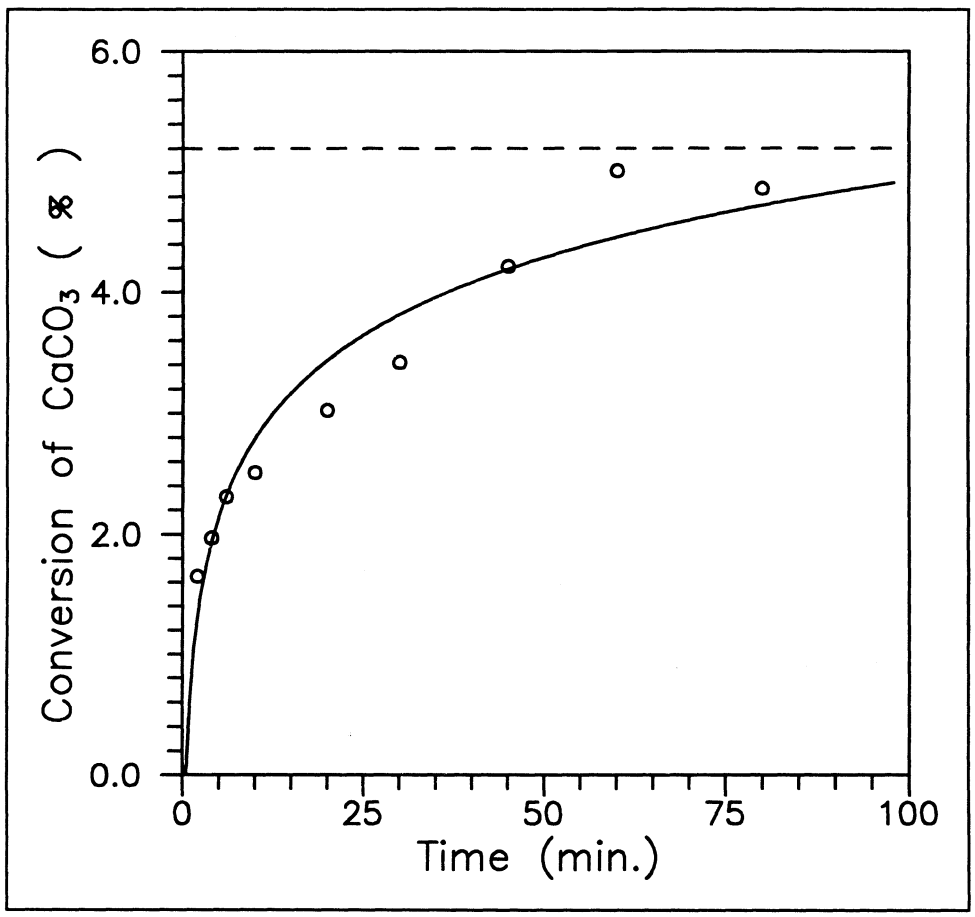

Figure 5-35: Conversion of Carey Limestone (53-75 μm) as a Function of Time at Flue Gas Relative Humidity = 95 %.

Limestone Type	$C_{SS,cr}$ (lbmole/ft^3) 10^2
Maxville	6.26
Mississippi	5.74
Vanport	4.53
Bucyrus	4.19
Carey	2.54

Table 5-5: Values for Critical Precipitate Concentrations.

In terms of fractional liquid coverage, f, and the surface area available for mass transfer, A_{mp}, the rate of transport, g_S, is given as :

$$g_S = k_{mc} C_{cle} f A_{mp} \tag{5-10}$$

By replacing A_{mp} as given in Equation (5-9), and letting $C_{SS}/C_{SS,cr} = C$, Equation (5-10) can be transformed into the following :

$$g_S = k_{mc} C_{cle} f A \left[1 - (C)^{\frac{n-1}{n}}\right] \tag{5-11}$$

Rearranging Equation (5-11) and taking the logarithm of both sides results in a linearized equation :

$$Ln\left(1 - \frac{g_S}{k_{mc} C_{cle} f A}\right) = \frac{n-1}{n} Ln[C] \tag{5-12}$$

Experimental values for reaction rates have been obtained at various points of the graphs shown as Figures 5-31 through 5-35. These data were fit to Equation (5-12), and the results are shown in Figures 5-36 through 5-40. As can be seen from these figures, straight lines have been constructed through the experimental data. The slope of each line, (n-1)/n, has been obtained and the model parameter, n, has been calculated. Values for the model parameter, n, are listed for the five limestones in Table 5-6, with an average value of 2.02.

Limestone Type	Precipitate Blinding Model Parameter (n)
Maxville	1.50
Mississippi	1.55
Vanport	2.61
Bucyrus	2.32
Carey	2.10

Table 5-6: Values for Precipitate Blinding Model Parameter, n.

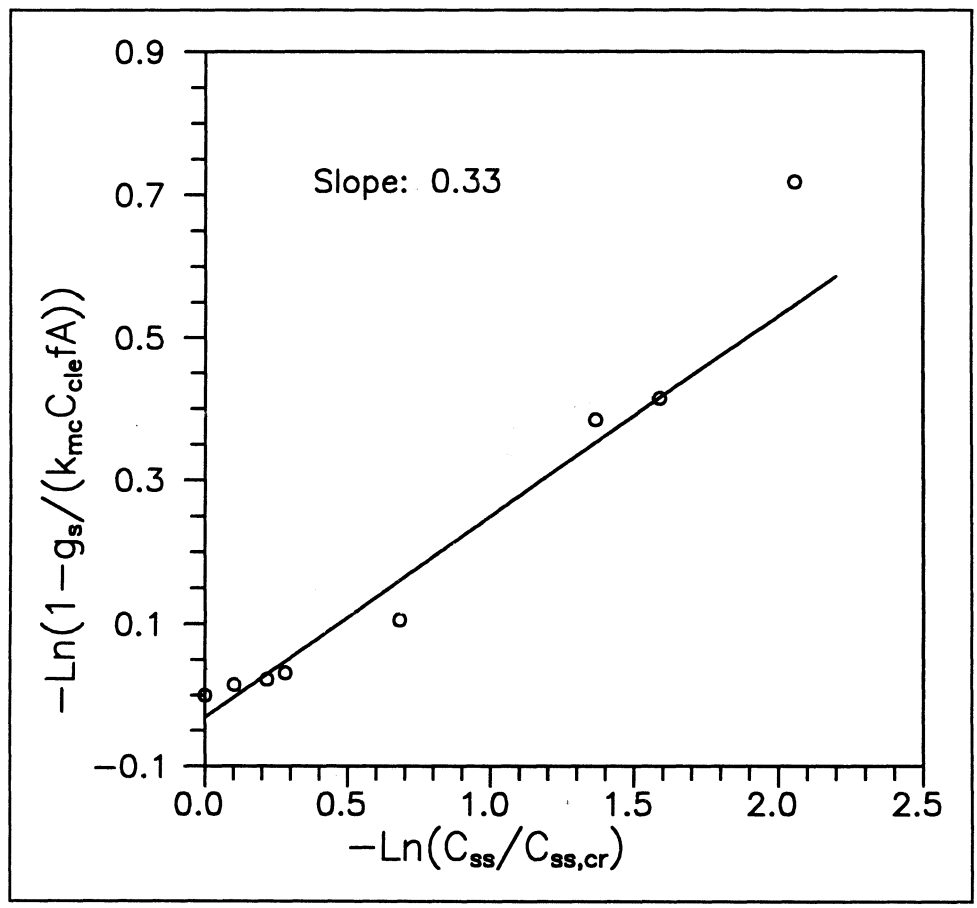

Figure 5-36: Determination of Blinding Model Parameter n for Maxville Limestone.

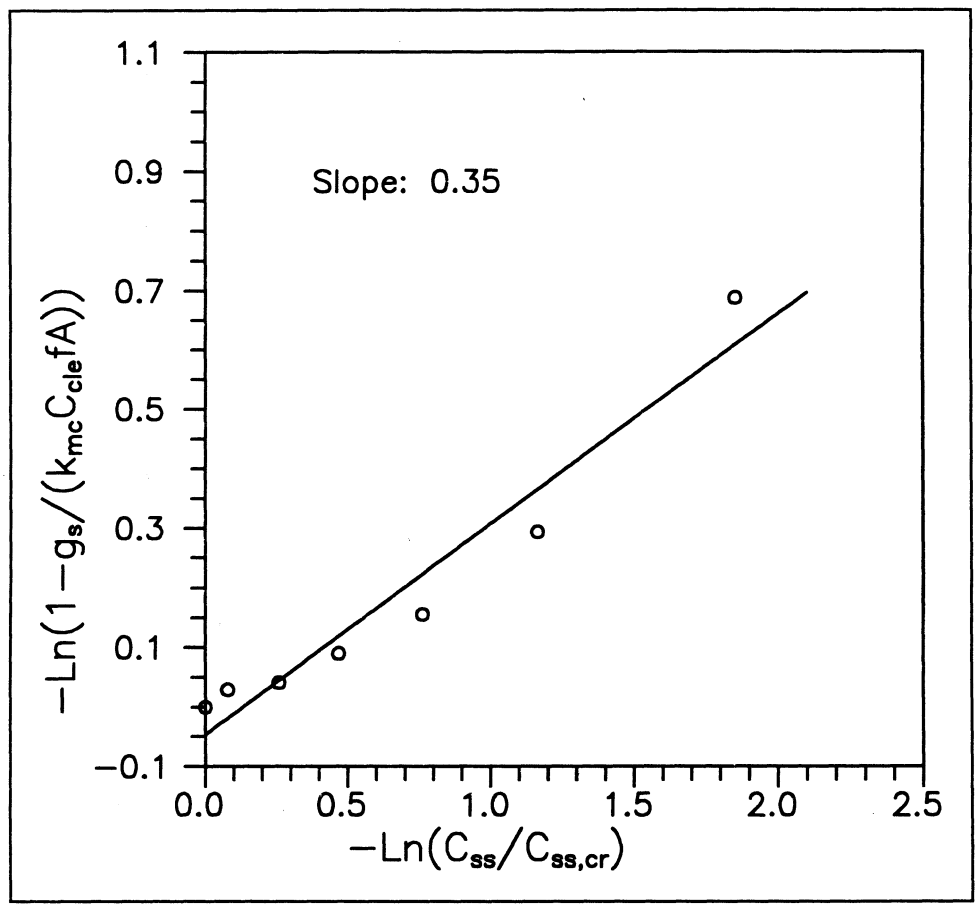

Figure 5-37: Determination of Blinding Model Parameter n for Mississippi Limestone.

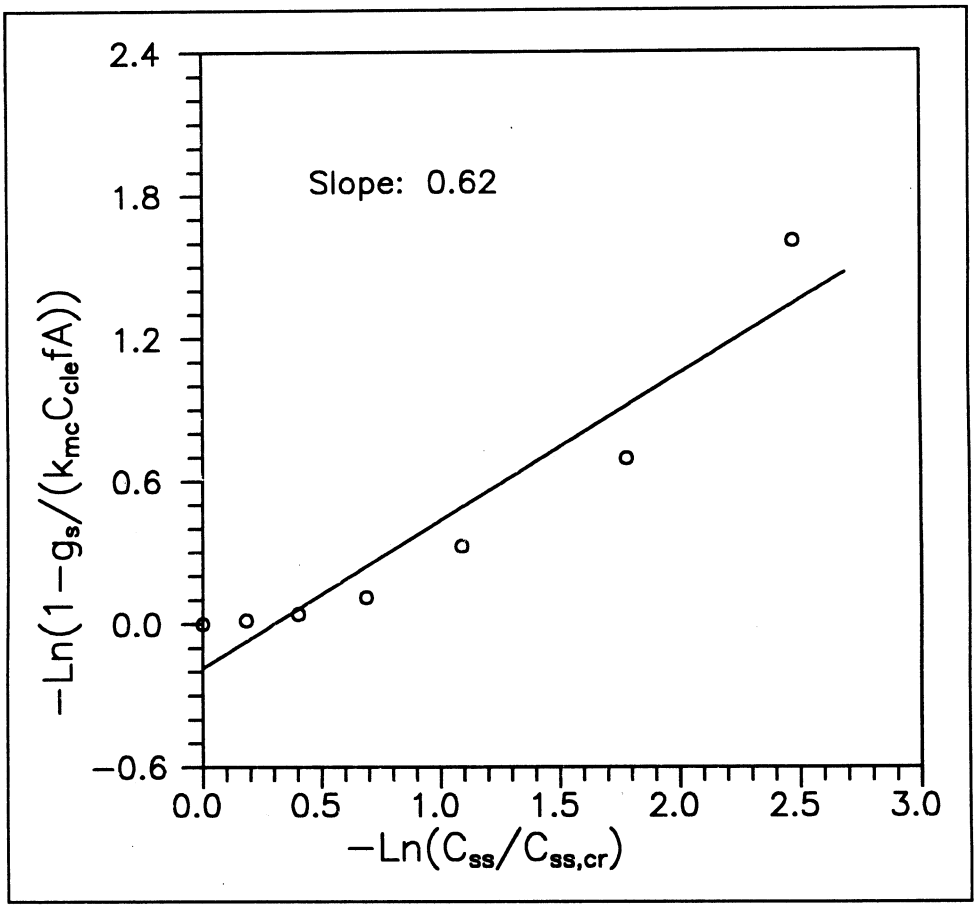

Figure 5-38: Determination of Blinding Model Parameter n for Vanport Limestone.

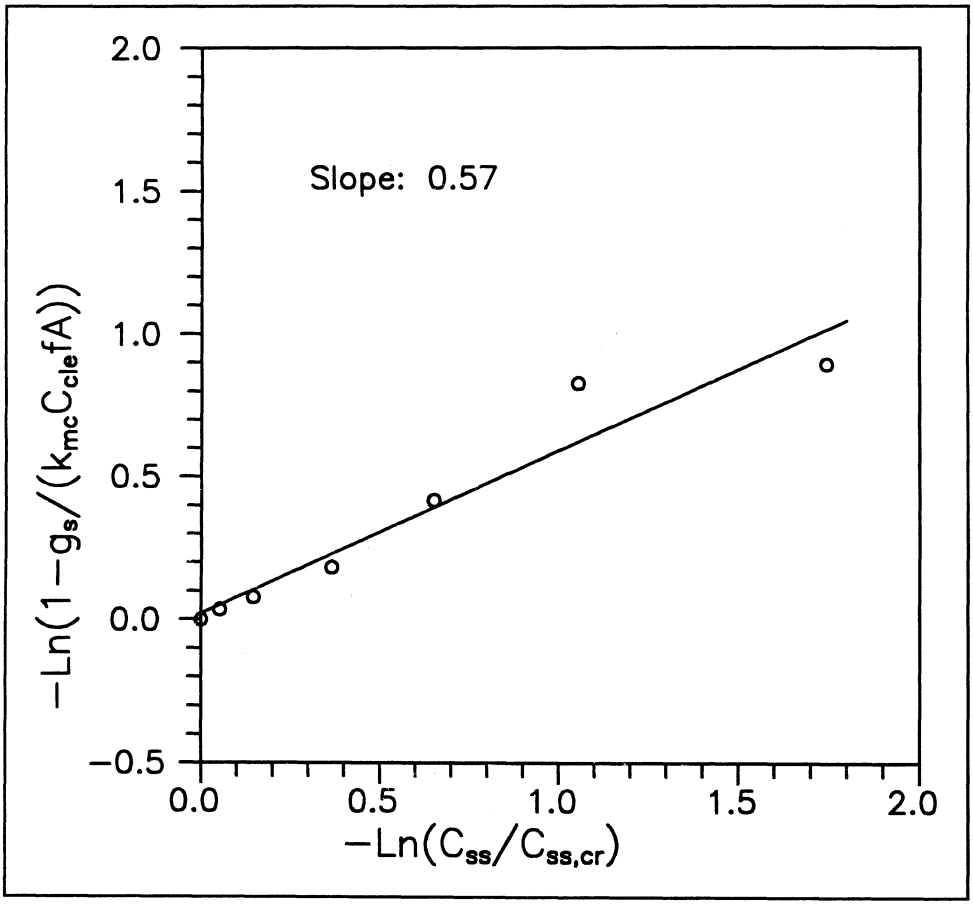

Figure 5-39: Determination of Blinding Model Parameter n for Bucyrus Limestone.

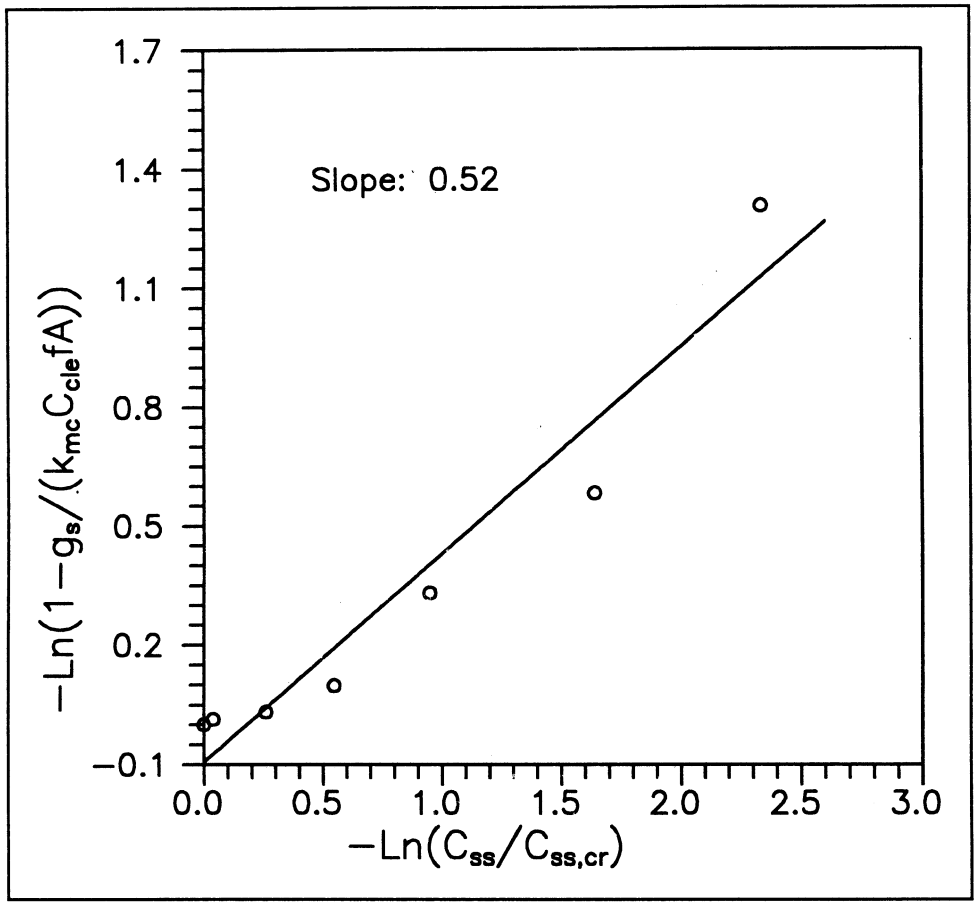

Figure 5-40: Determination of Blinding Model Parameter n for Carey Limestone.

5.3.5 Proposed Mechanism for Humidified/Dry Capture Regime

It has been shown through this experimental study that the SO_2/limestone reaction occurs only in the presence of water. Klingspor et al. (1983) suggested that as the number of monolayers of water on the limestone surface is increased (i.e. at high flue gas relative humidity), the SO_2 gas molecules penetrate into the adsorbed water. The proposed mechanism includes the following steps :

a. Adsorption of vapor water and SO_2 gas

$$H_2O(g) \rightleftarrows H_2O(ad) \qquad \textbf{(5-13)}$$

$$SO_2(g) \rightleftarrows SO_2(ad) \qquad \textbf{(5-14)}$$

b. Formation of reactive H_2O/SO_2 complexes

$$H_2O(ad) + SO_2(ad) \rightleftarrows Z^* \qquad \textbf{(5-15)}$$

c. Reaction with limestone

$$Z^* + CaCO_3(s) \rightleftarrows Y^* \qquad \textbf{(5-16)}$$

d. Formation of reaction products ($CaSO_3/CaSO_4$)

$$Y^* \rightarrow CaSO_3(s) + CO_2(g) + H_2O(ad) \qquad \textbf{(5-17)}$$

$$Y^* + \tfrac{1}{2}\, O_2 \rightarrow CaSO_4(s) + CO_2(g) + H_2O(ad) \qquad \textbf{(5-18)}$$

5.3.6 Evaluation of Kinetic Data in Terms of Shrinking Unreacted Core-Model

A chemical reaction controlled unreacted-core-model has been discussed in Chapter 4. The following equation gives the limestone conversion as a function of time :

$$1-(1-X_B)^{1/3}=\frac{bk_SC_{Ag}}{\rho_BR}t=k_ct \qquad (5\text{-}19)$$

Where: X_B: Fractional conversion

t: Time

k_C: Reaction constant

The kinetic data presented in Figure 5-18 and Figures D-1 through D-4 were fit to Equation (5-19). Straight line fits passing through the origin would be predicted by Equation (5-19). Figures 5-41 through 5-45 show that the experimental data do not reasonably fit straight lines passing through the origin. This indicates that the shrinking-unreacted-core model is not applicable to our system under the conditions being used.

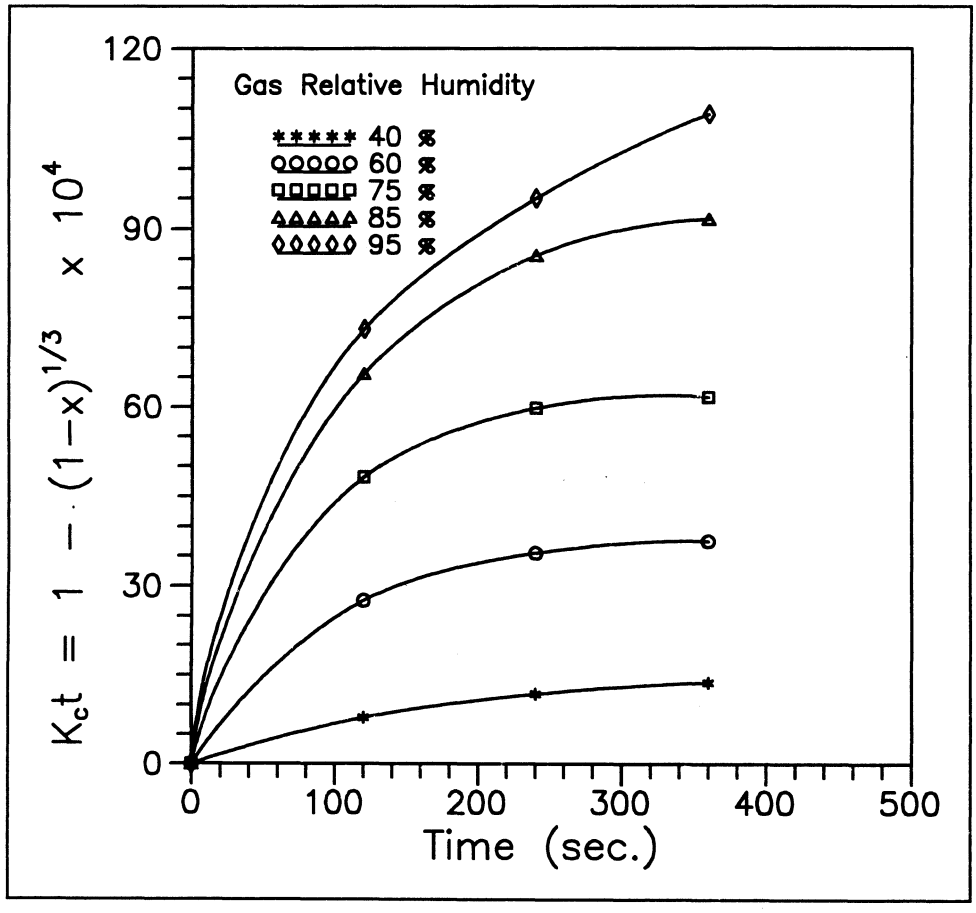

Figure 5-41: Test for Chemical Reaction Control at the Surface of a Shrinking Core of Unreacted Limestone Particle. Maxville Limestone.

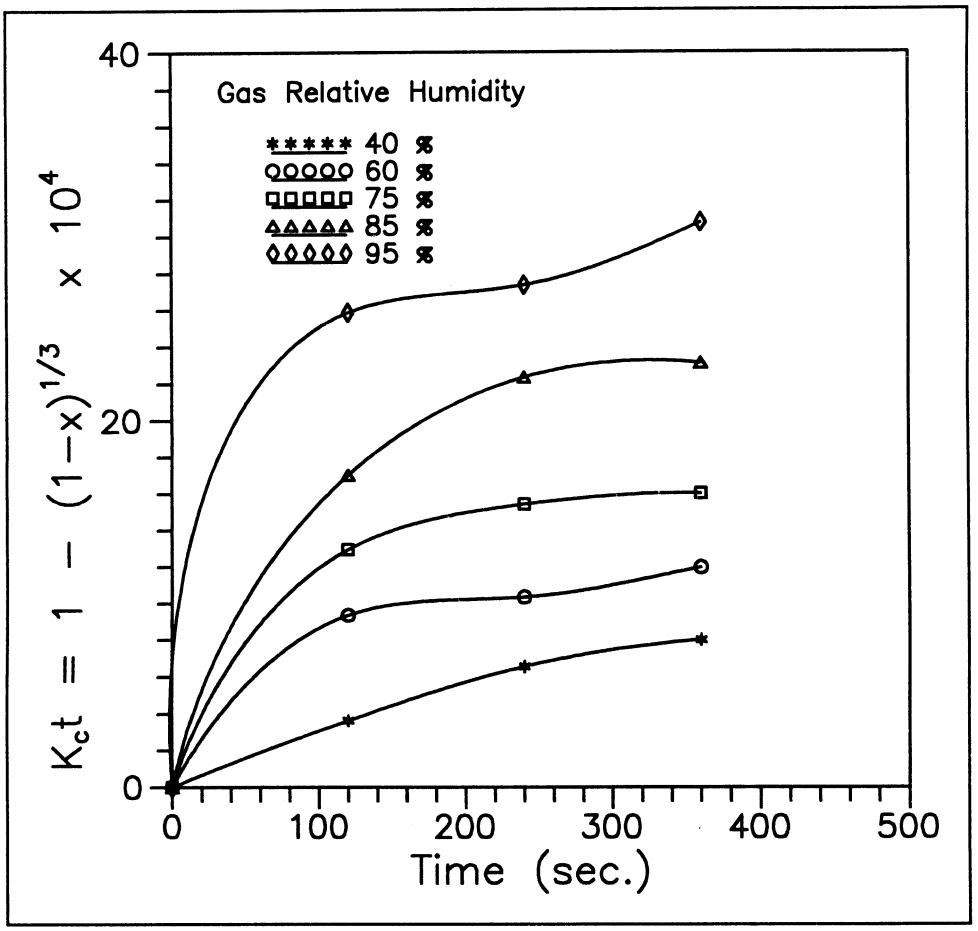

Figure 5-42: Test for Chemical Reaction Control at the Surface of a Shrinking Core of Unreacted Limestone Particle. Mississippi Limestone.

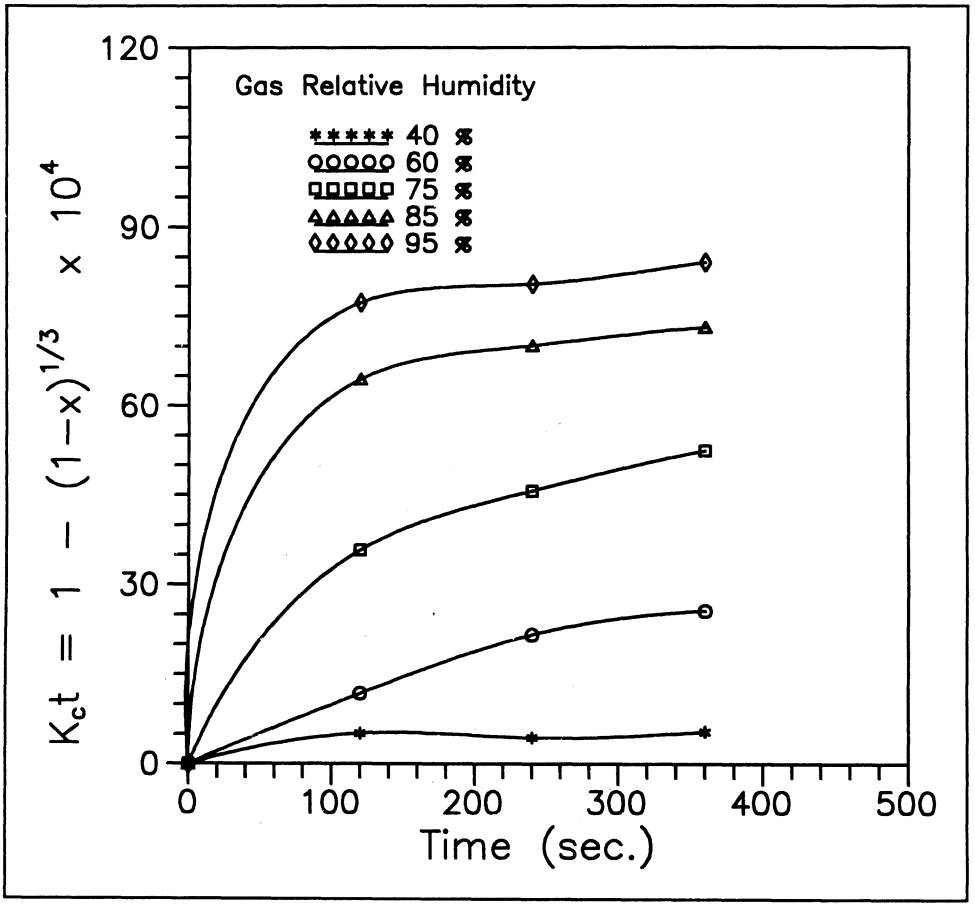

Figure 5-43: Test for Chemical Reaction Control at the Surface of a Shrinking Core of Unreacted Limestone Particle. Vanport Limestone.

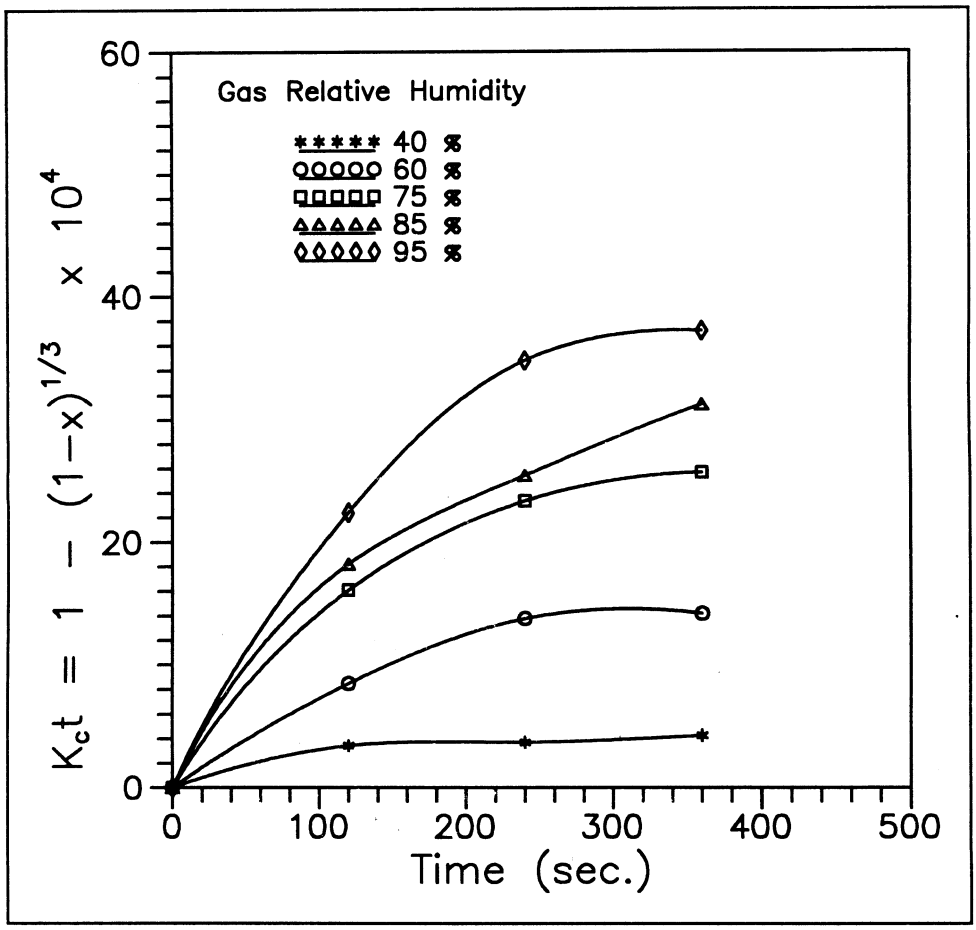

Figure 5-44: Test for Chemical Reaction Control at the Surface of a Shrinking Core of Unreacted Limestone Particle. Bucyrus Limestone.

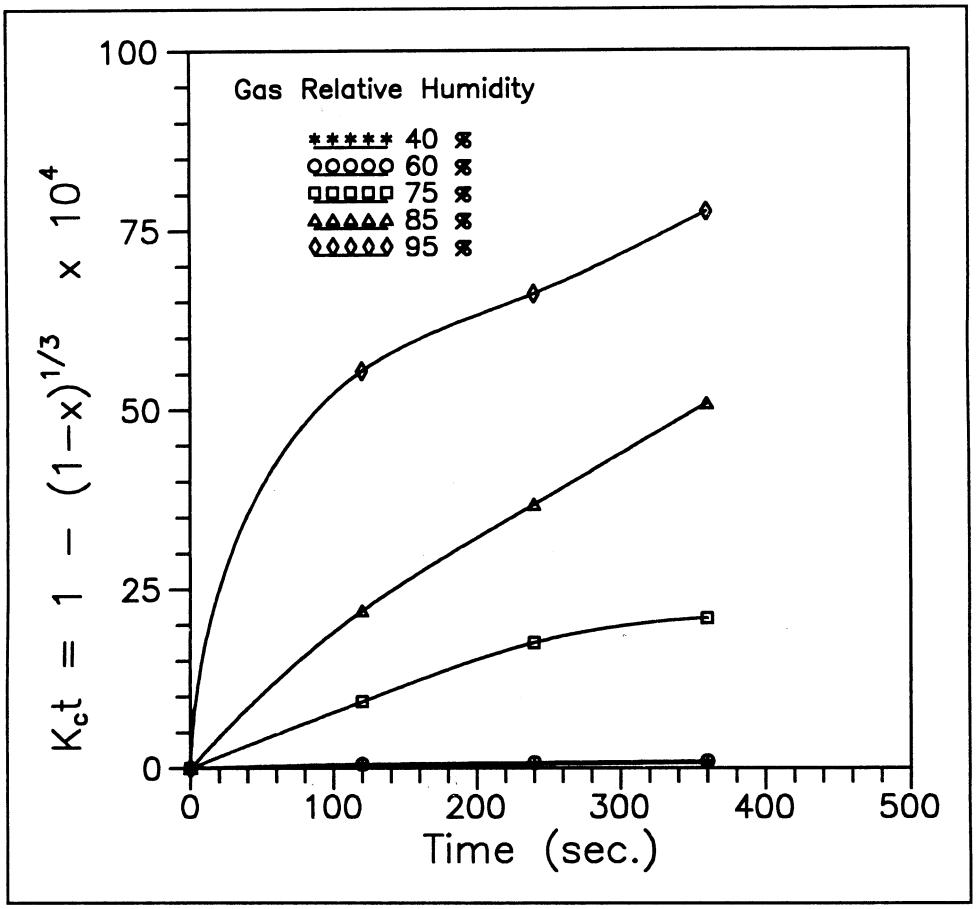

Figure 5-45: Test for Chemical Reaction Control at the Surface of a Shrinking Core of Unreacted Limestone Particle. Carey Limestone.

6.0 CONCLUSIONS AND RECOMMENDATIONS

6.1 Conclusions

An extension to an existing resistance-in-series kinetic model describing the reaction between SO_2 and limestone has been developed. The upgraded model includes the effects of $CaSO_3/CaSO_4$ product layer blinding as well as the effects of dry sorbent capture.

The model for the precipitate layer blinding idealizes the limestone surface by dividing it into blinded (i.e. nonactive area) and non-blinded (i.e. active area) regions. As the reaction between SO_2 and limestone progresses, the blinded area gradually increases until the limestone becomes entirely unreactive. The model takes the form of an empirical equation which relates the surface area available for mass transfer to the extent of reaction.

The model for dry sorbent capture has been developed based on experimentally observed behavior. The bench-scale kinetic experimental studies performed at 140 °F and at dry conditions using raw limestones revealed an exponential increase in the reaction rate as the flue gas relative humidity was increased. This model takes the form of an empirical equation which relates the fractional liquid coverage to the flue gas relative humidity.

Bench-scale experiments using differential reactor techniques were performed to obtain kinetic data under dry/humidified conditions and to investigate key experimental conditions which included limestone type, flue gas relative humidity and limestone particle size. The results indicated that the

reaction rate strongly depended on the flue gas relative humidity. At flue gas relative humidities of less than 40 %, the reaction rate was nearly zero. The reaction rate followed a power function with respect to flue gas relative humidity. The experimental results also indicated that the reaction rate was linearly proportional to the inverse of the particle radius. BET surface area data for limestones used in this study indicated that the reaction rate for limestones may be primarily a function of sorbent surface area available for reaction. The reaction rate was nearly proportional to the BET surface area.

The results of the differential experimental studies were used to determine the parameters of the dry capture and blinding models. The modeling results are used in the upgraded resistance-in-series kinetic model to calculate the sulfur dioxide removal rate in the dry portion of the limestone bed.

Bench-scale integral experiments which included the effects of inlet SO_2 concentration, flue gas relative humidity and limestone particle size were performed to test the SO_2 removal performance of a 2 inch diameter by 6 inch deep fixed-bed reactor. The results indicated that the SO_2 removal efficiency is decreased as the inlet SO_2 concentration is increased. More SO_2 removal for a longer period of time was achieved as the flue gas relative humidity was increased. The bench-scale integral experimental data indicated that significant amounts of SO_2 removal (5 to 15 %) took place in the dry portion of the limestone bed. This is in good agreement with the demonstration-scale LEC data (Prudich et al., 1988). Smaller limestone size ranges uniformly showed

higher SO_2 removal efficiency than larger size cuts over an initial operating period of about half an hour. The SO_2 removal efficiency was nearly the same after this initial operating period.

6.2 Recommendations

Some of the recommendations through which improvements to this research work can be achieved are listed below:

1. Experimental studies that investigate the effects of chemical additives would be an important contribution to the FGD process being studied.
2. An upgrade to the modeling effort that accounts for the effects of chemical additives can be developed so that a more comprehensive kinetic model would be readily available.
3. Computer simulations need to be carried out to evaluate the kinetic model and to compare the results with the experimental data.

REFERENCES

Appell, K. W., "A Mathematical Simulation of ETS' Limestone Emission Control Process Using the Method of Characteristics: Fixed Bed Configuration/Gas-phase Mass Transfer Control," M.S. Thesis, Ohio University, 1989.

Ben-Said L., M. E. Prudich, and K. J. Sampson, "Fundamental Studies of Low Temperature SO_2 Removal by Dry Calcium-Based Sorbents," Proceedings: 10 th Annual Pittsburgh Coal Conference, Pittsburgh, PA, September 20-24, 1993.

Borgwardt, R. H., and H. R. Bruce, "EPA Study of Hydroxide Reactivity in a Differential Reactor," paper 15, Proceedings: 1986 Joint Symposium on Dry SO_2 and Simultaneous SO_2/NO_x Control Technologies, 1, EPRI CS-4966, December, 1986.

Brunauer, S., P. H. Emmett, and E. Teller, "Adsorption of Gases in Multimolecular Layers," The Journal of the American Chemical Society, 60 (2), 309-319, 1938.

Davis, W. T., and T. G. Keener, "Chemical Kinetics Studies on Dry Sorbents," DOE/FC/10184-1 (DE82012765), 1982.

Harriott, P., and M. Kinzey, "Modeling the Gas and Liquid Phase Resistances in the Dry Scrubbing Process for SO_2 Removal," Proceedings: 3 rd Annual Pittsburgh Coal Conference, Pittsburgh, PA, September 8-12, 1986.

Irabien, A., F., Cortabitarte, J. Viguri, and M. I., Ortiz, "Kinetic Model for Desulfurization at Low Temperature Using Calcium Hydroxide," Chemical Engineering Science, Vol. 45, No. 12, 1990.

Ireland P. A., et al., "Site Specific Evaluation of Six Sorbent Injection Processes," FGD and Dry SO_2 Control Symposium, St. Louis, Missouri, October 25-28, 1988.

Jorgensen, C., C. S. Chang, and T. G. Brna, "Evaluation of Sorbents and Additives for Dry SO_2 Removal," Environmental Progress, Vol. 6, No. 1, 1987.

Klinsgpor, J., H. T. Karlsson, and I. Bjerle, "A Kinetic Study of the Dry SO_2-Limestone Reaction at Low Temperature," Chemical Engineering Communication, 22, 88, 1983.

Levenspiel, O., Chemical Reaction Engineering, John Wiley & Sons, Inc., New York, 1978.

Maldei, M., "Low Temperature Dry Scrubbing Reaction Kinetics and Mechanisms: Limestone Dissolution and Solubility," M.S. Thesis, Ohio University, 1993.

Mandal, D. K., "Production of Improved Calcium-Based Sorbents for Sulfur Dioxide Capture," M.S. Thesis, Ohio University, 1993.

Maurin P. G., "Controlling SO_2 Emissions, A Look at Wet and Dry Flue Gas Desulfurization Systems," Plant Engineering, 52, May 9, 1985.

McInnes R., and R. V. Royen, "Desulfurizing Flue Gases," Chemical Engineering, September, 1990.

Offen G. R. et al., "Assessment of Dry Sorbent Emission Control Technologies - Part III. Applications," Journal of Air Pollution Control Association, 37 (8), 968, 1987.

Perry, R. H., D. W., Green, and J. O. Maloney, Perry's Chemical Engineering Handbook, 6 th ed., McGraw-Hill, New York, 1987.

Prudich, M. E., K. W. Appel, M. J. Visneski, J. D. McKenna, D. A. Furlong, J. C. Mylock, J. F. Szalay, and J. E. Wright, "Small Pilot Plant Demonstration of ETS' Limestone Emission Control System," Final Report OCDO Grant No. CDO/R-86-24, May 1988.

Seeker, W. R., S. L. Chen, J. C. Kramlich, S. B. Greene, and B. J. Overmoe, "Fundamental Studies of Low Temperature Sulfur Capture by Dry Calcium Sorbent Injection," paper 32, Proceedings: 1986 Joint Symposium on Dry SO_2 and Simultaneous SO_2/NO_x Control Technologies, 2, EPRI CS-4966, December, 1986.

Uchida, S., K. Koide, and M. Shindo, "Gas Absorption with Fast Reaction into a Slurry Containing Fine Particles," Chemical Engineering Science, 30, 644-646, 1975.

Visneski, M. J., M. E. Prudich, and K. J. Sampson, "Modeling of the Low Temperature Reaction of Sulfur Dioxide and Limestone Using a Three Resistance Film Theory Instantaneous Reaction Model," 83 rd Annual Meeting of the AIChE, Nov. 11-16, 1990, Chicago.

Visneski, M. J., "Modeling of the Low Temperature Reaction of Sulfur Dioxide and Limestone Using a Three Resistance Film Theory Instantaneous Reaction Model," Ph.D. Dissertation, Ohio University, 1991.

Yoon, H., J. A. Withum, W. A. Rosenhoover, and F. P. Burke, "Sorbent Improvement and Computer Modeling Studies for Coolside Desulfurization," paper 33, Proceedings: 1986 Joint Symposium on Dry SO_2 and Simultaneous SO_2/NO_x Control Technologies, 2, EPRI CS-4966, December, 1986.

Yu, H. C., and S. V. Sotirchos, "A Generalized Pore Model for Gas-Solid Reactions Exhibiting Pore Closure," AIChE J., 33, 382, 1987.

APPENDICES

APPENDIX A

PROGRAM FOR DETERMINING MASS FLOW METER AND WATER PUMP SETTINGS

A.1 Program Description

The program listed below returns the settings of the mass flow meters and the water pump for the desired experimental conditions. These conditions are the source SO_2 concentration, the gas temperature, the gas superficial velocity through the reactor, the gas relative humidity, the desired SO_2 concentration of the gas entering the reactor, and the cross sectional area of the bed.

From this information, the program calculates the flow rates of gases from the air and SO_2 sources at STP and the necessary flow rate of water to be injected into the evaporation chamber. The calibration data for the mass flow meters and for the water pump is used to obtain the corresponding settings.

The input data to the program is entered through the computer screen and the output is stored in a file which can be printed later. Figure A-1 shows a typical output from the program.

Run I.D.: Figure A-1

SO_2 CONCENTRATION IN THE SO_2 SOURCE (ppm):	4500.0
SUPERFICIAL GAS VELOCITY (ft/sec):	1.0
GAS RELATIVE HUMIDITY (%):	75.0
SO_2 CONCENTRATION IN THE REACTOR (ppm):	1000.0
GAS TEMPERATURE (DEG. F) :	140.0
REQUIRED WATER FLOW RATE (cm^3/min):	1.72
FLOW RATE FROM SO_2 SOURCE (SLPM):	3.7
FLOW RATE FROM AIR SOURCE (SLPM):	12.8

GAS SOURCE	FLOW RATE (SLPM)	CHANNEL	SETTING
AIR	12.8	#1	64.2
SO_2	3.7	#2	13.4

WATER PUMP SETTING: 2.76

A.2 Program Listing

```
C*************************************************************
C     LANGUAGE : FORTRAN 77
C     COMPILER : MICROSOFT FORTRAN VERSION 5.0
C
C     COMMENTS:
C
C          1. This program calculates the flow rates of gases from the air
C          and SO2 sources for the desired experimental conditions and
C          returns the corresponding mass flow meter settings.
C          2. This program also calculates the flow rate of water, to be
C          injected into the evaporation chamber, necessary for obtaining
C          the desired gas relative humidity.
C
C*************************************************************
C
C      SO2CONC : Source SO2 concentration in ppm
C      GTF : Gas temperature in °F
C      VELF : Superficial gas velocity through the reactor in ft/sec
C      CSA : Cross sectional area of the bed
C      RHUM : Gas relative humidity in %
C      REQCONC : Desired SO2 concentration in the reactor in ppm
```

```
C       H: Molar flow rate of water in moles/min
C       FLOWSN : Gas flow from SO2 source in SLPM
C       FLOWN : Gas flow from air source in SLPM
C       A, B, C : Constants for Antoine equation
C       GTC : Gas temperature in °C
C       GTR : Gas temperature in °R
C       AVOLFS : Actual gas volumetric flow rate through the reactor in LPM
C       PS : Saturation vapor pressure of H2O in mm Hg
C       LYS : Saturation mole fraction of H2O
C       LY : Mole fraction of H2O
C       CY : Humidity, lbmole H2O/lbmole dry air
C       HPRIME : Water flow rate in cm3/min
C       H2OVF : Water flow rate in mole/min
C       READING : Mass flow meter setting or water pump reading


REAL SO2CONC,GTF,VELF, CSA, RHUM,REQCONC,H,FLOWSN,FLOWN
REAL A,B,C,GTC,GTR,AVOLFS,PS,LYS,LY,CY,HPRIME
REAL READING,H2OVF
CHARACTER*30 RUNID
WRITE(*,*)"ENTER RUN I.D. (MAX. 10 CHARACTERS)"
READ(*,*) RUNID
WRITE(*,*)"ENTER THE CONCENTRATION OF SO2 IN THE N2(AIR)/SO2"
CYLINDER, IN ppm"
READ(*,*) SO2CONC
WRITE(*,*)"ENTER THE GAS TEMPERATURE, IN DEG. F"
READ(*,*) GTF
WRITE(*,*)"ENTER THE SUPERFICIAL GAS VELOCITY THROUGH
THE BED, IN ft/sec"
READ(*,*) VELF
WRITE(*,*)"ENTER THE CROSS SECTIONAL AREA OF THE BED"
READ(*,*) CSA
WRITE(*,*)"ENTER THE DESIRED RELATIVE HUMIDITY OF THE GAS,IN %"
READ(*,*)RHUM
WRITE(*,*)"ENTER THE DESIRED SO2 CONCENTRATION IN THE
REACTOR, IN ppm"
READ(*,*) REQCONC
C
C       CHANGE TEMPERATURE TO DEG. C
C
        GTC=(5.0/9.0)*(GTF-32.0)
C
C       CHANGE TEMPERATURE TO DEG. R
```

```
C
      GTR=GTF+459.7
C
C     CALCULATE THE ACTUAL VOLUMETRIC FLOW RATE THROUGH
THE   BED, ft3/SEC
C
      AVOLFS=CSA*VELF/144.0

C     CALCULATE AVOLFS IN LPM
C
      AVOLFS=AVOLFS*28.32*60.0
C
C     ANTOINE EQUATION CONSTANTS FOR H2O
C
      A=7.96681
      B=1668.21
      C=228.0
C
C     CALCULATE THE SAT. VAP. PRESSURE OF H2O AT THE GAS
      TEMPERATURE, IN mm Hg
C
      PS=10.0**(A-(B/(C+GTC)))
C
C     CALCULATE THE SAT. MOLE FRACTION OF H2O
C
      LYS=(PS/760.0)*(14.7/17.7)
C
C     CALCULATE THE MOLE FRACTION OF H2O IN THE GAS
C
      LY=RHUM*LYS/100.0
C
C     CALCULATE THE HUMIDITY, lbmol H2O/lbmol DRY GAS
C
      CY=LY/(1.0-LY)
C
C     CALCULATE TOTAL GAS VOLUMETRIC FLOW AT STP (SLPM)
C
      AVOLFS=(17.7/14.7)*(529.7/599.7)*AVOLFS
C
C     CALCULATE THE FLOW RATE OF H2O VAPOR AT STP (SLPM)
C
      H2OVF=LY*AVOLFS
C
C     CALCULATE WATER FLOW RATE IN CM3/MIN
```

```
C
      HPRIME=H2OVF*18.0/24.145184
C
C     CALCULATE MOLES OF H2O PER MINUTE
C
      H=H2OVF/24.145184
C
      TOTFLOW=AVOLFS-H2OVF
      FLOWSN=(REQCONC/SO2CONC)*TOTFLOW
      FLOWN=TOTFLOW-FLOWSN
C
      WRITE(4,5) RUNID
5     FORMAT(/,A30)
      WRITE(4,6)
6     FORMAT(1X,'--------------------------------------------------------------------------------')
      WRITE(4,10) SO2CONC
10    FORMAT(/1X,'SO2 CONCENTRATION IN THE SO2 SOURCE (ppm):',
      F7.1)
      WRITE(4,20) VELF
20    FORMAT(1X,'SUPERFICIAL GAS VELOCITY (ft/sec):',F4.1)
      WRITE(4,30) RHUM
30    FORMAT(1X,'GAS RELATIVE HUMIDITY (%):',F5.1)
      WRITE(4,40) REQCONC
40    FORMAT(1X,'SO2 CONCENTRATION IN THE REACTOR (ppm):',F7.1)
      WRITE(4,50) GTF
50    FORMAT(1X,'GAS TEMPERATURE (DEG. F) :',F6.1)
      WRITE(4,60) HPRIME
60    FORMAT(1X,'REQUIRED WATER FLOW RATE (cm3/min):',F5.2)
      WRITE(4,80) FLOWSN
80    FORMAT(1X,'FLOW RATE FROM SO2 SOURCE (SLPM):',        F7.1)
      WRITE(4,90) FLOWN
90    FORMAT(1X,'FLOW RATE FROM AIR SOURCE (SLPM) :',F7.1)
      WRITE(4,100)
100   FORMAT(/1X,'GAS STREAM',4X,'FLOW RATE (SLPM)',4X,
      'CHANNEL',4X,'SETTING')
      WRITE(4,110)
110   FORMAT(1X,'----------',4X,'----------------',4X, '-------',4X,
      '--------------------')
C
      CALL FLOWMETER1(FLOWN,READING)
      WRITE(4,130)FLOWN,READING
130   FORMAT(3X,'AIR',7X,F7.1,13X,'#1',10X,F4.1)
C
      CALL FLOWMETER2(FLOWSN,READING)
```

```
      WRITE(4,140)FLOWSN,READING
140   FORMAT(3X,'SO2',3X,F7.1,13X,'#2',10X,F4.1)
C
      CALL PUMP(HPRIME,READING)
      WRITE(4,160)READING
160   FORMAT(/1X,'WATER PUMP READING :',F5.2)
      WRITE(4,170)
170   FORMAT(1X,'------------------')
      STOP
      END
C
C-----------------------------------------------------------------------------------------------
C
C     THIS SUBROUTINE RETURNS THE POTENTIOMETER READING FOR
C     FLOWMETER #1 (CHANNEL #1)
C
      SUBROUTINE FLOWMETER1(X,Y)
      REAL X,Y
      Y=(X/20.0)*100.0
      RETURN
      END
C
C-----------------------------------------------------------------------------------------------
C
C     THIS SUBROUTINE RETURNS THE POTENTIOMETER READING FOR
C     FLOWMETER #2 (CHANNEL #2)
C
      SUBROUTINE FLOWMETER2(X,Y)
      REAL X,Y
      Y=(X/20.0)*100.0*0.728
      RETURN
      END
C
C-----------------------------------------------------------------------------------------------
C
C     THIS SUBROUTINE RETURNS THE WATER PUMP READING
C
      SUBROUTINE PUMP(X,Y)
      REAL X,Y,A0,A1
      A0=-0.151291
      A1=1.69216
      Y=A0+A1*X
      RETURN
      END
```

APPENDIX B

WATER PUMP CALIBRATION

Pump Specifications:

* Masterflex L/S drive with ten-turn potentiometer speed control (Model No. 7520-35)
* Masterflex L/S Easy-Load pump head (Model No. 7518-10)
* Tygon tubing (size 13, 0.8 mm inside diameter)

Calibration data for this pump has been obtained and presented in Table B-1. Figure B-1 shows a plot of the data. The straight line passing through the data points is represented by the following equation.

$$Y = mX + b$$

Y: Pump setting, X: Water flow rate (cm^3/min)

Pump setting (# turns)	Water flow rate (cm^3/min)
0.0	0.0
0.5	0.110
1.0	0.405
1.5	0.802
2.0	1.123
2.5	1.402
3.0	1.620
3.5	1.985
4.0	2.212
4.5	2.341
5.0	2.805
5.5	3.110
6.0	3.323
6.5	3.752
7.0	3.989
7.5	4.214
8.0	4.528

Table B-1: Calibration Data for Water Pump

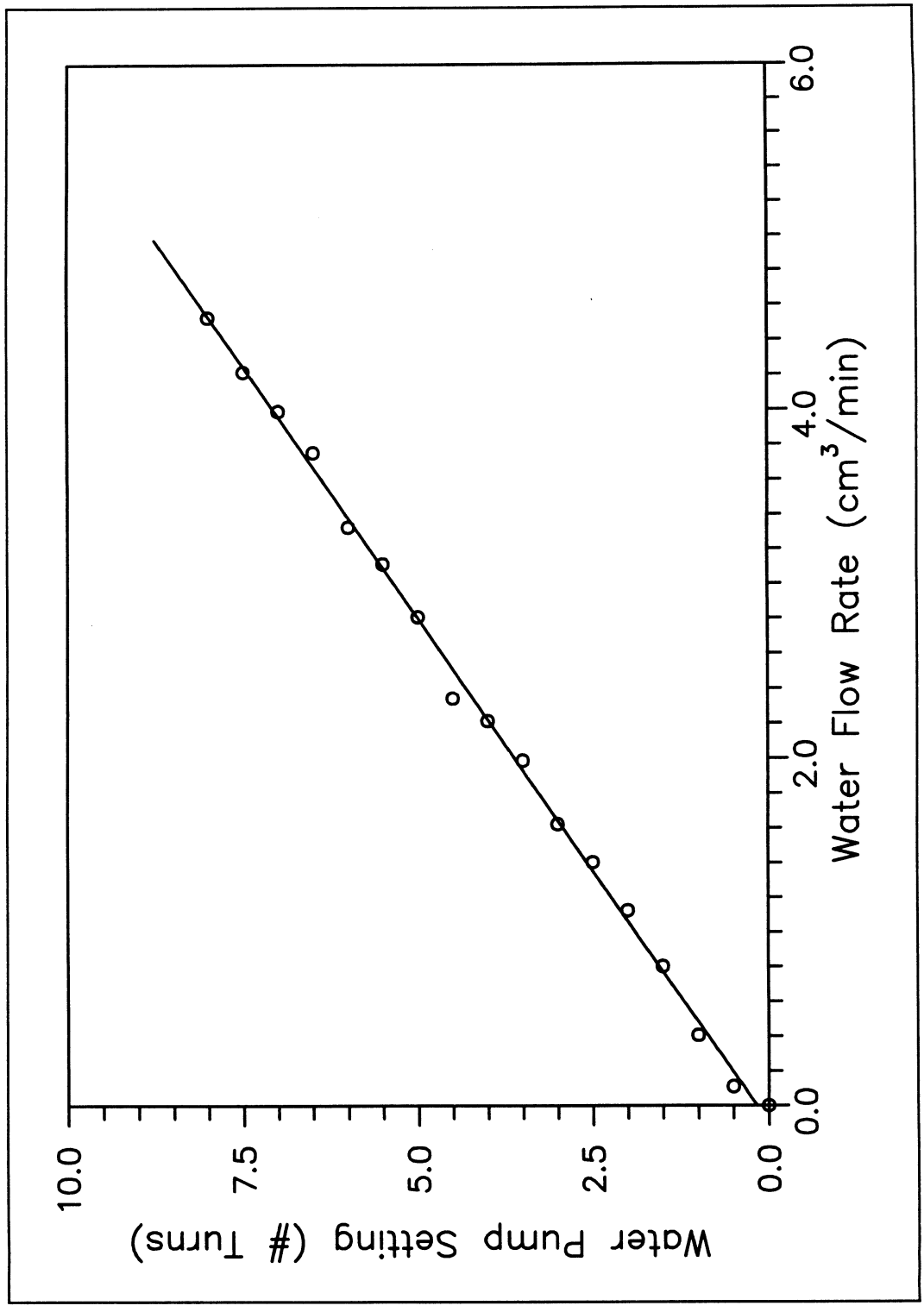

Figure B-1: Calibration Curve for Water Pump.

APPENDIX C

METHOD FOR DETERMING SULFUR CONTENT IN LIMESTONE SAMPLES

The sulfur content in the reaction products has been determined using a LECO-SC-32 sulfur analyzer. In this method, the sulfur is oxidized to sulfur dioxide during the combustion of the sample. An infrared (IR) cell is used to detect the total sulfur as sulfur dioxide. The sample analysis procedure is as follows:

1. Dry the samples at about 105 °C for at least one hour.
2. Weigh the sample (about 0.2 g) and enter the weight.
3. Add about 1.5 g of Lecocel 763-266 and 0.5 g of Iron powder (V_2O_5) 501-078 and mix thoroughly with sample.
4. Press "ANALYZE" key; when message center displays "LOAD FURNACE", slide the boat into the furnace, and press "ANALYZE" key again to start integration.
5. Calibrate the analyzer using a calibration standard and following steps 2 through 4.
6. Analyze samples using above procedure.

APPENDIX D

EXPERIMENTAL RESULTS

Time (min.)	Outlet SO_2 Conc. (ppm)	% SO_2 Removal
0.0	860.0	0.0
0.5	600.0	30.23
0.7	300.0	65.12
3.0	120.0	86.05
5.0	20.0	97.67
6.0	10.0	98.84
12.0	0.0	100.00
14.0	0.0	100.00
16.0	0.0	100.00
18.0	0.0	100.00
20.0	0.0	100.00
22.0	0.0	100.00
24.0	0.0	100.00
26.0	0.0	100.00
37.0	17.0	98.02
40.0	43.0	95.00
44.0	86.0	90.00
47.0	129.0	85.00
50.0	172.0	80.00
52.0	215.0	75.00
54.0	258.0	70.00
55.0	301.0	65.00
56.0	344.0	60.00
58.0	387.0	55.00
60.0	430.0	50.00
63.0	473.0	45.00
66.0	516.0	40.00
73.0	559.0	35.00
90.0	602.0	30.00

Table D-1: Experimental Results for Run #1 of Integral Reactor Study Maxville Limestone # LS890118A, Pre-Wet Bed,Gas S.V.: 1.0 ft/sec. Gas R.H.: 75%, Temp.: 60 °C, Inlet SO_2 Conc.: 860 ppm

Time (min.)	Outlet SO_2 Conc. (ppm)	% SO_2 Removal
0.0	825.0	0.0
0.5	620.0	24.85
0.7	220.0	73.33
3.0	100.0	87.88
5.0	20.0	97.58
6.0	10.0	98.79
14.0	0.0	100.00
16.0	0.0	100.00
18.0	0.0	100.00
20.0	0.0	100.00
24.0	0.0	100.00
30.0	17.0	97.94
37.0	41.0	95.03
42.0	83.0	89.94
46.0	124.0	84.97
49.0	165.0	80.00
52.0	206.0	75.03
54.0	248.0	69.94
57.0	289.0	64.97
59.0	330.0	60.00
61.0	371.0	55.03
64.0	413.0	49.94
67.0	454.0	44.97
69.0	495.0	40.00
73.0	536.0	35.03
79.0	578.0	29.94
95.0	619.0	24.97

Table D-2: Experimental Results for Run #2 of Integral Reactor Study Maxville Limestone # LS890118A, Pre-Wet Bed, Gas S.V.: 1.0 ft/*sec.* Gas R.H.: 75%, Temp.: 60 °C, Inlet SO_2 Conc.: 825 ppm

Time (min.)	Outlet SO_2 Conc. (ppm)	% SO_2 Removal
0.0	1750.0	0.0
0.5	1200.0	31.43
1.0	1000.0	42.86
4.0	650.0	62.86
10.0	200.0	88.57
12.0	150.0	91.43
14.0	150.0	91.43
15.5	175.0	90.00
19.5	263.0	84.97
23.0	350.0	80.00
25.5	438.0	74.97
29.0	525.0	70.00
31.5	613.0	64.97
34.5	700.0	60.00
38.0	788.0	54.97
41.5	875.0	50.00
45.0	963.0	44.97
48.5	1050.0	40.00
54.0	1138.0	34.97
66.0	1225.0	30.00

Table D-3: Experimental Results for Run #3 of Integral Reactor Study Maxville Limestone # LS890118A, Pre-Wet Bed, Gas S.V.: 1.0 ft/sec. Gas R.H.: 75%, Temp.: 60 °C, Inlet SO_2 Conc.: 1750 ppm

Time (min.)	Outlet SO_2 Conc. (ppm)	% SO_2 Removal
0.0	500.0	0.0
0.5	260.0	48.00
1.0	130.0	74.00
2.0	100.0	80.00
6.0	60.0	88.00
10.0	35.0	93.00
17.0	10.0	98.00
25.0	0.0	100.00
32.0	10.0	98.00
36.0	25.0	95.00
42.0	50.0	90.00
46.0	75.0	85.00
48.0	100.0	80.00
52.0	125.0	75.00
54.0	150.0	70.00
58.0	175.0	65.00
61.0	200.0	60.00
64.0	225.0	55.00
68.0	250.0	50.00
72.0	275.0	45.00
77.0	300.0	40.00
83.0	325.0	35.00
90.0	350.0	30.00
104.0	375.0	25.00
120.0	385.0	23.00

Table D-4: Experimental Results for Run #4 of Integral Reactor Study Maxville Limestone # LS890118A, Pre-Wet Bed, Gas S.V.: 1.0 ft/sec. Gas R.H.: 50%, Temp.: 60 °C, Inlet SO_2 Conc.: 500 ppm

Time (min.)	Outlet SO_2 Conc. (ppm)	% SO_2 Removal
0.0	500.0	0.0
0.5	270.0	46.00
1.0	120.0	76.00
2.0	90.0	82.00
6.0	55.0	89.00
10.0	35.0	93.00
15.0	20.0	96.00
25.0	5.0	99.00
30.0	0.0	100.00
37.0	0.0	100.00
49.0	10.0	98.00
56.0	25.0	95.00
60.0	50.0	90.00
63.0	75.0	85.00
65.0	100.0	80.00
68.0	125.0	75.00
70.0	150.0	70.00
72.0	175.0	65.00
75.0	200.0	60.00
78.0	225.0	55.00
80.0	250.0	50.00
84.0	275.0	45.00
88.0	300.0	40.00
97.0	325.0	35.00
107.0	350.0	30.00
121.0	370.0	26.00

Table D-5: Experimental Results for Run #5, Duplicate of Run #4

Time (min.)	Outlet SO_2 Conc. (ppm)	% SO_2 Removal
0.0	500.0	0.0
0.5	240.0	52.00
1.0	70.0	86.00
2.0	10.0	98.00
2.5	10.0	98.00
2.75	25.0	95.00
3.0	50.0	90.00
3.25	75.0	85.00
3.5	100.0	80.00
4.0	125.0	75.00
4.5	150.0	70.00
5.0	175.0	65.00
5.5	200.0	60.00
6.5	225.0	55.00
8.5	250.0	50.00
14.0	270.0	46.00
17.0	300.0	40.00
22.0	325.0	35.00
29.0	350.0	30.00
36.0	375.0	25.00
47.0	400.0	20.00
58.0	413.0	17.4

Table D-6: Experimental Results for Run #6 of Integral Reactor Study Maxville Limestone # LS890118A, Pre-Wet Bed, Gas S.V.: 1.0 ft/sec. Gas R.H.: 25%, Temp.: 60 °C, Inlet SO_2 Conc.: 500 ppm

Time (min.)	Outlet SO_2 Conc. (ppm)	% SO_2 Removal
0.0	500.0	0.0
0.1	450.0	10.00
0.2	350.0	30.00
0.4	250.0	50.00
0.5	196.0	60.80
0.6	207.0	58.60
1.0	230.0	54.00
1.2	253.0	49.40
1.5	276.0	44.8
2.0	299.0	40.20
2.8	322.0	35.60
4.0	345.0	31.00
6.7	368.0	26.40
12.0	391.0	21.80
32.0	414.0	17.20
46.0	415.0	17.00
62.0	420.0	16.00

Table D-7: Experimental Results for Run #7 of Integral Reactor Study Maxville Limestone # LS890118A, Dry Bed, Gas S.V.: 1.0 ft/sec. Gas R.H.: 25%, Temp.: 60 °C, Inlet SO_2 Conc.: 500 ppm

Time (min.)	Outlet SO_2 Conc. (ppm)	% SO_2 Removal
0.0	500.00	0.0
1.0	450.00	10.00
2.0	337.50	32.50
3.0	247.50	50.50
4.0	200.00	60.00
5.0	177.50	64.50
6.0	162.50	67.50
8.0	157.50	68.50
10.0	150.00	70.00
12.0	155.00	69.00
14.0	157.50	68.50
16.0	162.50	67.50
18.0	160.00	68.00
20.0	165.00	67.00
22.0	170.00	66.00
24.0	170.00	66.00
26.0	175.00	65.00
28.0	200.00	60.00
30.0	225.00	55.00
32.0	255.00	49.00
34.0	295.00	41.00
36.0	330.00	34.00
38.0	367.50	26.50
40.0	395.00	21.00
42.0	420.00	16.00
44.0	445.00	11.00
46.0	460.00	8.00
50.0	475.00	5.00
55.0	480.00	4.00
60.0	482.50	3.50

Table D-8: Experimental Results for Run #8 of Integral Reactor Study Maxville Limestone (2.00-2.36 mm), Pre-Wet Bed, Gas S.V.: 1.0 ft/sec. Gas R.H.: 50%, Temp.: 60 °C, Inlet SO_2 Conc.: 500 ppm

Time (min.)	Outlet SO_2 Conc. (ppm)	% SO_2 Removal
0.0	500.00	0.0
1.0	145.00	71.00
2.0	35.00	93.00
3.0	20.00	96.00
4.0	15.00	97.00
5.0	12.50	97.50
6.0	15.00	97.00
8.0	40.00	92.00
10.0	57.50	88.50
12.0	70.00	86.00
14.0	85.00	83.00
16.0	105.00	79.00
18.0	120.00	76.00
20.0	130.00	74.00
22.0	140.00	72.00
24.0	150.00	70.00
26.0	160.00	68.00
28.0	175.00	65.00
30.0	200.00	60.00
32.0	230.00	54.00
34.0	275.00	45.00
36.0	315.00	37.00
38.0	365.00	27.00
40.0	395.00	21.00
42.0	420.00	16.00
44.0	435.00	13.00
46.0	445.00	11.00
50.0	455.00	9.00
55.0	460.00	8.00
60.0	460.00	8.00

Table D-9: Experimental Results for Run #9 of Integral Reactor Study Maxville Limestone (1.00-1.18 mm), Pre-Wet Bed, Gas S.V.: 1.0 ft/sec. Gas R.H.:50%, Temp.: 60 °C, Inlet SO_2 Conc.: 500 ppm

Time (min.)	Outlet SO_2 Conc. (ppm)	% SO_2 Removal
0.0	500.00	0.0
1.0	95.00	81.00
2.0	20.00	96.00
3.0	15.00	97.00
4.0	12.50	97.50
5.0	10.00	98.00
6.0	10.00	98.00
8.0	10.00	98.00
10.0	10.00	98.00
12.0	7.50	98.50
14.0	17.50	96.50
16.0	80.00	84.00
18.0	90.00	82.00
20.0	110.00	78.00
22.0	125.00	75.00
24.0	155.00	69.00
26.0	180.00	64.00
28.0	210.00	58.00
30.0	240.00	52.00
32.0	290.00	42.00
34.0	345.00	31.00
36.0	400.00	20.00
38.0	430.00	14.00
40.0	450.00	10.00
42.0	465.00	7.00
44.0	475.00	5.00
46.0	477.50	4.50
50.0	480.00	4.00
55.0	485.00	3.00
60.0	490.00	2.00

Table D-10 Experimental Results for Run #10 of Integral Reactor Study Maxville Limestone (0.50-0.60 mm), Pre-Wet Bed, Gas S.V.: 1.0 ft/sec. Gas R.H.: 50%, Temp.: 60 °C, Inlet SO_2 Conc.: 500 ppm

Time (sec.)	Conversion of $CaCO_3$ (%)
0.0	0.0
120	0.235
240	0.353
360	0.412

Table D-11: Conversion Versus Time Data for Maxville Limestone (53-75 μm) at Flue Gas Relative Humidity = 40 %

Time (sec.)	Conversion of $CaCO_3$ (%)
0.0	0.0
120	0.824
240	1.059
360	1.118

Table D-12: Conversion Versus Time Data for Maxville Limestone (53-75 μm) at Flue Gas Relative Humidity = 60 %

Time (sec.)	Conversion of $CaCO_3$ (%)
0.0	0.0
120	1.437
240	1.780
360	1.834

Table D-13: Conversion Versus Time Data for Maxville Limestone (53-75 μm) at Flue Gas Relative Humidity = 75 %

Time (sec.)	Conversion of $CaCO_3$ (%)
0.0	0.0
120	1.953
240	2.543
360	2.721

Table D-14: Conversion Versus Time Data for Maxville Limestone (53-75 μm) at Flue Gas Relative Humidity = 85 %

Time (sec.)	Conversion of $CaCO_3$ (%)
0.0	0.0
120	2.177
240	2.824
360	3.235
600	3.834
1200	6.864
1800	7.504
2700	9.306
3600	9.498
4800	9.200

Table D-15: Conversion Versus Time Data for Maxville Limestone (53-75 μm) at Flue Gas Relative Humidity = 95 %

Time (sec.)	Conversion of $CaCO_3$ (%)
0.0	0.0
120	0.109
240	0.196
360	0.239

Table D-16: Conversion Versus Time Data for Mississippi Limestone (53-75 μm) at Flue Gas Relative Humidity = 40 %

Time (sec.)	Conversion of $CaCO_3$ (%)
0.0	0.0
120	0.280
240	0.309
360	0.357

Table D-17: Conversion Versus Time Data for Mississippi Limestone (53-75 μm) at Flue Gas Relative Humidity = 60 %

Time (sec.)	Conversion of $CaCO_3$ (%)
0.0	0.0
120	0.387
240	0.461
360	0.478

Table D-18: Conversion Versus Time Data for Mississippi Limestone (53-75 μm) at Flue Gas Relative Humidity = 75 %

Time (sec.)	Conversion of $CaCO_3$ (%)
0.0	0.0
120	0.509
240	0.668
360	0.691

Table D-19: Conversion Versus Time Data for Mississippi Limestone (53-75 μm) at Flue Gas Relative Humidity = 85 %

Time (sec.)	Conversion of $CaCO_3$ (%)
0.0	0.0
120	0.774
240	0.819
360	0.920
600	1.980
1200	3.396
1800	4.493
2700	5.615
3600	6.540
4800	6.277

Table D-20: Conversion Versus Time Data for Mississippi Limestone (53-75 μm) at Flue Gas Relative Humidity = 95 %

Time (sec.)	Conversion of $CaCO_3$ (%)
0.0	0.0
120	0.154
240	0.132
360	0.162

Table D-21: Conversion Versus Time Data for Vanport Limestone (53-75 μm) at Flue Gas Relative Humidity = 40 %

Time (sec.)	Conversion of $CaCO_3$ (%)
0.0	0.0
120	0.353
240	0.647
360	0.765

Table D-22: Conversion Versus Time Data for Vanport Limestone (53-75 μm) at Flue Gas Relative Humidity = 60 %

Time (sec.)	Conversion of $CaCO_3$ (%)
0.0	0.0
120	1.070
240	1.362
360	1.563

Table D-23: Conversion Versus Time Data for Vanport Limestone (53-75 μm) at Flue Gas Relative Humidity = 75 %

Time (sec.)	Conversion of $CaCO_3$ (%)
0.0	0.0
120	1.920
240	2.088
360	2.178

Table D-24: Conversion Versus Time Data for Vanport Limestone (53-75 μm) at Flue Gas Relative Humidity = 85 %

Time (sec.)	Conversion of $CaCO_3$ (%)
0.0	0.0
120	2.300
240	2.393
360	2.501
600	3.675
1200	3.958
1800	4.611
2700	5.789
3600	4.842
4800	5.332

Table D-25: Conversion Versus Time Data for Vanport Limestone (53-75 μm) at Flue Gas Relative Humidity = 95 %

Time (sec.)	Conversion of $CaCO_3$ (%)
0.0	0.0
120	0.103
240	0.111
360	0.127

Table D-26: Conversion Versus Time Data for Bucyrus Limestone (53-75 μm) at Flue Gas Relative Humidity = 40 %

Time (sec.)	Conversion of $CaCO_3$ (%)
0.0	0.0
120	0.254
240	0.411
360	0.423

Table D-27: Conversion Versus Time Data for Bucyrus Limestone (53-75 μm) at Flue Gas Relative Humidity = 60 %

Time (sec.)	Conversion of $CaCO_3$ (%)
0.0	0.0
120	0.481
240	0.697
360	0.767

Table D-28: Conversion Versus Time Data for Bucyrus Limestone (53-75 μm) at Flue Gas Relative Humidity = 75 %

Time (sec.)	Conversion of $CaCO_3$ (%)
0.0	0.0
120	0.544
240	0.760
360	0.933

Table D-29: Conversion Versus Time Data for Bucyrus Limestone (53-75 μm) at Flue Gas Relative Humidity = 85 %

Time (sec.)	Conversion of $CaCO_3$ (%)
0.0	0.0
120	0.670
240	1.039
360	1.110
600	1.622
1200	2.851
1800	3.520
2700	4.831
3600	5.615
4800	5.523

Table D-30: Conversion Versus Time Data for Bucyrus Limestone (53-75 μm) at Flue Gas Relative Humidity = 95 %

Time (sec.)	Conversion of $CaCO_3$ (%)
0.0	0.0
120	0.012
240	0.017
360	0.023

Table D-31: Conversion Versus Time Data for Carey Limestone (53-75 μm) at Flue Gas Relative Humidity = 40 %

Time (sec.)	Conversion of $CaCO_3$ (%)
0.0	0.0
120	0.017
240	0.023
360	0.029

Table D-32: Conversion Versus Time Data for Carey Limestone (53-75 μm) at Flue Gas Relative Humidity = 60 %

Time (sec.)	Conversion of $CaCO_3$ (%)
0.0	0.0
120	0.278
240	0.523
360	0.625

Table D-33: Conversion Versus Time Data for Carey Limestone (53-75 μm) at Flue Gas Relative Humidity = 75 %

Time (sec.)	Conversion of $CaCO_3$ (%)
0.0	0.0
120	0.657
240	1.097
360	1.513

Table D-34: Conversion Versus Time Data for Carey Limestone (53-75 μm) at Flue Gas Relative Humidity = 85 %

Time (sec.)	Conversion of $CaCO_3$ (%)
0.0	0.0
120	1.652
240	1.969
360	2.309
600	2.510
1200	3.022
1800	3.416
2700	4.213
3600	5.015
4800	4.867

Table D-35: Conversion Versus Time Data for Carey Limestone (53-75 μm) at Flue Gas Relative Humidity = 95 %

Time (sec.)	Conversion of $CaCO_3$ (%)
0.0	0.0
120	1.813
240	2.206
360	2.735

Table D-36: Conversion Versus Time Data for Maxville Limestone (150-180 μm) at Flue Gas Relative Humidity = 95 %

Time (sec.)	Conversion of $CaCO_3$ (%)
0.0	0.0
120	1.552
240	1.805
360	1.890

Table D-37: Conversion Versus Time Data for Maxville Limestone (250-300 μm) at Flue Gas Relative Humidity = 95 %

Time (sec.)	Conversion of $CaCO_3$ (%)
0.0	0.0
120	1.098
240	1.220
360	1.412

Table D-38: Conversion Versus Time Data for Maxville Limestone (300-425 μm) at Flue Gas Relative Humidity = 95 %

Gas Relative Humidity (%)	Initial Reaction Rate (mole/kg hr)
0.0	0.0
40.0	0.51
60.0	1.91
75.0	5.80
85.0	9.90
95.0	15.44

Table D-39: Initial Reaction Rate Versus Gas Relative Humidity for Maxville Limestone (53-75 μm)

Gas Relative Humidity (%)	Initial Reaction Rate (mole/kg hr)
0.0	0.0
40.0	0.38
60.0	0.90
75.0	1.32
85.0	3.50
95.0	6.48

Table D-40: Initial Reaction Rate Versus Gas Relative Humidity for Mississippi Limestone (53-75 μm)

Gas Relative Humidity (%)	Initial Reaction Rate (mole/kg hr)
0.0	0.0
40.0	0.14
60.0	1.04
75.0	4.16
85.0	6.88
95.0	8.41

Table D-41: Initial Reaction Rate Versus Gas Relative Humidity for Vanport Limestone (53-75 μm)

Gas Relative Humidity (%)	Initial Reaction Rate (mole/kg hr)
0.0	0.0
40.0	0.25
60.0	0.34
75.0	0.67
85.0	1.11
95.0	1.46

Table D-42: Initial Reaction Rate Versus Gas Relative Humidity for Bucyrus Limestone (53-75 μm)

Gas Relative Humidity (%)	Initial Reaction Rate (mole/kg hr)
0.0	0.0
40.0	0.005
60.0	0.006
75.0	0.45
85.0	1.38
95.0	3.81

Table D-43: Initial Reaction Rate Versus Gas Relative Humidity for Carey Limestone (53-75 μm)

Average Particle Diameter (μm)	Initial Reaction Rate (mole/kg hr)
363	2.27
275	3.16
165	4.02
64	15.44

Table D-44: Initial Reaction Rate Versus Average Particle Diameter for Maxville Limestone at Flue Gas Relative Humidity = 95 %

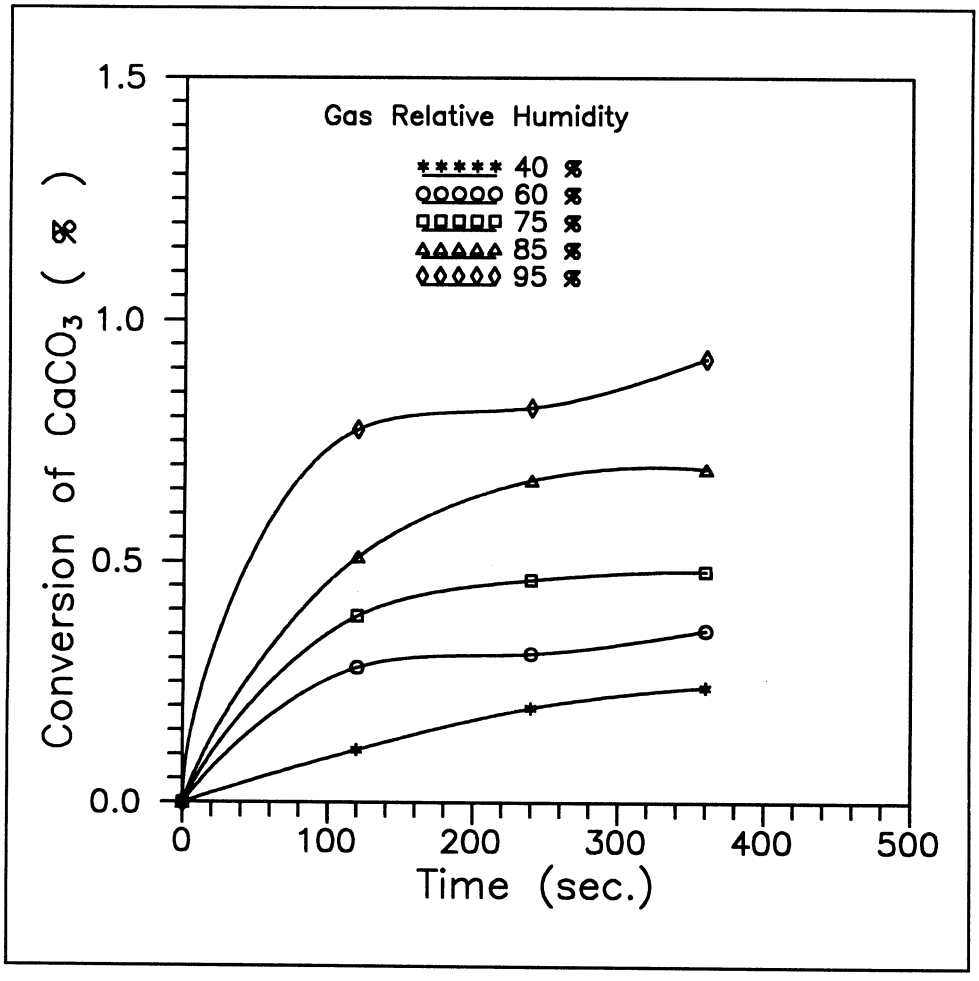

Figure D-1: Conversion of Mississippi Limestone (53-75 μm) as a Function of Time for Various Flue Gas Relative Humidities.

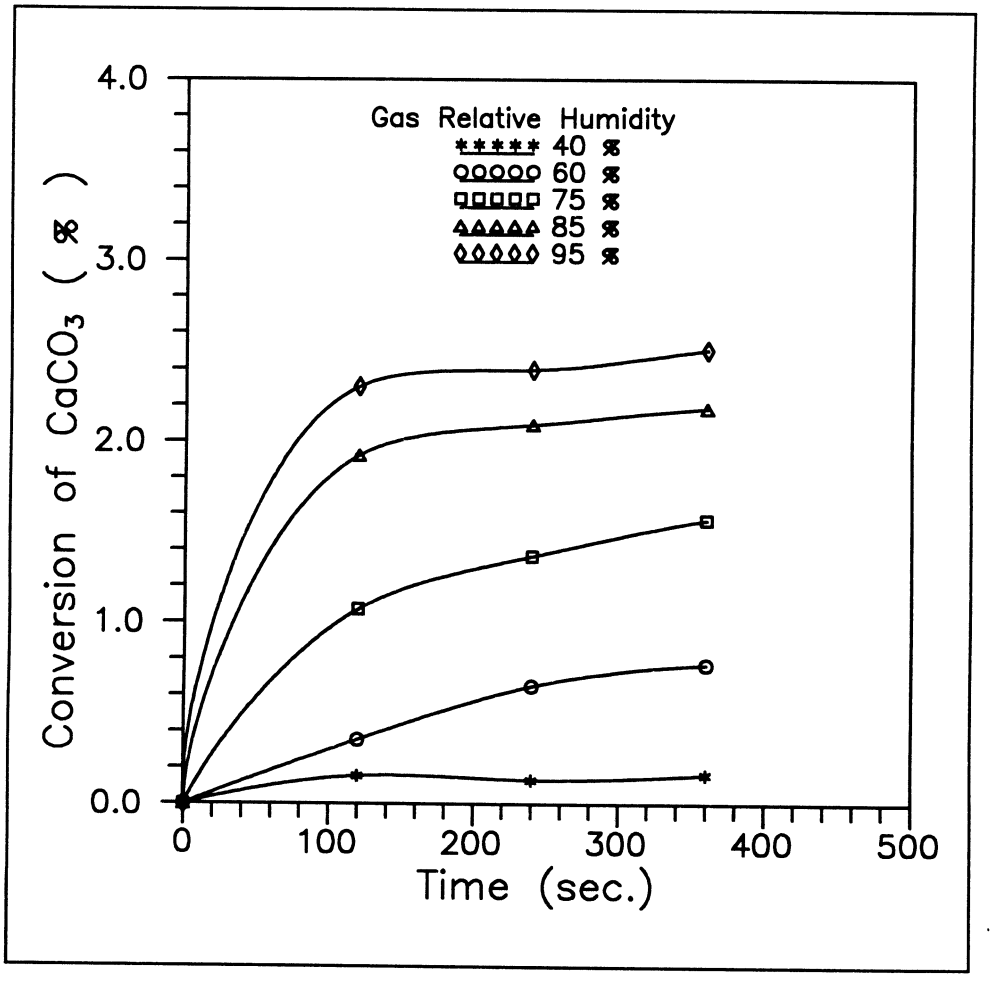

Figure D-2: Conversion of Vanport Limestone (53-75 μm) as a Function of Time for Various Flue Gas Relative Humidities.

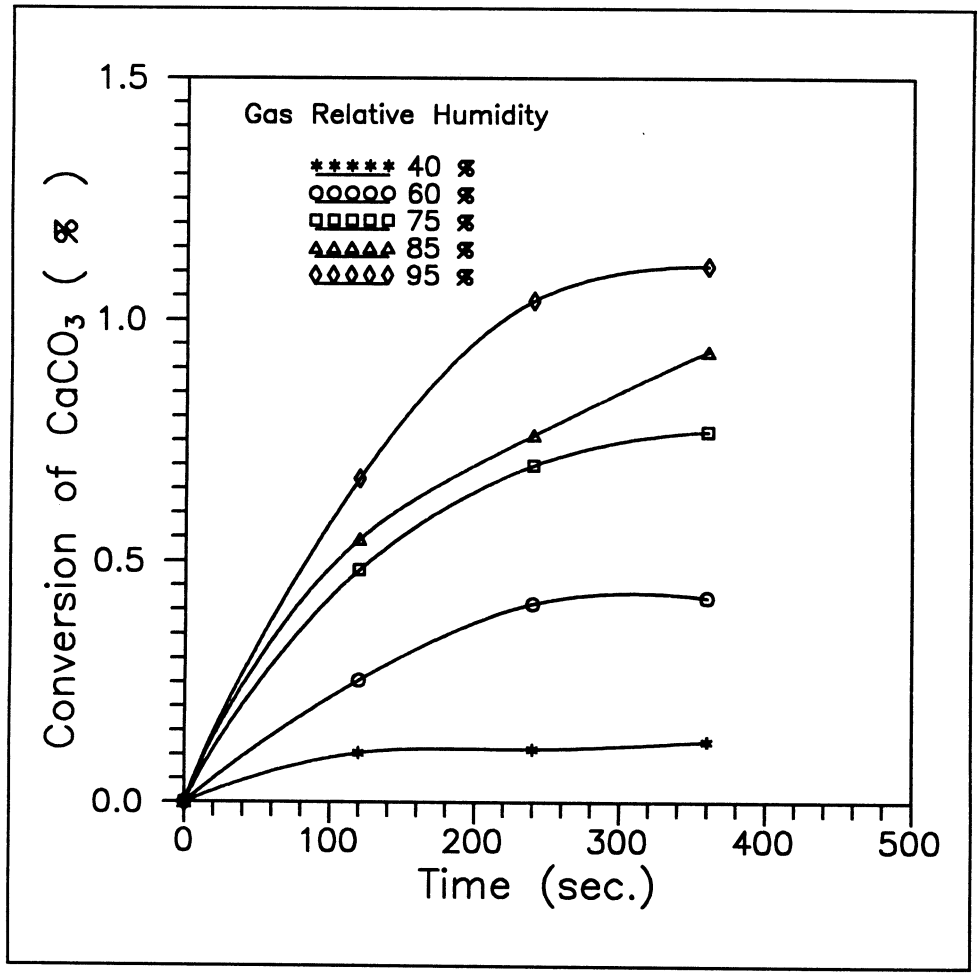

Figure D-3: Conversion of Bucyrus Limestone (53-75 μm) as a Function of Time for Various Flue Gas Relative Humidities.

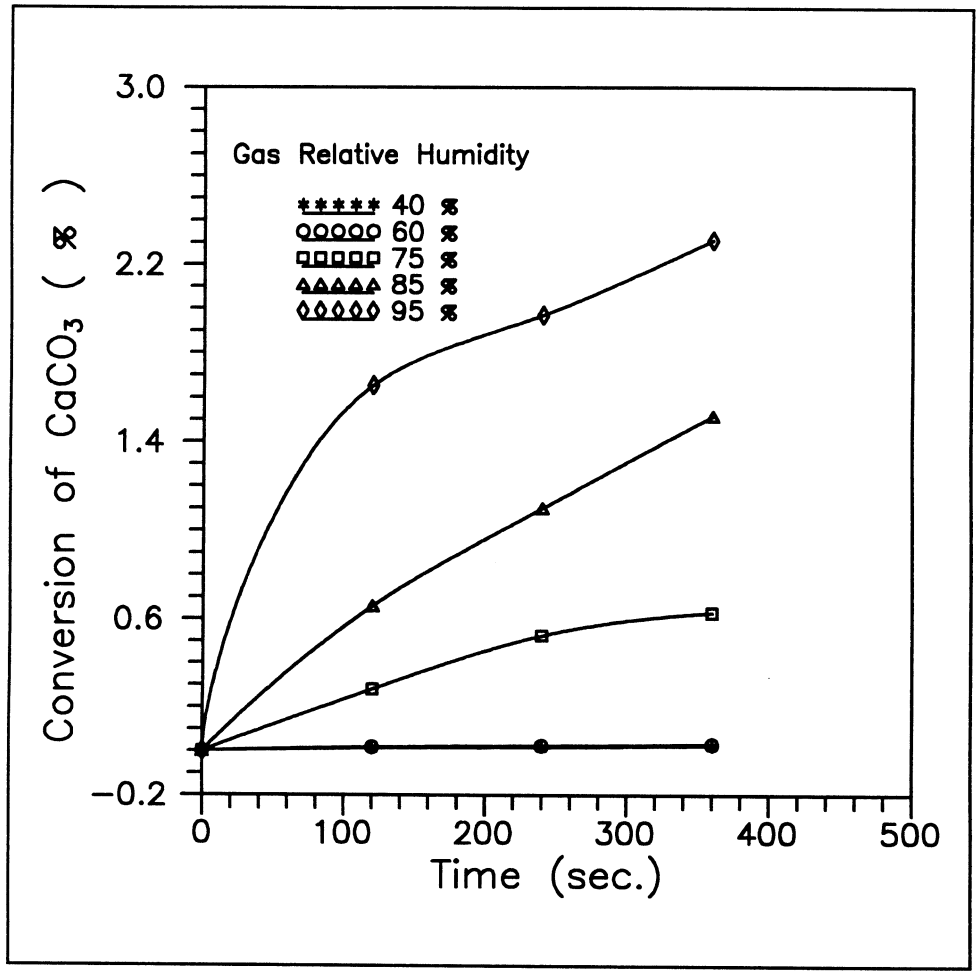

Figure D-4: Conversion of Carey Limestone (53-75 μm) as a Function of Time for Various Flue Gas Relative Humidities.